AD-A122 217 IMPURITY AND DEFECT INTERACTIONS IN GAAS(U) WASHINGTON 1/3
UNIV ST LOUIS MO SEMICONDUCTOR RESEARCH LAB
C M WOLFE ET AL. 30 SEP 82 WU/SRL-64422-10
UNCLASSIFIED N00014-80-C-0762 F/G 20/2 NL

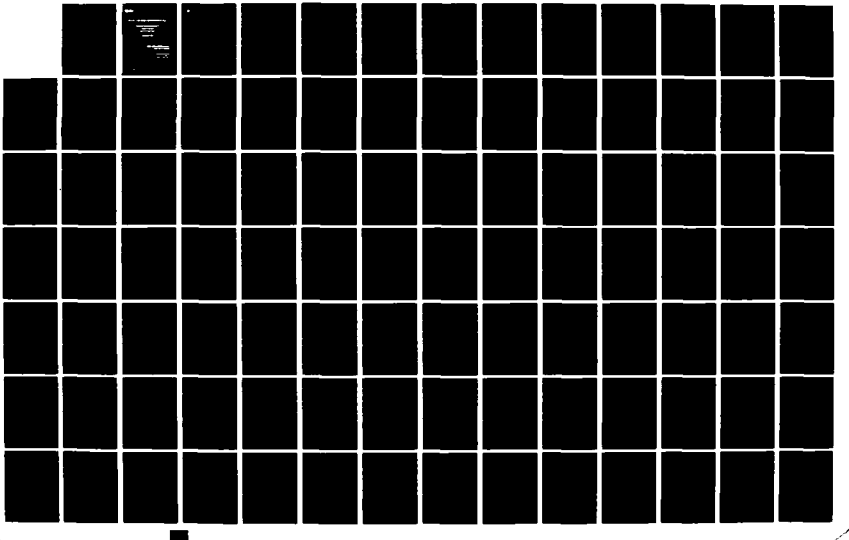

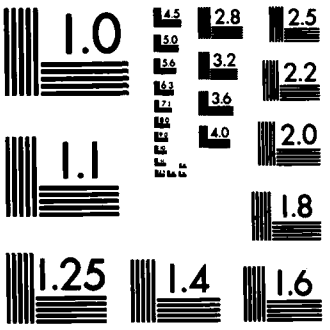

(12)

WASHINGTON UNIVERSITY IN ST. LOUIS

IMPURITY AND DEFECT INTERACTIONS IN GaAs

SEMICONDUCTOR RESEARCH LABORATORY

Washington University

Saint Louis, Missouri 63130

30 September 1982

ANNUAL TECHNICAL REPORT NO. 64422-10

1 August 1981 to 31 July 1982

Office of Naval Research
Code 414
Arlington, Virginia 22217

Contract: N00014-80C-0762

Approved for public release, distribution unlimited.

Unclassified

SECURITY CLASSIFICATION OF THIS PAGE (When Data Entered)

REPORT DOCUMENTATION PAGE		READ INSTRUCTIONS BEFORE COMPLETING FORM
1. REPORT NUMBER	2. GOVT ACCESSION NO. AD-A122217	3. RECIPIENT'S CATALOG NUMBER
4. TITLE (and Subtitle) Impurity and Defect Interactions in GaAs		5. TYPE OF REPORT & PERIOD COVERED Annual Technical Report 1 Aug 1981-31 Jul 1982
		6. PERFORMING ORG. REPORT NUMBER WU/SRL 64422-10
7. AUTHOR(s) C.M. Wolfe, P.A. Fedders, G.E. Stillman, Camellia M.L. Yee, R.T. Green, T.S. Low, B.J. Skromme		8. CONTRACT OR GRANT NUMBER(s) N00014-80C-0762
9. PERFORMING ORGANIZATION NAME AND ADDRESS Semiconductor Research Laboratory Box 1127 Washington University St. Louis, MO 63130		10. PROGRAM ELEMENT, PROJECT, TASK AREA & WORK UNIT NUMBERS PE 61153N RR 021-02-03 NR 243-032
11. CONTROLLING OFFICE NAME AND ADDRESS Office of Naval Research Code 414 Arlington, Virginia 22217		12. REPORT DATE 30 Sep 1982
		13. NUMBER OF PAGES 209
14. MONITORING AGENCY NAME & ADDRESS(if different from Controlling Office)		15. SECURITY CLASS. (of this report) Unclassified
		15a. DECLASSIFICATION/DOWNGRADING SCHEDULE

16. DISTRIBUTION STATEMENT (of this Report)

Approved for public release; distribution unlimited.

17. DISTRIBUTION STATEMENT (of the abstract entered in Block 20, if different from Report)

18. SUPPLEMENTARY NOTES

ONR Scientific Officer
Telephone: (202) 696-4218

19. KEY WORDS (Continue on reverse side if necessary and identify by block number)

GaAs, impurities, defects, complexes, epitaxy, ion implantation, Cr redistribution, impurity incorporation, complex formation, lineshape analysis.

20. ABSTRACT (Continue on reverse side if necessary and identify by block number)

The electrostatic effects on the energy of a hydrogenic donor complex in the presence of an externally applied magnetic field are investigated. The complex is defined as an impurity of net charge one whose charge distribution is not equivalent to a single simple point charge. The results are discussed with respect to photoconductivity measurements of the 1s-2p shallow donor lines in GaAs.

(over)

DD FORM 1 JAN 73 1473 EDITION OF 1 NOV 65 IS OBSOLETE

Unclassified

SECURITY CLASSIFICATION OF THIS PAGE (When Data Entered)

20. Abstract (Cont.)

The effects of fluctuations in the Coulomb potential due to charged impurities in high-purity n-type III-V semiconductors are examined at low temperatures. Assuming that charged donors and acceptors are randomly distributed at high temperatures, we conclude that the donors are selectively filled at low temperatures leaving non-random distributions of charged and filled donors. The potential fluctuations from these distributions can approximately account for a number of experimental observations on low-temperature high-purity GaAs including the apparent decrease of donor binding energy with increasing impurity concentration observed in Hall measurements, the sharpness and temperature dependence of the 1s-2p transition along with the diffuse 1s-conduction band edge observed in photoconductivity experiments, and the fact that experimentally observed photoconductivity lineshapes are narrower than those previously predicted.

Static strains in piezoelectric semiconductors give rise to an electric field or potential which can have an effect on the electrical properties of the material. We have calculated the electric potential due to the strain field arising from a random distribution of point defects. This potential contributes a term to the mobility that is proportional to $T^{1/2}$ and a Hall factor of 1.10. Crude estimates of strain strengths indicate that this scattering mechanism may contribute significantly to the mobility of electrically rather pure III-V semiconductors below room temperature when neutral impurity concentrations are greater than $10^{18}cm^{-3}$. The mechanism may also constitute a dominant one in the mobility of some III-V alloys at fairly low temperatures. The existence of strain induced electric potentials also provides at least a possible mechanism whereby different donors can have different lineshapes as measured in photoconductivity experiments.

A model of Cr in GaAs which is consistent with a large body of experimental data has been developed. It relies on recent spectroscopic models and on our interpretation of redistribution and electrical data, all of which indicate the existence of Cr complexes. The existence of rapidly diffusing interstitial Cr donors is assumed and justified. The model offers a unified picture of the effects of implantation on the Cr profile. It contains mechanisms for compensation and redistribution, which offer an explanation of the semi-insulating properties of Cr doped GaAs and of the two apparently incompatible classes of diffusion and anneal data. The redistribution depends on how the Cr was incorporated and on the vacancy concentration profiles. A study of representatives of the two classes of redistribution data allows us to estimate a lower limit of interstitial Cr diffusion constant and of the vacancy diffusion lengths in GaAs.

During the annealing of ion-implanted Cr-doped GaAs, Cr often redistributes and accumulates at the surface. Although this behavior has been attributed to strain fields and other mechanisms, the widths of these accumulation regions suggest that electric fields due to surface states are a limiting factor in Cr redistribution. For this reason we have developed a thermodynamic model for Cr redistribution which takes into account the electric field due to surface states. A qualitative fit to SIMS data on annealed unimplanted GaAs samples can be obtained with this model. We have also used applied voltages during annealing to modify the amount of band bending and Cr buildup at the surface. This experiment indicates that the accumulated ions are positively charged. We conclude from these experiments that electric fields play a significant role in the redistribution of Cr at GaAs surfaces.

20. Abstract (Cont.)

In this report we present a model of impurity redistribution during epitaxial growth of semiconductors due to diffusion, drift in the built-in electric field, and the growth itself. Examples show unexpected impurity profiles for the minority species and indicate how undesirable conductivity regions can occur.

The incorporation of Group IV impurities as donors and as acceptors in high purity epitaxial GaAs has been investigated using photothermal ionization spectroscopy and variable temperature photoluminescence to detect donors and acceptors respectively. Samples from several sources of high purity LPE, $AsCl_3$-VPE, AsH_3-VPE, MOCVD, and MBE grown GaAs were measured to establish the typical residual impurities present and their relative concetnrations. For AsH_3-VPE, MOCVD and MBE GaAs, impurity incorporation data are presented as a function of III/V ratio. The relative incorporation of amphoteric impurities as donors and acceptors is compared with the model of Teramoto (1972) for LPE and its extension to $AsCl_3$-VPE by Ashen et al. (1975).

Photothermal ionization measurements on Si doped GaAs grown by molecular beam epitaxy (MBE) have indicated that the impurity peak previously assigned to Si was incorrect. Data leading to the new identification are presented, and the results leading to the earlier identification are reexamined. Implications of the new identification on the importance of Si as a residual donor in GaAs grown by various techniques are discussed.

Photothermal ionization spectroscopy has also been used to determine the residual donor species present and their relative concentrations in the highest purity MBE n-GaAs yet reported. Data are presented for samples grown in two different MBE growth reactors; one using elemental As and the other using cracked AsH_3 as the arsenic source. In spite of the substantial differences between growth systems, the donor backgrounds are quite similar.

To directly examine possible impurity interactions or complexing in GaAs, multiply-doped epitaxial layers were prepared. Samples doped both homogeneously and inhomogeneously with H_2O and H_2S exhibit effects which indicate that: (1) H_2O produces free carrier compensation and deep donor behavior; and (2) H_2O affects the incorporation and/or diffusion of sulfur. Experiments are being performed to obtain more insight into these interactions.

A

TABLE OF CONTENTS:

TABLE OF CONTENTS (Continued)

1. RESEARCH OBJECTIVES

The purpose of this work is to investigate the interactions among impurities, defects, and complexes in GaAs which adversely affect the yield and performance of high-speed GaAs integrated circuits. To achieve this objective the following experimental approach is being employed: Impurities are introduced into GaAs by gas-phase doping during epitaxial growth and by ion-implantation into bulk samples. Annealing is performed under controlled atmospheres with applied fields. The resulting samples are characterized by a combination of low and high temperature resistivity and Hall measurements, differential capacitance measurements, far and near infrared photoconductivity measurements, photoluminescence, electron spin resonance, and secondary ion mass spectroscopy. These data are then analyzed with impurity incorporation, redistribution, complex formation, and other models. In the theoretical part of the program various aspects of the experimental results are investigated to obtain new insights into impurity and defect interactions.

2. PHOTOCONDUCTIVITY SPECTRA FOR HYDROGENIC DONOR COMPLEXES

Although the study of the spectra of shallow donors in semiconductors is a rather old subject, many problems of understanding the linewidths, lineshapes, and even the line positions remain unsolved. This is somewhat unfortunate since photoconductivity experiments cannot only detect shallow donor impurities that have densities of $10^{12}/cm^3$ or less, but can also yield resolvable lineshapes. With such a fantastically sensitive spectroscopic tool, one might hope to obtain a wealth of information about the structure and environment of shallow donor impurities.

One major difficulty is that different species of shallow donors ought to yield identical lineshapes whose positions are controlled by central cell corrections and whose intensities are proportional to the densities of the species.[1] As has been discussed in the literature, this is not the case quantitatively and is sometimes not even the case qualitatively. For example, linewidths for different species in GaAs are usually different[1-3] and often even lineshapes are grossly different.[4-6]

2.1 EFFECTIVE MASS APPROXIMATION

Towards a partial understanding of these discrepancies we investigate the electrostatic effects on the energy levels of a hydrogenic shallow donor complex in the presence of an applied magnetic field. For our purposes here, a simple shallow donor is described by an effective mass Hamiltonian where the potential is due to a point charge of magnitude e. A complex (or complex shallow donor) is also described by an effective mass Hamiltonian but the potential is due to a charge density $\rho(\vec{r})$ whose integrated weight is e but which in general is not the charge density of a single point charge.

The Hamiltonian for an electron in the field of a donor and a magnetic field $\vec{B}$ which defines the z-axis is

$$H = (p^2/2m^*) + \frac{1}{2}\omega_c(xp_y - yp_x) + \frac{1}{8}m^*\omega_c^2(x^2+y^2) - (e/\varepsilon_0)\int d^3r'\ \rho(\vec{r}')/|\vec{r}-\vec{r}'|,$$
$$\int d^3r'\ \rho(\vec{r}') = e \qquad (1)$$

where $\omega_c = eB/m^*c$ is the cyclotron frequency. We are assuming that the effective mass approximation is valid and thus m^* and ε_0 are the effective mass and dielectric constant of the medium. We shall further assume that $\rho(\vec{r})$ is zero outside of a volume whose dimensions are small compared to a Bohr radius. The effects of charged impurities many Bohr radii from the center of the charge distribution can be treated as perturbations.

The effective mass approximation yields excellent results in a wide variety of semiconductors[7] and its validity will not be discussed here. Of course, in a real material, $\rho(\vec{r})$ is not the actual charge distribution but is the actual charge distribution minus the charge distribution of the perfect lattice. Further, the use of a dielectric constant in and very near the charge distribution is clearly not valid. The details of the interactions in this volume are contained in the central cell correction to the energy of the 1s state which we shall assume to be given. These corrections are quite small in GaAs because the effective Bohr radius is 99 Å.

2.2 ANALYSIS

In this section we outline the calculation of the effects of a complex on the energy levels of a shallow donor. Initially we ignore the effects due to any remote charges. In reduced units, the zero order Hamiltonian, H_0, is that for a simple donor at the origin,

$$H_0 = -\nabla^2 + (\gamma/i)(\partial/\partial\phi) + \frac{1}{4}\gamma^2\rho^2 - 2/r \quad , \tag{2}$$

where lengths and energies are taken in units of the effective Bohr radius, $a_0 = \varepsilon_0 \hbar^2/m^*e^2$, and the effective Rydberg, $R = m^*e^4/2\varepsilon_0^2\hbar^2$. The dimensionless magnetic field strength is γ where $\gamma = \hbar\omega_c/2R$, $\rho^2 = r^2\sin^2\theta$, and the magnetic field $\vec{B}$ defines the z direction. In what follows, we shall always assume γ is much larger than any other (dimensionless) perturbation.

We define the complex by a set of charges $Z_i e$ at the points $\vec{r}_i$ where

$$\sum_i Z_i = 1 \quad . \tag{3}$$

(If the charge distribution is a continuum, the appropriate sums can trivially be converted to integrals.) Thus H', the perturbation due to the complex, can be written as a sum of terms, one from each member of the complex.

$$H' = \sum_i V_i$$

$$V_i = -2Z_i(|\vec{r}-\vec{r}_i|^{-1} - r^{-1}) \quad . \tag{4}$$

At this point it is important to note that the origin of the charge distribution is irrelevant. Thus, if we translate all of the charges

by $\vec{r}_o$ so that

$$\vec{r}_i \rightarrow \vec{r}_i + \vec{r}_o \quad , \tag{5}$$

the problem remains unchanged.

Using the usual multipole expansion, V_i can be expanded as

$$V_i = -8Z_i\pi \sum_{\ell=1} \sum_m \frac{r_i^\ell}{r^{\ell+1}} \frac{Y^*_{\ell m}(\Omega_i) Y_{\ell m}(\Omega)}{2\ell + 1} \quad , \qquad r > r_i \tag{6a}$$

$$V_i = -2Z_i \left(\left(\frac{1}{r_i} - \frac{1}{r} \right) + 4\pi \sum_{\ell=1} \sum_m \frac{r^\ell}{r_i^{\ell+1}} \frac{Y^*_{\ell m}(\Omega_i) Y_{\ell m}(\Omega)}{2\ell + 1} \right) \quad , \quad r < r_i \tag{6b}$$

where the $Y_{\ell m}(\Omega)$ are the usual spherical harmonics and Ω and Ω' refer to the solid angles for $\vec{r}$ and $\vec{r}_i$ respectively. As noted earlier, we have assumed that the charge distribution has dimensions d and that $d \ll 1$ in reduced units. Assuming that the origin in the problem is chosen to lie within a distance d of the charge distribution, the contribution to the energy of an s state from $r < r_i$ will be of order d^2 and will be independent of the angles Ω_i. The corresponding energies of other states will be proportional to the fourth or higher powers of d. Such contributions can be lumped into a central cell correction and will temporarily be ignored while we concentrate on the contributions from Eqs. (4) and (6a).

Although the final answers must be independent of origin, some choices are more convenient than others. The perturbations described by Eq. (6a) contains a sum over ℓ and the ℓth term is proportional to d^ℓ. If we chose the origin to eliminate the $\ell = 1$ term, then first order perturbation theory will yield the correct answer to order d^2. Any other choice will require second order perturbation theory to obtain answers to order d^2. This choice is accomplished by choosing the origin so that

$$\sum_i Z_i \vec{r}_i = 0 \quad , \tag{7}$$

that is, so that the dipole moment of the charge distribution vanishes. Now, to order d^2, H' can be written with only the $\ell = 2$ terms as

$$H' = -(8\pi/5) \sum_m \left| \sum_i Z_i r_i^2 \, Y^*_{2m}(\Omega_i) \right| Y_{2m}(\Omega)/r^3 \quad . \tag{8}$$

Only the $m = 0$ term in Eq. (8) will contribute in lowest order perturbation theory. The energy shift of the state x can be written as

$$\Delta E_x = -\alpha_Q(x) Q(\Omega_i) \tag{9a}$$

$$\alpha_Q(x) = \langle x | (3\cos^2\theta - 1)/r^3 | x \rangle \tag{9b}$$

$$Q(\Omega_i) = \frac{1}{2} \sum_i Z_i r_i^2 (3\cos^2 \theta_i - 1) \quad . \tag{9c}$$

The $\vec{r}_i$ in Eq. (9c) are determined by Eq. (7) and θ_i refers to the i^{th} charge in the coordinate system defined by the magnetic field. Equation (9c) will be presented in a more convenient form in the next section. Before presenting our calculations of $\alpha_Q(x)$ for the 1s and $2p_-$ states, we wish to briefly comment on the coupling of terms arising from the complex with terms describing the electric field from remote charges.

The Hamiltonian describing an electron interacting with an electric field $\vec{E}$ generated by remote charges is

$$H_s = -e\vec{E} \cdot \vec{r}/\varepsilon_o r^3 \quad . \tag{10}$$

Since this term has an odd parity, bound states (in the presence of a magnetic field) are unaffected by H_s to first order. They are, of course, affected to second order and this Hamiltonian gives rise to the second

order Stark shift. As has been extensively discussed in the literature, different donors are under the influence of different electric fields generated by remote defects. This leads to a characteristic lineshape that is usually observed in photoconductivity experiments.

Since in general there will be a "length" vector $\vec{d}$ associated with the charge distribution of a complex, one might have expected a term in the complex Hamiltonian that was linear in d and had odd parity. If such a term existed, the cross term of it and the Stark term in second order perturbation theory would lead to an energy shift proportional to Ed; i.e., an effective first order Stark shift. In fact, such a term did exist in the Hamiltonian for a complex before we transformed it to zero via Eq. (7). If we had not transformed this dipole term to zero, every energy level would have been shifted by a term proportional to Ed. However, the multiplicative coefficient would be the same for all states and thus the term would cancel out for any energy difference.

A term linear in E whose coefficient depends on the charge configuration could be useful in trying to explain anomalous linewidths from different donor species. However, our argument does not rule out such a term,[8] it merely rules it out for a medium described by only an isotropic dielectric constant.[9] Terms depending on other less isotropic properties of the media may yield such terms.

2.3 CALCULATIONS

The energy shift of a shallow donor state due to the electrostatic effects of a complex is given by Eqs. (9) in the reduced units discussed at the beginning of Sect. II. For GaAs, lengths are measured in terms of the Bohr radius $a_o = 99$ Å, energies are measured in terms of the Rydberg $R = 5.77$ meV $= 46.5$ cm^{-1}, and γ is the dimensionless magnetic field strength where B (in kG) $= 65.6\,\gamma$. In this section we present and discuss the results of our calculations for the energy difference of the 1s and $2p_-$ states only since this is the most important spectroscopic transition.

The wave functions of the 1s and $2p_-$ states for the zero order Hamiltonian, Eq. (2), describing an hydrogenic atom in a magnetic field were obtained by variational calculations. The trial wave functions used were

$$\psi_{1s}(\vec{r}) = A \exp(-ar - b^2\rho^2 - c^2z^2) \quad , \tag{11a}$$

$$\psi_{2p_-}(\vec{r}) = A\rho \exp(-ar - b^2\rho^2 - c^2z^2 - i\phi) \quad , \tag{11b}$$

where a, b, and c were varied in each case to minimize the energy. One reason for the choice in Eqs. (11) is that all radial integrals can be expressed in terms of the parabolic cylinder function and only the θ integrals had to be performed numerically. Thus the energies and all derivatives with respect to a, b, and c are easily computed and one can minimize the energies with very few iterations. The energies obtained are not quite as low as have been obtained with better trial wavefunctions. For example we obtain

$$\left(\frac{E_h(\gamma) - E_L(\gamma)}{E_L(\gamma) - E(0)}\right) \leq 2 \times 10^{-3} \tag{12}$$

for all values of γ less than 10. In this expression $E_h(\gamma)$ is our computed energy as a function of γ for the 1s state, $E_L(\gamma)$ is the energy as a function of γ as obtained by Larson[10] using better trial wave functions, and E(0) is the 1s energy in zero magnetic field.

Using the above wavefunctions we have calculated $\alpha_Q(x)$ where x refers to the 1s and $2p_-$ states. Since it is the energy shift between the 1s and $2p_-$ states that is important, we write

$$\Delta E(\gamma) = \beta(\gamma) Q(\Omega_i),$$
$$\beta(\gamma) = \alpha_Q(1s) - \alpha_Q(2p_-) \qquad (13)$$

where $\Delta E(\gamma)$ is the shift in $E_{2p_-} - E_{1s}$ due to the complex. $Q(\Omega_i)$, given by Eq. (9b) in reduced units, depends only on the structure of the complex and its orientation. At $\gamma = 0$,

$$\beta(0) = 1/60 \quad . \qquad (14)$$

The quantity $\beta(\gamma)$ is plotted vs γ in Figure 1. For purposes of comparison, the magnetic field dependence of the central cell correction $E_c(\gamma)$ is also plotted on Figure 1 where

$$E_c(\gamma) \propto 1/|\psi_{1s}(r=0)|^2 \quad . \qquad (15)$$

There are two features that distinguish the complex shift from the central cell shift. First of all, the complex shift changes much more rapidly with magnetic field. Secondly, and more important, the complex shift depends on the orientation of a complex with respect to the magnetic field. As can be seen from Fig. 1, the effects of a complex as a function of field orientation can best be observed at highest magnetic fields.

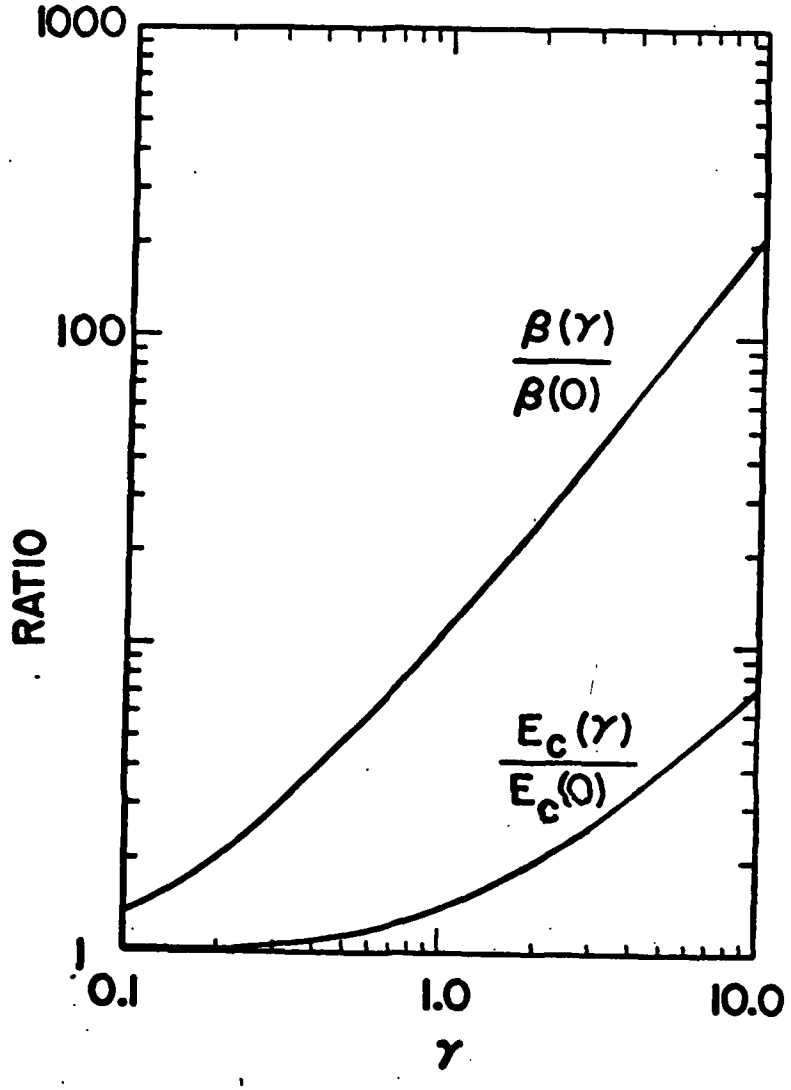

Fig. 1. Magnetic field dependence of $\beta(\gamma)$. The quantity plotted in $\beta(\gamma)/\beta(0)$ vs. the magnetic field in dimensionless units. For purposes of comparison, the magnetic field dependence of the central cell correction is also give.

As an example consider a complex consisting of two charges $Z_1 = 2$ and $Z_2 = -1$ separated by a dimensionless distance a. Using Eqs. (7) and (9c) we obtain

$$Q(\Omega) = a^2(3\cos^2\theta - 1) \tag{16}$$

where θ is the angle between the magnetic field and a line connecting the two charges. Suppose, for instance, such a complex could be oriented along any one of the four independent <111> axes. If $\vec{B}$ was pointing along one of the three independent <100> axis, Q would be zero in all cases. On the other hand, if $\vec{B}$ were pointing along one of the <111> axes, complexes pointing along that axis would have $Q = 2a^2$ and complexes pointing along the other three axes would have $Q = -\frac{2}{3}a^2$. Numerically, for GaAs in a magnetic field of 65.6 kG, the above complex with length of a equal to one lattice spacing could give rise to a shift that moves over a range of 0.0816 cm^{-1} as a function of magnetic field angle.

There is, of course, no guarantee that a given complex of net charge one is a shallow donor. The question of whether it is or not is beyond the scope of this paper and will not be discussed further. Besides substitutions of two or more atoms to form a complex there could be configurations where a single substitution plus a shift in position forms one. For example, suppose a C atom replaces an As atom but, because of its small size, the C atom moves slightly from the normal As position. Such a complex might be described by a charge Z_c at the C site and a charge $1-Z_c$ at the old As site where Z_c is an effective charge for the C.

Figures 2 and 3 exhibit photoconductive response data of doped GaAs epitaxial layers.[11] The arrows in the figures point to structure that could be interpreted as resolved, partially resolved, and unresolved splittings due to a complex. This data exists only at one orientation and therefore it is not known whether the structure shifts with magnetic field angle. Thus one could also obviously interpret the data as structure due to different chemical species.

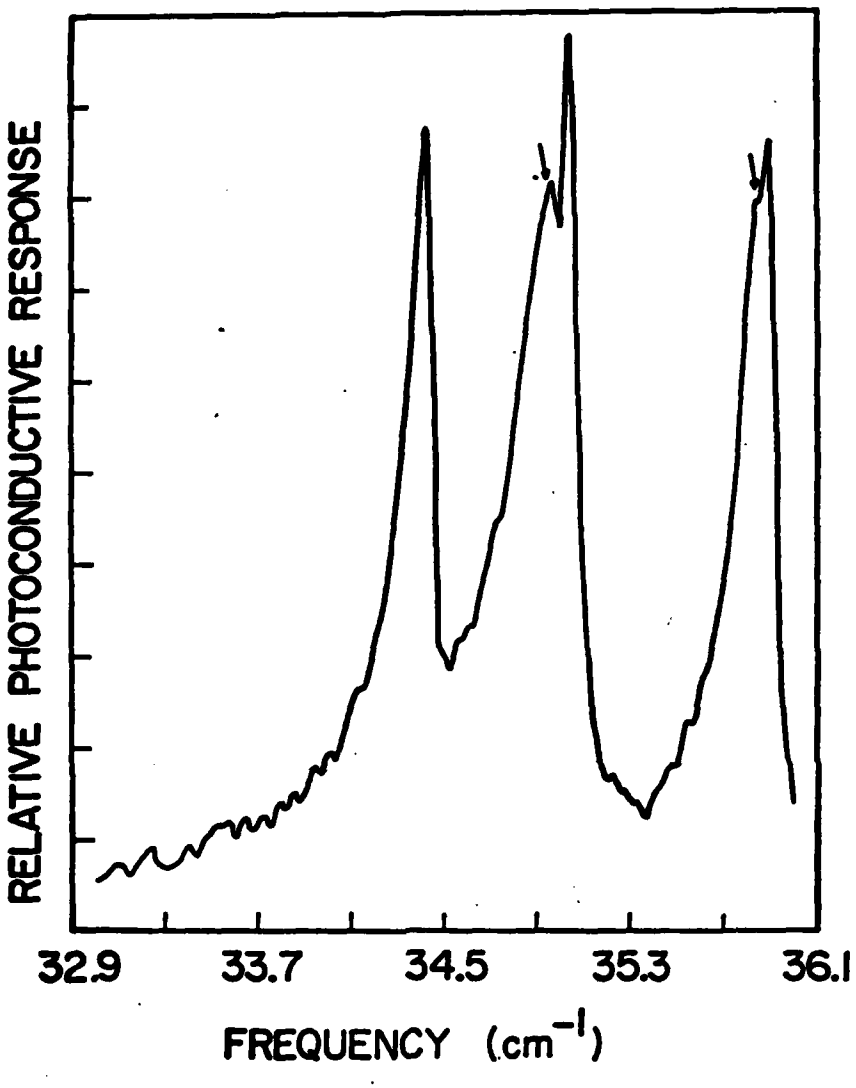

Fig. 2. High resolution photoconductivity spectra of a GaAs epitaxial layer at a magnetic field of 50 kG and a temperature of 42 K. (See ref. 1.) The arrows point to structure that could be interpreted as resolved and partially resolved splittings due to complexes.

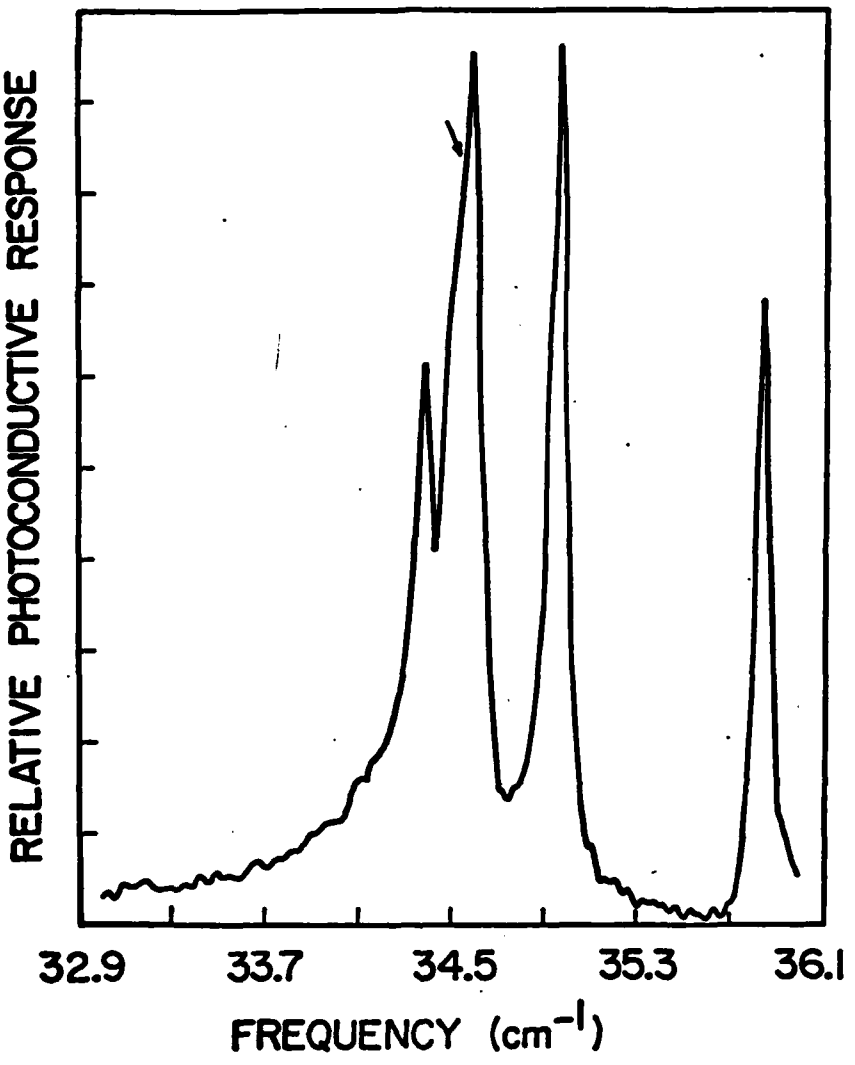

Fig. 3. High resolution photoconductivity spectra of a GaAs epitaxial layer at a magnetic field of 50 kG and a temperature of 4.2 K. (See ref. 1.) The arrow points to structure that could be interpreted as an unresolved splitting due to a complex.

2.4 REFERENCES

1. D. M. Korn and David M. Larsen, Solid State Commun, 13, 807 (1973).
2. David M. Larsen, Phys. Rev. B 8, 535 (1973).
3. David M. Larsen, Phys. Rev. B 13, 1681 (1976).
4. C. M. Wolfe, D. M. Korn, and G. E. Stillman, Appl. Phys. Lett. 24, 78 (1974).
5. C. M. Wolfe, G. E. Stillman, and D. M. Korn, Gallium Arsenide and Related Compounds 1976 (Inst. Phys. Conf. Ser. 33a) p. 119.
6. G. E. Stillman, private communication.
7. With respect to GaAs see, for example, G. E. Stillman, David M. Larsen, C. M. Wolfe, and R. C. Brandt, Solid State Commun. 9, 2245 (1971).
8. The Hamiltonian used here does contain an odd parity term proportional to d^3. This term is too small to exhibit observable effect.
9. Preliminary calculations that such a term is generated by strains emanating from the defect in conjunction with the piezoelectric effects.
10. David M. Larsen, Phys. Rev. B, to be published.
11. G. Stillman, private communication.

3. COULOMB FLUCTUATIONS FROM NON-RANDOM DONOR DISTRIBUTIONS

For years it has been known that a random distribution of equal concentrations of fixed positive and negative charges will yield infinite fluctuations in the Coulomb potential in the limit of an infinite volume.[1] These fluctuations can be damped, of course, by screening due to additional mobile charges or by a rearrangement of the fixed charges themselves. In light of this, consider a high-purity n-type semiconductor at low temperatures. As the temperature is lowered, the number of free carriers is reduced toward zero, and thus the screening or Debye radius tends toward infinity.[2] Since one does not normally think of the charged donors and acceptors as being mobile, one would naively expect the Coulomb fluctuations to become huge and finally infinite.

However, there is another available mechanism for partially screening these fluctuations that consists of the spatially selective filling of donor states rather than the usual picture of filling these states randomly. That is, the Coulomb fluctuations, and of course the free energy, will be lowered by selectively filling the charged donor states. The purpose of this section is to theoretically investigate this process including the magnitude and consequences of the remaining finite fluctuations. We shall limit our discussion and arguments to n-type III-V semiconductors with low impurity concentrations of shallow donors and acceptors. For the purposes of this report low concentrations mean $n_d^{1/3} a_o \ll 1$ where n_d is the number density of donors and a_o is the Bohr radius of a shallow donor. Thus, for GaAs with $a_o = 99$ A, our limit would include samples with $n_d \lesssim 10^{15}$ cm^{-3}. These concentrations are low enough so that impurity band conduction becomes very difficult.[3]

Given a random distribution of donors and acceptors, finding the actual distribution of filled and empty donors from first principles is an extremely difficult problem that will not be attempted here. Instead we approach the problem in a much more phenomenological (and less rigorous) way as follows. We assume that each acceptor can be paired with an unfilled or charged donor. This pairing radius is described by the probability distribution function for being able to construct a charge neutral volume around an acceptor with that radius. The distribution of Coulomb potentials can then be obtained and used to deduce various properties of the system.

The picture that emerges from our analysis of the system at low temperatures is as follows. There must, of course, be fluctuations in the Coulomb potential due to the charged impurities. However, these fluctuations are quite different from those which one would obtain from a random distribution of charged impurities. This non-random distribution of fluctuations due to the selective filling of donors has two important aspects. In the first place, the average potential energy that electrons feel from charged donors and acceptors is negative in regions of the crystal near filled donors even though the average Coulomb potential throughout the crystal is, of course, zero. Secondly, there are finite fluctuations in the potential energy of an electron about this mean value that are smaller than the average fluctuations in the crystal as a whole.

Further, our analysis provides at least an approximate explanation of a number of puzzling phenomena observed in relatively pure n-type GaAs at low temperatures. These include the apparent decrease in E_d, the donor binding energy, with increasing n_d as observed in Hall measurements[4,5] and the decrease in mobility of many samples below about 10 K.[5] It also includes the sharpness and temperature dependence of the 1s-2p transition

along with the lack of a sharp 1s-conduction band edge observed in photoconductivity experiments.[5,6] Finally, it gives an explanation for the fact that experimentally observed photoconductivity lineshapes are narrower than those predicted theoretically[7,8] using the familiar Holzmark distribution of electric fields in a sample.

There have been a number of previous explanations of some of the above phenomena that depend on the banding of impurity states.[5] However, as will be discussed, the Coulomb fluctuations are much greater than typical overlap integrals at low concentrations of impurities which should preclude banding.[3]

3.1 BASIC MODEL

First, it is instructive to pursue the concept of the random filling of charged donor states in somewhat more detail. Thus, we consider the distribution of electric potentials at a given point due to a random distribution of point charges with a density n_t. The potential at the origin due to single positive charge at $\vec{r}$ is the screened Coulomb potential

$$\phi(\vec{r}) = (e/\varepsilon_0 r)\exp(-r/r_s) \quad , \tag{1}$$

where ε_0 is the static dielectric constant of the medium and r_s is a screening radius. We assume that the system is charge neutral so that the number of positively charged impurities is equal to the number of negatively charged impurities plus the number of conduction electrons. Finally, we take the low-concentration limit where n_t is much smaller than the density of lattice points.

The calculation of the distribution of potentials for the above system is easily obtained as a special case of the calculation described below. For our purposes here it is sufficient to characterize the Coulomb potential fluctuations by their second moment and one obtains

$$\phi_r^2 = \langle\phi^2\rangle = 2\pi n_t r_s \; e^2/\varepsilon_0^2 \quad . \tag{2}$$

In order to apply this to an n-type semiconductor we take r_s to be the Debye screening radius,

$$r_s = (kT\varepsilon_0/4\pi ne^2)^{1/2} \quad , \tag{3}$$

where n is the density of conduction electrons (assumed nondegenerate)

and

$$n_t = (2n_a + n) \quad , \tag{4}$$

where n_a is the density of charged acceptors and $n_a + n$ is equal to the density of charged donors. At this point one can see that as the density of conduction electrons tends toward zero, the Debye radius and ϕ_r tend toward infinity.

To proceed further we assume a crude model where the charged donors have only one bound state with binding energy E_d and, using effective mass theory,

$$E_d = e^2/2a_0\varepsilon_0 \quad . \tag{5}$$

Since the potential energy fluctuations at different donor sites span a width in energy of order $e\phi_r$ we approximate these fluctuations by a band of width U_0 where

$$U_0 = \alpha e \phi_r \quad , \tag{6}$$

and α is a constant of order one. Thus, assuming that the conduction band edge lies at the potential energy, the bound donor states have energies with respect to the lowest part of conduction band edge of

$$E(x) = -E_d + U_0 x \quad , \tag{7}$$

where x lies between zero and one. From Eqs. (2) through (6) we obtain

$$(U_0/E_d) = \alpha[(8\pi kT/E_d)(n_t^2 a_0^3/n)]^{\frac{1}{4}} \quad . \tag{8}$$

Now, as n decreases, U_0 increases. However, if U_0 becomes too large, many of the charged donor states will no longer bind an electron because $E > 0$ in Eq. (7). This will self-consistently stabilize the Coulomb fluctuations at $U_0 \sim E_d$. One can obtain quantitative results from this

model by performing the standard calculation[2] for n using Eq. (7) with x taking on all values between zero and one with equal probabilities. The results of this calculation show that if $E_d \gg kT$, the number of conduction electrons will not decrease exponentially as the temperature is lowered but will be proportional to kT. Since this argument does not depend on the density of donors or acceptors, it predicts impurity-induced conduction electrons at low temperatures for any concentration of impurities. Further, n will be proportional to kT and thus the effective E_d measured in Hall measurements would be zero.

At least for small enough concentrations of charged impurities the above scenario does not occur. In our picture we still assume that the original distribution of donors and acceptors is random since at the temperatures at which materials are usually synthesized there are plenty of conduction electrons available to screen the fluctuations. However, as the temperature is lowered and donor states start to fill, they will not be filled at random. Instead they will fill in such a manner as to lower the Coulomb fluctuations and also the energy of the system.

We now consider in more detail a system with a density n_d of shallow donors, a density n_a of charged acceptors, and a compensation ratio,

$$K = n_a/n_d \quad , \tag{9}$$

less than one. Both types of charged impurities are distributed at random. If at low temperatures all of the conduction electrons are frozen out, then there must be n_a unfilled or charged donors and $(K^{-1}-1)n_a$ filled or neutral donors. The large fluctuations discussed earlier are due to the long-range nature of the Coulomb potential and arise from regions of the sample that are not charge neutral. They are in no way due to the divergence of the Coulomb potential at the origin.

In order to understand the length scale of these fluctuations we ask the following question: Given a charged acceptor at the origin, what is the probability P(r) of being able to enclose that acceptor in a charge-neutral sphere of radius r. Besides the acceptor at the origin the sphere may enclose k other acceptors and n donors. Since the number of charged donors must be equal to the number of acceptors, all integral values of n and k with

$$n-1 \geq k \geq 0 \tag{10}$$

are allowed. This is a well defined mathematical problem whose solution will yield some information about how small the Coulomb fluctuations can be made.

The solution to this problem is obtained below and the result is

$$\begin{aligned} P(r) &= 1 - Q(r) \\ Q(r) &= e^{-x} + (2xK^{1/2})e^{-x} \int_0^1 dz\, I_1(2xz\,K^{1/2})\exp(-z^2 x\,K) \quad , \\ x &= (r/r_d)^3 \quad , \end{aligned} \tag{11}$$

where I_1 is the modified Bessel function and r_d is the average distance between donors

$$r_d = (3/4\pi n_d)^{1/3} \quad . \tag{12}$$

Plots of Q(r) for various values of K are given in Figure 1 and, for very large values of r one can easily derive the asymptotic expression

$$\begin{aligned} Q(r) &\approx (K\,16\pi^2 z^2)^{-1/4}\, e^{-z} \quad , \\ z &= (r/r_d)^3(1-K^{1/2})^2 \quad . \end{aligned} \tag{13}$$

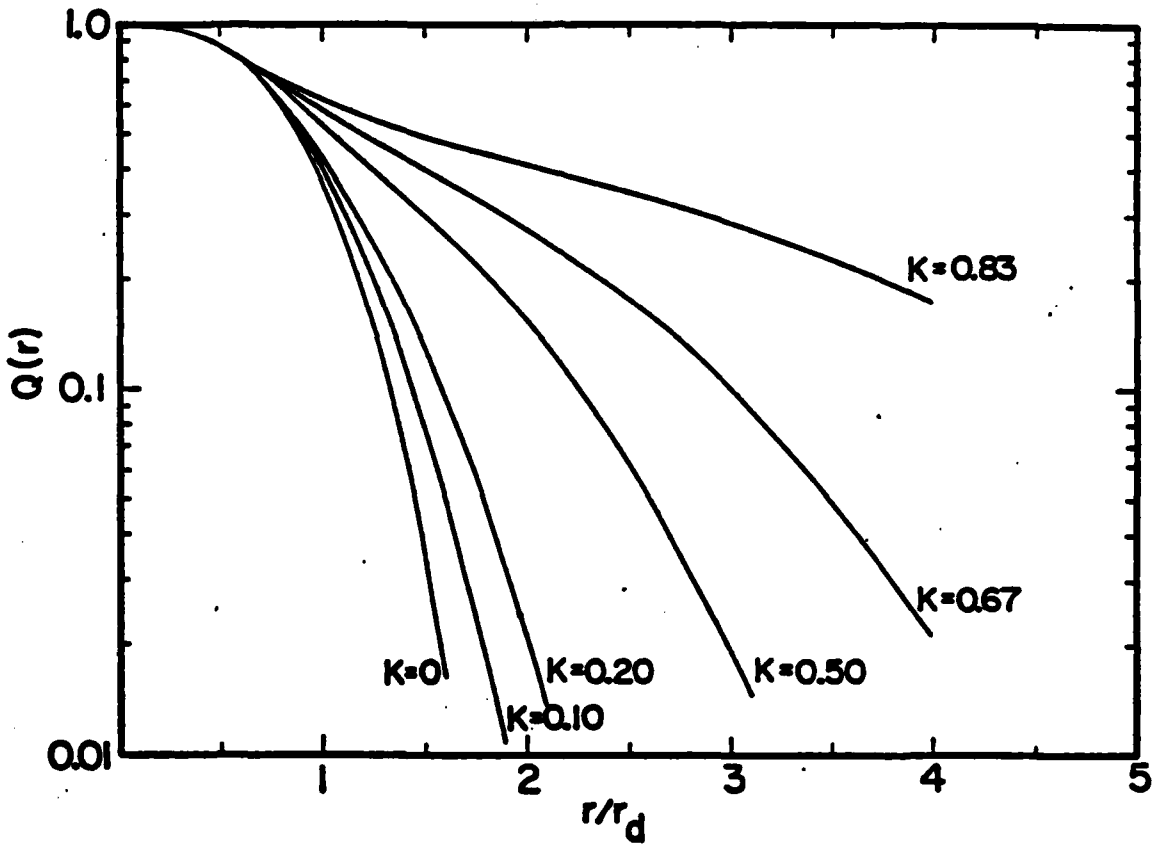

Fig. 1. Q(r), the probability of not being able to enclose an acceptor in a charge neutral volume of radius r, vs. r in units of an average interdonor spacing r_d. Q(r) is plotted for various values of the compensation ratio $K = n_a/n_d$.

For small values of r/r_d or for small values of K, P(r) is dominated by the probability of enclosing a single donor in the volume. However, as K increases, it is increasingly difficult to enclose more donors than acceptors and thus the probability of large positively charged volumes increases.

On one hand the above results are exact and do yield useful information about the distribution of Coulomb potentials. On the other hand they do not give any quantitative measurable properties of the system. Therefore, in order to make quantitative calculations, we assume that at low temperatures each acceptor can be associated with an unfilled or charged donor and that the probability density p(r) that the two are separated by a distance r is related to P(r) by the equation

$$4\pi r^2 p(r) = dP(r)/dr \quad . \tag{14}$$

Further, we assume that a filled donor cannot be closer to an acceptor than the acceptor's partner is because otherwise the acceptor would have paired with the filled donor. Although the actual situation is far more complex than our simple model suggests, our model does correctly reflect the basic physics discussed above.

With this model we can calculate the distribution of potentials in the sample due to the acceptors and charged donors. This is done below. The distribution function itself can only be expressed in terms of several integrals so we have computed the first two moments of the distribution. These results are plotted in Figure 2 in the form

$$\begin{aligned} \langle U\rangle/E_d &= -(U_1/E_d) = -y_a\, f_1(K) \quad , \\ \langle (U-\langle U\rangle)^2\rangle^{1/2}/E_d &= (U_2/E_d) = y_a\, f_2(K) \quad , \end{aligned} \tag{15}$$

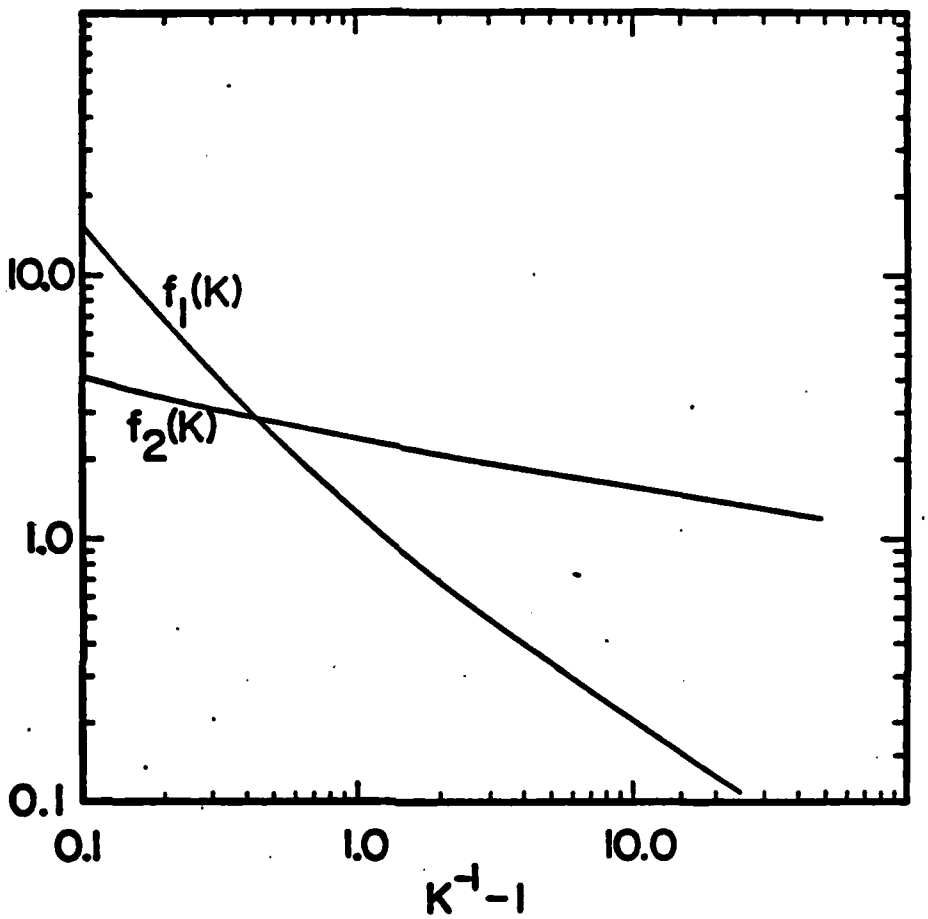

Fig. 2. The quantities $f_1(K)$ and $f_2(K)$ defined by Eqs. (15), describing the average and rms fluctuations of the potential energy of an electron, vs. K.

where the functions f_1 and f_2 are defined below.
Further, U_1 and U_2 are both positive, E_d is given by Eq. (5), y_a is a dimensionless measure of the average spacing between acceptors,

$$y_a = a_o/r_a \quad ,$$
$$r_a = (3/4\pi n_a)^{1/3} \quad , \tag{16}$$

and K is the compensation ratio. The quantity $-U_1$ is the average potential energy of an electron near a filled donor due to charged donors and acceptors and U_2 is the rms potential energy fluctuation about $-U_1$ for the electron. The average potential energy of an electron anywhere in the sample is, of course, zero and the rms fluctuations about this value are $\sqrt{2}\,U_2$. Thus, because of the spatially non-random distribution of charged donors and acceptors, electrons in regions of the sample near filled donors have a lower (more negative) average potential energy with smaller rms fluctuations than electrons at arbitrary positions.

3.2 APPLICATIONS

Based on the ideas and calculations of the previous section we can now present an approximate picture of a low-temperature n-type III-V semiconductor with a low concentration of impurities and compare this picture to experimental observations on GaAs. When discussing shallow donors we shall use effective mass theory and, unless discussing transitions between hydrogenic states, we shall ignore any excited states of the donors. Including other hydrogenic states is not warranted by the accuracy of our model.

As discussed above, the potential energy of an electron due to charged donors and acceptors is zero with an rms fluctuation equal to $\sqrt{2}\,U_2$. Because of these fluctuations the bottom of the conduction band is not a well defined quantity. However, we view it as a spatially varying quantity with minimum value denoted by E_c,

$$E_c = -\sqrt{2}\,\alpha\,U_2 \quad , \tag{17}$$

where α is a constant of order one. Electrons that are bound at donor sites feel an average potential energy of $-U_1$ with an rms fluctuation of U_2. Thus we take the binding energy of these electrons to be

$$E_B(x) = E_d + U_1 + \alpha\, x\, U_2 \tag{18}$$

where x varies between plus and minus one and E_d is the effective mass binding energy. Therefore the binding energy of an electron with respect to the minimum of the conduction band is given by E(x) where

$$E(x) = E_d + U_1 + \alpha U_2(-\sqrt{2} + x) \quad , \quad -1 \leq x \leq 1 \quad . \tag{19}$$

That is, the energy of a bound electron is an amount E(x) below the minimum of the conduction band.

Thus we predict a spread or distribution of donor binding energies with

$$E_{max} = E_d + U_1 - (\sqrt{2} - 1)\alpha U_2$$
$$E_{av} = E_d + U_1 - \sqrt{2}\,\alpha\, U_2 \qquad (20)$$
$$E_{min} = E_d + U_1 - (\sqrt{2} + 1)\alpha U_2$$

where E_{max}, E_{av}, and E_{min} are the maximum, average, and minimum binding energies respectively. At temperatures such that U_2 is of order kT but not much less than kT we would expect E_{av} to control the temperature dependence of n in a Hall measurement. For $U_2 >> kT$ we would expect E_{min} to be the controlling factor assuming that $E_{min} > 0$. If $E_{min} < 0$ the whole picture breaks down although there may be a temperature range where the analysis is partly valid.

Of course the potential energy distribution of electrons averaged over the whole crystal or averaged over regions near filled donors does not cut off sharply in our model. The cut-off at energies of order the rms fluctuation is taken as a convenience. Since the distribution of potential energy involves simplifying assumptions anyway, we feel little is lost by taking this convenience. However we note that our distribution predicts an exponentially small probability for large potential energies and we believe that the exact distribution would also have this property. This means that a few electrons could never be bound to donors although they could be trapped in regions of very small potential energy. We shall not pursue this fact in the remainder of this report.

We now consider a qualitative and quantitative comparison of our theory with some experimental observations on GaAs. First we consider the dependence of the donor binding energy observed in Hall measurements on the concentrations of donor and acceptors. Table I contains values of impurity concentrations, observed donor binding energies, and computed values of K, U_1, and U_2 for various samples of high-purity GaAs. According to Eq. (20) and the ensuing discussion the observed donor binding energy, E_{do}, should be E_{av} which is related to U_1, U_2, and the effective mass donor binding energy, E_d by the equation

$$[E_d + U_1 - E_{do})/E_d = \sqrt{2}\ \alpha\ U_2/E_d \quad . \tag{21}$$

In order to check this and to determine the parameter α discussed above we have plotted $(E_d + U_1 - E_{do})/E_d$ vs U_2/E_d in Figure 3 using the values in Table I and $E_d = 5.8$ meV.

The experimental points fall on a remarkably straight line with a slope corresponding to a value for α of 1.26. The fact that a line through the points does not pass through the origin indicates a value for E_d of 6.6 meV. This is somewhat higher than the 5.8 meV effective mass energy and the difference is larger than any expected central cell correction. However, in view of the straight line fit, this discrepancy appears to be independent of charged impurities. Since U_1, which is not an adjustable parameter, varies between 20% and 50% of $E_d - E_{do}$, we regard the excellent fit as evidence that our model has a reasonable quantitative validity.

Table I

The quantities n_a, n_d, E_{do}, and K are the observed acceptor concentrations, donor concentrations, observed donor binding energies, and compensation ratios. The quantities U_1/E_d and U_2/E_d were computed using Eqs. (15).

Ref.	$n_a \times 10^{-12}$ cm^3	$n_d \times 10^{-12}$ cm^3	E_{do} in meV	K	U_1/E_d	U_2/E_d
a	21.3	48.0	5.52	0.44	0.046	0.103
a	40.7	204	5.09	0.20	0.022	0.103
a	136	502	4.51	0.27	0.045	0.166
a	327	1060	3.88	0.31	0.069	0.230
b	200	860	4.3	0.23	0.043	0.182
b	390	490	4.2	0.80	0.641	0.414
b	350	610	3.8	0.57	0.192	0.293
c	37.6	72.5	5.30	0.52	0.190	0.132
c	104	489	4.59	0.21	0.031	0.143

a) G. E. Stillman, C. M. Wolfe, and J. O. Dimmock, Proc. 3rd Int. Conf. Photocond., Stanford, 1969, p. 265, Pergamon, Oxford, 1971.

b) Ref. 11.

c) G. E. Stillman and C. M. Wolfe, private communication.

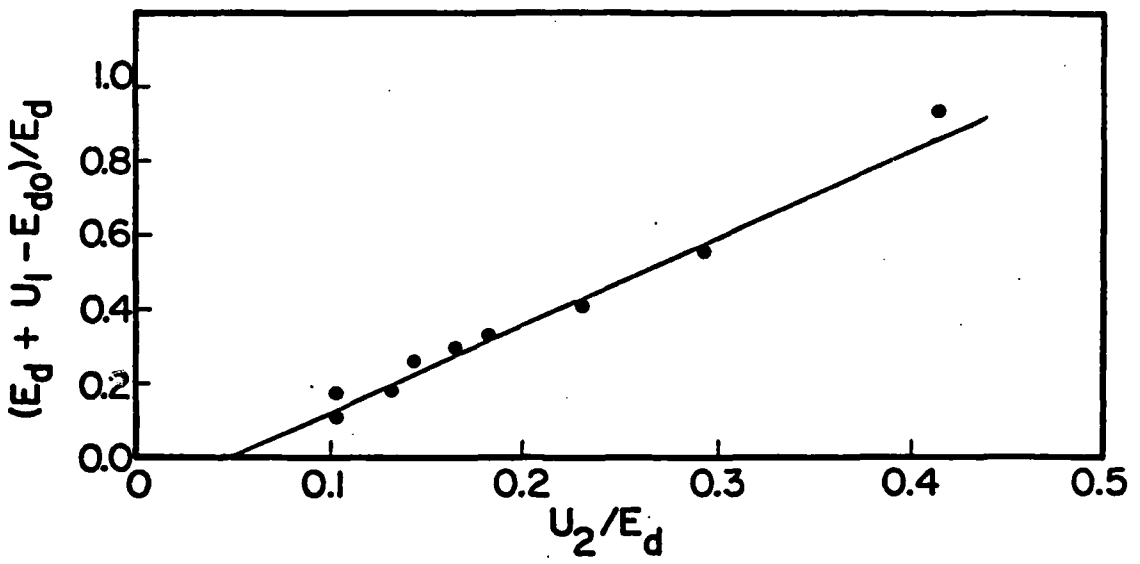

Fig. 3. Plot of $(E_d + U_1 - E_{do})/E_d$ vs U_2/E_d for the samples in Table I.

In photoconductivity experiments on high-purity GaAs at low temperatures one observes a very sharp 1s-2p transition whose magnetic field dependence is in excellent agreement with effective mass theory with no corrections for fluctuations.[9] On the other hand, the 1s-conduction band edge is either non-existent or very diffuse. Photoconduction from the 1s-2p transition is believed to be thermally activated from the 2p level to the conduction band. However, the activation energy of the strength of the transition is less than either $E_{do}/4$ or $E_d/4$ as would be expected from effective mass theory.[10]

Our picture is in agreement with all of these observations. Since the Coulomb fluctuations take place on a length scale much greater than a_o, they will have little effect on the low lying hydrogenic states and thus E_{1s}-E_{2p} will be little affected as is observed.[8] However, the conduction band edge is spatially varying on a length much greater than a_o and thus the 1s-conduction band transition will have a spread of order $2\alpha U_2$ which will smear it considerably as is observed. For the first sample in Table I, $2\alpha U_2$ is 1.5 meV. This is quite close to the observed smearing for this sample.[11] Further, the 2p-conduction band energy gap will be given by Eqs. (19) and (20) with E_d replaced by $E_d/4$. Using the same analysis as that leading up to Eq. (21) we obtain

$$E_{av}(2s) = (E_d/4) + U_1 - \sqrt{2}\,\alpha U_2 \quad . \tag{22}$$

For the first sample in Table I this yields an activation energy of 0.65 meV which is reasonably close to the measured value[10] of 0.47 meV and much closer than the effective mass value of 1.45 meV.

Next, we examine what we consider a most puzzling and most underrated piece of evidence obtained from high-purity GaAs at low temperatures. It is apparently widely believed that the Holtzmark

distribution describing the distribution of electric fields from a random distribution of charged impurities explains the lineshapes observed in photoconductivity experiments. However, in the few careful comparisons between theory and experiment it has been noted that while the lineshape predicted by the theory is fairly good, the number density of charged impurities necessary for quantitative agreement is considerably smaller than that obtained from transport measurements.[7,8] This is particularly disturbing since the observed line is narrower than the predicted line and thus additional broadening mechanisms cannot be invoked to explain the discrepancy.

Our picture provides a qualitative and even a semiquantitative explanation of this behavior. Although the charged acceptors do constitute a random distribution, the charged donors do not because they are more likely to lie near an acceptor than one would deduce from a random distribution. Further, the filled donors, which photoconductivity experiments sample, are not randomly placed either but are likely to be further from an acceptor than one would deduce from a random distribution. Both of these effects tend to decrease the electric fields at filled donor sites. Preliminary calculations on the distribution of electric fields have been performed with the following results. As K approaches one, the distribution of electric fields is exactly a Holtzmark distribution with the effective number of impurities reduced by a factor of four. For values of K nearly one the distribution of electric fields is nearly Holtzmark with the effective number of impurities reduced by somewhat more than four.

Of course for small values of K the distribution of electric fields will more closely resemble a distribution from dipoles with a density n_a and a dipole moment of $r_d = K^{1/3} r_a$. We consider these

lineshape effects to be the strongest evidence in support of our picture because they most clearly depend on the non-randomness of the distribution of charges.

Finally, we briefly consider the mobility of samples where $E_d >> kT$ but at temperatures high enough so that hopping conduction can be ignored. At temperature $kT \sim U_2$ and below, the fluctuations in the Coulomb potential should constitute a significant scattering mechanism for the conduction electrons that is not included in the potential scattering due to charged impurities. In fact when kT is considerably less than U_2 there must be significant volumes of the sample that are virtually inaccessible to the electrons. Since U_2 depends on K for fixed n_a, this mechanism should be more pronounced as K approaches one. In fact this sort of behavior is observed, for example, with sample P128(b) and P121(a) of ref. 11 which have almost identical values of n_a. However, the above argument only indicates that our theory has the correct trend. Actual calculations on this effect would be very useful.

3.3 PROBABILITIES

In this section we sketch the solution to the following mathematical problem. We are given a lattice with probabilities c_1 and c_2 of having particles of type 1 (donors) and type 2 (acceptors) respectively on a given site where

$$c_2 < c_1 \ll 1 \quad . \tag{23}$$

We wish to find Q(N), the probability that a volume of N lattice sites does not contain more particles of type 1 than of type 2. Thus,

$$Q(N) = \sum_{m_1=0}^{N} \sum_{m_2=m_1}^{N} \binom{N}{m_1}\binom{N}{m_2} c_1^{m_1}(1-c_1)^{N-m_1}\, c_2^{m_2}(1-c_2)^{N-m_2} \tag{24}$$

$$\binom{N}{m} = \frac{N!}{m!(N-m)!} \quad .$$

The summation over m_2 can be expressed in terms of the incomplete beta function yielding

$$Q(N) = \sum_{m=0}^{N} Q_m(N) \quad ,$$

$$Q_0(N) = (1-c_1)^N \quad , \tag{25}$$

$$Q_m(n) = c_1^m(1-c_1)^{N-m} \binom{N}{m}^2 \int_0^{c_2} t^{m-1}(1-t)^{N-m}\, dt \quad ,$$

$$m \geq 1 \quad .$$

The summation over m can be performed exactly by constructing the sum

$$[(1+xe^{i\theta})(1+xe^{-i\theta})]^N = \sum_{m_1=0}^{N} \sum_{m_2=0}^{N} \binom{N}{m_1}\binom{N}{m_2} x^{m_1+m_2}\, e^{i\theta(m_1-m_2)} \quad , \tag{26}$$

integrating θ from 0 to 2π, and taking a derivative to obtain

$$\frac{x}{4\pi}\frac{d}{dx}\int_0^{2\pi} d\theta[1+x^2+2x\cos\theta]^N = \sum_{m=1}^{\infty}\left(\frac{N}{m}\right)^2 m\,x^{2m} \quad . \tag{27}$$

Thus we can write

$$Q(N) = (1-c_1)^N + \int_0^{c_2} dt \int_0^{2\pi} \frac{d\theta}{4\pi} \frac{(1-c_1)^N(1-t)^N}{t}$$

$$x\,\frac{d}{dx}[1+x^2+2x\cos\theta]^N \quad , \tag{28}$$

$$x = (c_1 t/(1-c_1)(1-t))^{1/2} \quad .$$

Since c_1 and c_2 are much less than one we can expand

$$[1+x^2+2x\cos\theta]^N = \exp(N\ln(1+x^2+2x\cos\theta)) \cong \exp(2Nx\cos\theta) \quad , \tag{29}$$

the expansion being valid if $x^2N \ll 1$. One can easily check that values of N violating this restriction would constitute 10^{14} atoms for concentrations of impurities of order 10^{15} cm^{-3}. For N this large Q(N) is ridiculously small. Further, by similar arguments,

$$(1-c)^N \cong \exp(-Nc) \quad ,$$
$$(1-t)^N \cong \exp(-Nt) \quad ,$$
$$x \cong (c_1 t)^{1/2} \quad . \tag{30}$$

When Eqs. (28) through (30) are combined, the θ integration can be expressed exactly in terms of a Bessel function of imaginary argument and one obtains

$$Q(N) = e^{-Nc_1}\left[1+\int_0^{c_2}\frac{dt}{t}\,e^{-tN}(C_1 t)^{1/2}\,N\,I_1[2(C_1 t)^{1/2}N]\right] \quad . \tag{31}$$

Equation (11) can be obtained by a simple change of variables and by noting that

$$(Nc_1) = (r/r_d)^3 \tag{32}$$

for a sphere of radius r containing N lattice points.

3.4 DISTRIBUTION FUNCTION

In this section we derive the distribution function and first two moments for the Coulomb potential of an electron due to the non-random distributions of charged donors and acceptors. We consider a random distribution of a small concentration of acceptors where $U_a(\vec{r})$ is the potential energy of an electron at the origin due to an acceptor at $\vec{r}$. Further, for each acceptor; there is a donor with a probability density $p(\vec{r})$ that the donor is at a position $\vec{r}$ away from the acceptor. The contribution to the potential energy of an electron at the origin from a donor at $\vec{r}$ is $U_d(\vec{r})$. By a straightforward generalization of a method used earlier,[13] one can easily obtain F(U)dU, the probability that an electron at the origin has a potential energy between U and U + dU.

$$F(U) = \int_{-\infty}^{\infty} \frac{dt}{2\pi} e^{iUt} e^{-I(t)} \quad ,$$

$$I(t) = n_a \int d^3r\, d^3r'\, p(\vec{r}-\vec{r}')\{1 - \exp[it(U_a(\vec{r}) + U_d(\vec{r}'))]\} \quad , \qquad (33)$$

where n_a is the density of acceptors.

In this case,

$$U_a(\vec{r}) = -U_d(\vec{r}) = e^2/\varepsilon_0 r \quad . \qquad (34)$$

For an electron at an arbitrary position Eqs. (33) are correct as they stand. However, for an electron bound (or near to) a filled donor, the acceptor must be closer to its paired donor than to the filled donor and thus there is a restriction on the $\vec{r}$ and $\vec{r}'$ integrations such that

$$|\vec{r}| > |\vec{r} - \vec{r}'| \quad . \qquad (35)$$

The moments of the distribution can be obtained by expanding I(t) in a power series to obtain

$$M_k = n_a(e^2/\varepsilon_o)^k \int d^3r\, d^3r'\, p(\vec{r}')(r^{-k} - |\vec{r} - \vec{r}'|^{-k}) \quad , \quad r > r' \; . \tag{36}$$

For k = 1,2, one of the integrals in (36) can easily be performed yielding

$$M_1 = -(2\pi n_a e^2/3\varepsilon_o)J_2 = \langle U \rangle$$

$$M_2 = (2n_a \pi e^4/\varepsilon_o^2)J_1 = \langle (U - \langle U \rangle)^2 \rangle$$

$$J_k = \int d^3r\, r^k\, p(\vec{r}) \quad . \tag{37}$$

By using Eq. (14), integrating by parts once, and changing variables from r to $N = 4\pi\rho r^3/3$ where ρ is the density of lattice points we obtain

$$J_k = (3/4\pi\rho)^{k/3}\,(k/3)\int_0^\infty N^{(k-3)/3} Q(N)\,dN \tag{38}$$

where Q(N) is in Section 3.3. By using Eq. (31) for Q(N), the N integral is a tabulated Laplace transform of a Bessel function and we obtain

$$J_k = (3/4\pi\rho)^{k/3}(k/3)\left[\Gamma(k/3)c_1^{-k/3} + \Gamma(2+k/3)\sqrt{c_1 c_2}\int_0^1 dx\right. -$$

$$\left. x^{-1/2}(c_1 - c_2 x)^{-1-k/3}\; P_{k/3}^{-1}((c_1 + c_2 x)/(c_1 - c_2 x))\right] \quad , \tag{39}$$

where c_1 and c_2 are defined in Section 3.3, $\Gamma(z)$ is the gamma function, and $P_{k/3}^{-1}$ is the Legendre function. By combining Eqs. (39) with Eqs. (37) and making another change of variables one obtains Eqs. (15) with

$$f_1(K) = (2K^{2/3}/3)\Gamma(2/3)[1 + (10/9)L_2(K)]$$

$$(f_2(k))^2 = (2K^{1/3})\Gamma(1/3)[1 + (4/9)L_1(K)]$$

$$L_k(K) = \int_0^{K/1-K} (x+1)^{(k-3)/3}\; F(-k/3, 1+k/3; 2, -x)\,dx \tag{40}$$

where F(a,b;c,z) is the hypergeometric function. The integral is performed numerically to obtain Figure 2.

3.5 REFERENCES

1. B. I. Shklovskiĭ and A. L. Éfros, Zh. Eksp. Teor. Fiz. 60, 867 (1971) [Sov. Phys. -JETP 33, 468 (1971).
2. See, for example, J. S. Blakemore, Semiconductor Statistics, (Pergamon Press, Oxford, 1962).
3. N. F. Mott and E. A. Davis, Electronic Processes in Non-Crystalline Materials, (Clarendon Press, Oxford, 1971).
4. C. M. Wolfe, G. E. Stillman in Gallium Arsenide and Related Compounds (Proc. 3rd Int. Symp., Aachen, 1970) Inst. Phys. and Phys. Soc., London, 1971,
5. G. E. Stillman, C. M. Wolfe, and O. J. Dimmock, in Far Infrared Photoconductivity in High Purity GaAs in Semiconductors and Semimetals, Vol. 12, Academic Press, New York, 1977.
6. G. E. Stillman, C. M. Wolfe, and D. M. Korn, in 11th Conf. Phys. Semicond. Warsaw, Poland, 1972, p. 863. Polish Sci. Publ., Warsaw, 1973.
7. D. M. Korn and David M. Larsen, Solid State Commun, 13, 807 (1973).
8. David M. Larsen, Phys. Rev. B 13, 1681 (1976).
9. G. E. Stillman, David M. Larsen, C. M. Wolfe, and R. C. Brandt, Solid State Commun. 9, 2245 (1975).
10. G. E. Stillman, C. M. Wolfe, and O. J. Dimmock, in Far Infrared Photoconductivity in High Purity GaAs in Semiconductors and Semimetals, Vol. 12, Academic Press, New York, 1977, p. 226.
11. G. E. Stillman, C. M. Wolfe, and J. O. Dimmock, Proc. 3rd Int. Conf. Photocond., Stanford, 1969, p. 265, Pergamon, Oxford, 1971.
12. J. Whitaker and D. E. Bolger, Solid State Commun. 4, 181 (1966).
13. P. A. Fedders, Phys. Rev. B 11, 1020 (1975).

4. PIEZOELECTRIC STRAIN SCATTERING FROM NEUTRAL IMPURITIES

It is well known that static strains in piezoelectric materials give rise to an electric field or an electric potential. Thus in piezoelectric semiconductors, such as III-V compounds, static strains can have an effect on the electrical properties of the materials. In this report we discuss some of these electrical effects that are due to a distribution of strains generated by a random distribution of point defects.

More particularly, we calculate the mobility due to a concentration of charge neutral defects that each produce a given strain field. The electric potential due to a strain producing point defect in a piezoelectric crystal is quite similar to the potential due to a point dipole and both will produce a mobility that is proportional to $T^{\frac{1}{2}}$ in the effective mass approximation. Except for scattering by ionized impurities, this is the only mechanism that produces a mobility that decreases as the temperature decreases. Crude estimates of the strain field associated with a single defect are estimated from linewidth measurements on a Si sample with known concentrations of specific impurities. These estimates indicate that the piezoelectric static strain scattering mechanism may contribute significantly to the mobility of electrically rather pure semiconductors below room temperature when neutral impurity concentrations are greater than 10^{18} cm^{-3}. Further, it could be a dominant mechanism in determining the mobility of III-V semiconducting alloys in some regimes. Other electrical effects, such as donor lineshapes as measured in photoconductivity experiments, are also qualitatively discussed.

4.1 POINT DEFECT MODEL

According to elastic continuum theory[1] a defect will produce a lattice displacement proportional to r^{-2} and a strain field proportional to r^{-3} at distances r that are large compared to the size of the defect. In this paper we shall make use of a "model defect" defined so that $\vec{u}(\vec{r})$, the displacement of a material point at $\vec{r}$ due to a defect at the origin, is given by the equation

$$u(\vec{r}) = b^3\vec{r}/r^3 \quad , \tag{1}$$

where b has the units of length. This gives rise to a strain field

$$u_{ij}(\vec{r}) = \frac{1}{2}\left[(\partial u_i/\partial r_j) + (\partial u_j/\partial r_i)\right] = (r^2\delta_{ij} - 3r_i r_j)b^3/r^5 \quad . \tag{2}$$

Several cautionary and explanatory remarks are appropriate at this point. The model defect described by Eq. (1) is a fairly common model[2] because it is rather easy to manipulate analytically and it does, of course, possess the correct long range behavior which determines the dominant features of our results. However Eq. (1) is not to be taken very seriously at distances within a few atomic spacings of the defect. In fact the displacement near the defect is a very difficult problem that is largely irrelevant to the present problem because the behavior of u_{ij} at distances of a few atomic spacings will not contribute to any

expressions in this report. Further, although Eq. (1) implies a dilatation or volume change of order b^3, this is incidental to this report. The piezoelectric coupling in III-V semiconductors occurs only through the shear strain components u_{ij} $(i \neq j)$ which describes a trigonal shape change of a material element and not a volume change. An appreciable shear strain in a crystal may or may not be accompanied by any volume change. Thus, while one expects b to be related to the dimensions of a defect, it cannot be related to a volume change or a nearest neighbor displacement. In this report b will be estimated by examining experimental determinations of strain fields in samples with known defect concentrations. We also note that Eq. (1) describes a spherically symmetric displacement. This is almost surely not the case in any real material. Even in an isotropic continuum no finite number of force pairs will produce a spherically symmetric displacement and the situation is worse in a nonisotropic material. In general

$$u_{ij}(\vec{r}) = f_{ij}(\Omega)/r^3 \tag{3}$$

where $f_{ij}(\Omega)$ is a very complicated function of angles. Thus, any detailed angular dependence predicted by our model strain cannot be viewed as reliable.

4.2 DERIVATIONS

In this section we derive expressions for the quantities used in the rest of this report. First we obtain an expression for the electric potential, Φ, due to the model defect described by Eq. (1). We use the notation and basic equations from ref. (3) which includes cgs units and the summation equation for repeated indices. In the presence of a strain field (and to first order in the strains) the equation[3] connecting the electric and displacement fields is

$$D_i = \varepsilon_o E_i - 4\pi e_{i,jk} u_{jk} \quad , \tag{4}$$

where we assume an isotropic dielectric constant ε_o. For the cubic sphalerite structure the only non-zero element of the piezoelectric coupling constant $e_{i,jk}$ is e_{14} if i, j, and k are all distinct and is zero otherwise. The quantity e_{14} has the units of charge/length^2. The equations $\vec{\nabla}\cdot\vec{D} = 0$ and $\vec{E} = -\vec{\nabla}\Phi$ together with Eq. (4) yield

$$\nabla^2\Phi(\vec{r}) = -4\pi\rho(\vec{r}) \tag{5}$$

where ρ is an effective charge density,

$$\rho(\vec{r}) = (\partial/\partial x_i)(e_{i,jk} u_{jk}(\vec{r})/\varepsilon_o) \quad . \tag{6}$$

Using Eq. (2) for our model defect yields

$$\rho(\vec{r}) = (90b^3 e_{14}/\varepsilon_o)(xyz/r^7) \quad , \tag{7}$$

where spatial directions refer to the crystalline axes.

Equations (5) and (7) can be solved in a variety of different ways and we have found Fourier transforming the equations to be most convenient. Thus all functions $f(\vec{r})$ have a Fourier transform

$$f(\vec{k}) = \int d^3r f(r) e^{-i\vec{k}\cdot\vec{r}} \quad ,$$

$$f(\vec{r}) = \int \frac{d^3k}{(2\pi)^3} f(\vec{k}) e^{i\vec{k}\cdot\vec{r}} \quad , \tag{8}$$

and Eq. (5) can be written as

$$k^2\phi(\vec{k}) = 4\pi\rho(\vec{k}) \quad . \tag{5'}$$

By using standard methods one can easily find that

$$\phi(\vec{k}) = (96\pi^2 i e_{14} b^3/\epsilon_o)(k_x k_y k_z/k^4) \quad ,$$

$$\phi(\vec{r}) = (36\pi b^3 e_{14}/\epsilon_o)(xyz/r^5) \quad . \tag{9}$$

The effects of Debye screening can also easily be included and the results are

$$\phi(\vec{k}) = (96\pi^2 i e_{14} b^3/\epsilon_o)(k_x k_y k_z/(k^2(k^2 + k_s^2)))$$

$$\phi(\vec{r}) = (-24\pi e_{14} b^3/\partial_o)(\partial/\partial x)(\partial/\partial y)(\partial/\partial z)(r_D^2/r)(1 - \exp(-r/r_D)), \tag{9s}$$

where r_D is the Debye screening length and $k_s = 1/r_D$. Thus, $\phi(\vec{r})$ is proportional to r^{-2} if $r << r_D$ and proportional to r^{-4} if $r >> r_D$.

Given the electrical potential, the calculation for the elastic scattering relaxation rate and thus the mobility is perfectly straightforward, at least in the Born approximation. The calculation is virtually identical to the one described by Rode[4] for ionized impurities except that the Coulomb potential is replaced by the piezoelectric strain field potential and only one point needs further clarification. Where the $|\Phi(\vec{k})|^2$ enters the calculation we replace it by its angular average analogue $|\bar{\Phi}(k)|^2$ where

$$|\bar{\Phi}(k)|^2 = \langle|\Phi(\vec{k})|^2\rangle = (3.2^{10}\pi^4/35)(e_{14}b^3/\varepsilon_o)^2/k^2 \quad . \tag{10}$$

for the unscreened version. This simplifying approximation is well within the spirit of neglecting any detailed angular dependence discussed above. The relaxation rate in the effective mass approximation is

$$\nu = (3\cdot 2^9\cdot\pi^3/5\cdot 7)(e\, e_{14}\, b^3/\varepsilon_o)^2\, m^*n/\hbar^3k \quad . \tag{11}$$

If this is the only scattering mechanism under consideration then the mobility is easily calculated to be

$$\mu = (5\cdot 7/2^6\cdot\pi^3\cdot 3^2)(\varepsilon_o\hbar/em^*\, e_{14}b^3)^2(e/n)(2m^*kT/\pi)^{\frac{1}{2}} \tag{12}$$

and the Hall factor r_H is

$$r_H = \Gamma(7/2)\Gamma(5/2)/\Gamma^2(3) \approx 1.10 \quad . \tag{13}$$

Equations (11) through (13) were obtained by ignoring screening. The effects of screening can easily be added, if necessary, by starting with Eq. (9s) for $\Phi(\vec{k})$ instead of Eq. (9).

In order to make contact with other effects from the strains we consider the distribution of strains due to a random distribution of model defects. In the limit where the number of defects is a small fraction of the number of lattice sites the calculation is straightforward.[5] If p(e)de is the probability that the strain at a given point is between e and e + de then

$$p(e) = (e_o/\pi)[e^2 + e_o^2]^{-1} \quad ,$$

$$e_o = (4\pi/3)nb^3 \quad , \qquad \text{for } e = u_{xy}$$

$$e_o = (8\pi^2/9\sqrt{3})nb^3 \quad , \qquad \text{for } e = u_{xx} \quad . \tag{14}$$

Finally we note that if there are concentrations n_i of several impurities with associated values of b_i then

$$e_o \sim \Sigma_i n_i b_i^3 \quad ,$$

$$\nu \sim \mu^{-1} \sim \Sigma_i n_i b_i^6 \quad . \tag{15}$$

These equations can also include the effects of more extended defects such as complexes or dislocation loops in which b^3 is roughly proportional to the volume of the loop. At distances far from the defect the same r dependence will be obtained[1] and thus the k dependence of ν and the T dependence of μ will remain the same.

4.3 EXPERIMENTAL COMPARISONS

One major result of Sec.4.2 is that the strains generated by point defects in a piezoelectric semiconductor produce a mobility that is proportional to $T^{-\frac{1}{2}}$ and a Hall factor of $r_H = 1.10$. These are the same as would have been produced by a distribution of point dipoles. Except for scattering by ionized impurities, these are the only mechanisms that we know of that decrease the mobility as the temperature decreases.

The obvious question is whether the strength of the static strain piezoelectric scattering mechanism is large enough to cause a measurable effect in mobilities. Concentrations of neutral defects of order 10^{18} cm^{-3} are common in almost all materials. Further EPR, infrared, and optical measurements on defects in many materials yield splittings or inhomogeneous line broadening of about 1 cm^{-1}. Since splittings are typically of order 10^4 cm^{-1} per unit strain, this implies typical random strains of order 10^{-4}. Measurements of neutral impurity concentrations in well characterized III-V semiconductors are rare. There are, however, reports that concentrations of order 10^{18} cm^{-3} are quite common even in electrically rather pure GaAs.[6] However, we know of no quantitative analysis of strains in any III-V semiconductors. There is one quantitative determination of the strains due to oxygen impurities in Czochralski grown silicon that was obtained by their effect on the resonance lineshape of deep In acceptors. Mozurkewich,[7] using a backward wave phonon spectroscopy technique, measured linewidths corresponding to strains of about 0.5×10^{-4} in a sample with an oxygen content of 0.5×10^{18} cm^{-3}. Using Eq. (14) this implies a value of $b^3 \sim 0.3 \times 10^{-22}$ cm^{-3}.

From these numbers we estimate that $n = 10^{18}$ cm^{-3} and $b^3 = 0.3 \times 10^{-22}$ cm^{-3} are at least not unreasonable. For GaAs with $\epsilon_o = 12.5$, $e_{14} = 4.7 \times 10^4$ esu/cm^2, and $m^* = 0.0665$ m, this yields a mobility of 1.5×10^5 cm^2/V sec at a temperature T = 20°K. This is lower than the mobility of good samples whose mobilities are published. However, our numerical estimates for b^3 are uncertain to at least an order of magnitude which will lead to a change in the mobility of a factor of one hundred. We feel that our estimates are certainly no better than that but that they do show that the mechanism is worth considering.

We have included the possibility of static strain piezoelectric scattering in analyzing the mobility of one well studied very good sample of GaAs. Using reasonable parameters the fit could be made slightly better than without the mechanism. However, the fit could also be improved by changing the number of donors and acceptors by about 10% and thus we regard this attempt as inconclusive. Unfortunately, there is probably a tendency for data on well characterized samples with only the highest mobilities to reach the literature and these samples are the worst candidates for the effect.

One might expect strain effects to be more important in III-V semiconducting alloys than in the pure materials. Our analysis, of course, is valid only for rather dilute alloys although we expect the qualitative features to be present at all concentrations. We would also expect much smaller values for b^3 in alloys than for many impurities in purer substances. There have been a number of mobility measurements on $Ga_{1-x}Al_xAs$ at temperatures low enough so that static strain piezoelectric scattering might be detectable.[8-10] That is, at low enough temperatures the various lattice scattering mechanisms[4] should have become quite ineffective leaving

only scattering by charged impurities, alloy scattering, and possibly static strain piezoelectric scattering. One expects a $T^{-\frac{1}{2}}$ temperature dependence in the mobility for what is usually called alloy scattering. Although the $T^{-\frac{1}{2}}$ really obtains from a weak scattering limit, it is difficult to see how scattering from short range fluctuations due to alloying could lead to a mobility that decreases as the temperature does. That is, as the temperature is decreased the conduction electron's average momentum is lowered and these electrons are less affected by spatially small potential variations.

GaAs and AlAs have almost identical lattice parameters and thus one might expect rather small effects for $Ga_{1-x}Al_xAs$. However, most mobility measurements do exhibit a low temperature regime where the mobility decreases with decreasing temperature and with increasing alloy concentration x. This is usually interpreted as an increasing number of donors and acceptors as x increases even though n (the number of conduction electrons at 77°K or at room temperature) is not correlated with the composition. We suggest that at least part of the decrease in mobility with decreasing temperature and increasing x may be due to static strain piezoelectric scattering. In order to conclusively verify this, independent determinations of N_A and N_D would have to be made.

We have crudely analyzed some of the mobility data of Chandra and Eastman[10] in order to see if static strain piezoelectric scattering could be a dominant mechanism. The analysis was limited to temperatures between 25°K and 45°K so that lattice scattering mechanisms could be safely ignored. Assuming that inverse mobilities add and that the number of charged impurities was largely independent of x, one can obtain concentration or x dependent mobilities by subtracting inverse mobilities of different samples.

This was done with the higher concentration sample pairs (F14,F16), (F14,F18), (F16,F18) and (F15,F19). The results yielded mobilities that varied by less than 5% over the temperature range. Either a $T^{\frac{1}{2}}$ or $T^{-\frac{1}{2}}$ temperature dependence would have given a mobility that varied by more than 30% over this range although the right combination of $T^{\frac{1}{2}}$ and $T^{-\frac{1}{2}}$ would be consistent with our analysis. Further, all pairs gave a μ^{-1} that was roughly proportional to x with a value of b^3 about one hundred times smaller than discussed earlier. We regard this analysis as suggestive but certainly not conclusive.

Finally we wish to make a few qualitative comments on the effect of strain produced electrostatic potentials on the donor lineshapes measured in photoconductivity experiments. First we note that the 1s-2p-lineshapes measured in alloys are much broader and more symmetric than in pure compounds. The typical narrow asymmetric line obtains because the electric field from impurities separated by distances much greater than a Bohr radius contribute only to second order in the 1s-2p energy difference. This will not be true for the electric potential due to strain centers that are separated by distances small compared to the Bohr radius. Secondly we note that different donors are characterized by different linewidths (or even lineshapes) in pure III-V semiconductors. A possible explanation of this is a strain generated potential from the donor defect itself contributes to the lineshape. These ideas are presently being pursued quantitatively.

4.4 REFERENCES

1. L. D. Landau and E. M. Lifshitz, Theory of Elasticity (Pergamon Press, London, 1959).
2. C. P. Flynn, Point Defects and Diffusion (Clarendon Press, Oxford, 1972), Chap. 3.
3. L. D. Landau and E. M. Lifshitz, Electrodynamics of Continuous Media (Pergamon Press, London, 1960), Chap. II.
4. D. L. Rode in Semiconductors and Semimetals, edited by R. K. Willardson and Albert C. Beer (Academic Press, New York, 1975), Vol. 10, Chap. 1.
5. See, for instance, P. A. Fedders, Phys. Rev. B 11, 1020 (1975).
6. C. W. Wolfe, G. E. Stillman, and E. B. Owens, J. Electrochem. Soc. 117, 129 (1970).
7. George Mozurkewich, Ph.D. Thesis, Washington University, 1981 (unpublished).
8. G. B. Stringfellow, J. App. Phys. 50, 4178 (1979).
9. K. Kaneko, M. Ayabe, and N. Watanabe, Int. Phys. Conf. Ser. 33a, 216 (1977).
10. A. Chandra and L. F. Eastman, J. App. Phys. 51, 2669 (1980); J. Electrochem. Soc. 127, 211 (1980).

5. Cr COMPLEXES AND BULK REDISTRIBUTION DURING DIFFUSION AND ANNEALING

Cr-doped GaAs has been studied for some 20 years. The experimental data that have been generated over this period fall mainly into three categories: spectroscopic results, electrical properties, and redistribution phenomena. Many properties of the GaAs:Cr system are still not well understood. In this report we present a model consistent with a wide spectrum of experimental data from the three classes.

We start by reviewing indications of Cr interacting with other defects in GaAs, and evidence of the existence of highly mobile interstitial Cr donors. We can then give a unifying picture of the effect of implantation on Cr, and reinterpret the compensation and redistribution mechanisms of Cr in GaAs.

5.1 DEFECT INTERACTIONS

It is becoming increasingly clear that one cannot in general model Cr independently from other defects that are present. We will therefore start with a short survey of experimental data indicating defect interaction with Cr.

White [1a] has assigned excitonic recombination at an isoelectronic Cr-complex $(Cr_{Ga}D_{As})^{o}$ as the cause of the observed 0.84-eV photoluminescence line earlier attributed to an internal Cr transition ^{5}E-$^{5}T_{2}$. This assignment is supported by the Zeeman anisotropy [1b] and by the angular dependence of the optically detected magnetic resonance [1c]. Picoli et al. [1d] proposed an interesting alternative: an interstitial Cr coupled with an acceptor A on an arsenic site. This would, according to the authors, explain the 0.575/0.535 eV transition.

Favennec et al. [2] observed trapping of Cr in GaAs implanted with oxygen. The dose was rather large, which could indicate gettering due to damage. However, implantation of neon under the same conditions (same dose and energy) did not cause a build-up of Cr in the implanted region. The authors give complexing of Cr and O as a possible explanation. Favennec and L'Haridon [3,1e] implanted Se and Zn into GaAs:Cr. Their results do not indicate any complexing; i.e., no trapping of Cr was observed in the implanted region. Asbeck et al. [4] implanted Se and Kr. No trapping of Cr in either case was reported. However, Evans et al. [5] did see Cr trapping in the Se implanted region. They used a dose 3 orders of magnitude larger than in the two aforementioned papers. In

the latter case the Cr pile-up disappeared and formed again at the surface after further annealing. An interesting case was reported by Magee et al. [6]. They annealed GaAs implanted with high doses of B (isoelectronic with Ga). This increased the outdiffusion of Cr, compared to annealing without implantation, and resulted in a stable Cr depletion channel. A small tendency for Cr pile-up at the implant peak was observed for high Cr content. Ne implantation [2] also enhances Cr outdiffusion.

Tuck et al. [7] observed that S doping of an epitaxial layer grown on a Cr doped substrate decreases the Cr outdiffusion more than an undoped layer. This indicates some interaction between Cr and S.

It is possible that Cr is sensitive to lattice strain. Clegg et al. [8] point out that Cr doping of GaAs reduces the lattice constant. In regions of large concentrations of As vacancies (e.g. at the surface) the lattice constant is larger. The gettering of Cr in such regions may decrease the lattice strain energy. Strain due to interfaces between encapsulants and GaAs may also interact with Cr. Eu et al. [9] suggest that the surface pile-up of Cr would be caused by precipitation of Cr at dislocations generated at the interface. They attribute the generally smaller accumulation of Cr at unencapsulated surfaces to smaller dislocation densities. This contrasts with the behavior in the bulk. Simondet et al. [1f] observe that Cr prefers to

migrate rather than to precipitate. They perform implantation of Cr and study the redistribution during the post-implantation encapsulated anneal. The Cr peak flattens out and Cr accumulates at the interface and in the encapsulant (silicon nitride). A higher dose of Cr causes more damage, and if Cr had a tendency to precipitate in damaged regions, the Cr peak would disappear at a less rapid rate, if at all. However, at higher doses the Cr shows the same tendency to leave the region of implantation.

Mullin et al. [10] observed that the deep-level-forming species in their samples were present at one percent or less of the total Cr concentration in the crystal. This led them to propose that Cr gives rise indirectly to the species that controls the Fermi level. They mentioned a Cr-O complex as one possibility.

Brozel et al. [11] studied the electrical compensation mechanism of Cr in GaAs doped with Cr and Si. Using localized vibrational mode absorption measurements they concluded that there were no signs of near-neighbor Si-Cr pairs. However, they did observe an increase of the Cr concentration when the Si concentration was increased. They actually observed a geometrical adjustment of the Cr concentration to the Si concentration. This behavior

certainly indicates some kind of interaction between Cr and Si.

Hobgood et al. [12] observed that the post-implantation activation of Si is more efficient when the Cr background is higher. Although this suggested to them a Cr-Si interaction, it does not seem likely that this is due to Cr_{Ga} forming pairs with Si. This is because most of the Si atoms as donors reside on the Ga sublattice where Cr is also thought to reside. This would indicate that a Cr-Si pair is not as favorable as, for example, a Cr-O pair.

5.2 INTERSTITIAL DONOR

It has been suggested that Cr can exist as an interstitial donor in GaAs [13]. In a paper to be discussed in detail later, Tuck and Adegboyega [14] model their diffusion data, which exhibit exceedingly rapid diffusion of Cr, by invoking a very mobile interstitial Cr-species (Cr_i). We will assume the existence of very mobile interstitial Cr donors. There have been experimental data reported which support this. Deveaud and Favennec [15] observed a new PL line in substrates that had been Cr-implanted and annealed, and also in contaminated epitaxial layers; i.e., layers into which Cr had outdiffused from the substrates. A very interesting feature of the latter is that, although the part of the

layer into which Cr had outdiffused contained almost as much Cr as the substrate itself, it was not semi-insulating. Furthermore, the new PL line was much stronger than those usually assigned to Cr. The authors suggested that Cr may be located non-substitutionally. Asbeck et al. [4] observed a spurious n-type layer just below the GaAs-Si_3N_4 interface after encapsulated annealing, and in this region Cr is always observed to accumulate at concentrations above the expected solubility [3,16]. Andre and Le Duc [17] actually concluded that Cr incorporated into LPE layers form shallow donors, contrary to Cr incorporated during bulk growth. As mentioned in section 2.1, Picoli et al. [1d] argue the formation of (Cr_iA)-pairs. With our assumption this seems very likely to be enhanced by an electrostatic interaction.

5.3 ION IMPLANTATION EFFECTS

The spectroscopic models invoking Cr complexes appear well justified. The existence of these complexes would certainly affect both redistribution of Cr and the electrical properties of Cr doped GaAs. Actually, successful reinterpretation of both the redistribution and compensation mechanisms in terms of Cr complexes is possible, as we will see in the following sections. In this section we will focus on the cause of Cr

redistribution about implants, and present a unifying qualitative interpretation.

The redistribution of implanted Cr discussed above, indicates that Cr is much more prone to outdiffuse and precipitate at the interface, than to be gettered in damaged regions. If Cr actually does accumulate in regions of implantation of a different ion, it is therefore presumably not because Cr is attracted by the damage, but instead due to a direct interaction between Cr and the implanted species. The observed redistribution of Cr upon post-implantation annealing therefore suggests that Cr tends to complex with the column VI elements (probably most strongly with O), but that the barriers to be overcome in the complexing reaction are so large that the material has to be nearly amorphous before this takes place; Simondet et al. [1f] point out that doses of about $10^{15}cm^{-2}$ effectively disorder the material, and it is in this range that trapping is observed. The dependence on the dose is well illustrated in [1g] where implanted S traps Cr for a dose larger than about $10^{14}cm^{-2}$. The proposed mechanism also conforms well with the depletion of Cr in regions of B implantation. The damage will undoubtedly produce a large amount of interstitial Cr, which will have to compete with B for Ga sites. Excess interstitial Cr will not accumulate in damaged regions, but instead outdiffuse rapidly, by a mechanism that will be discussed in detail in section 6.

In summary, Cr does not appear to be attracted, or repelled, by bulk damage caused by implantation. Any accumulation, or depletion, of Cr in implanted regions is likely to occur by an attraction, or effectively a repulsion, by the specific implanted ions. The damage only promotes the processes.

5.4 COMPENSATION MECHANISM

Our model of Cr in GaAs relies on the existence of ($Cr_{Ga}D_{As}$) complexes and rapidly diffusing interstitial Cr donors. Even though the (Cr_iA) complexes were proposed as an alternative to the ($Cr_{Ga}D_{As}$) complexes, it appears likely that both kinds can occur. This would offer an alternative interpretation of the compensation in Cr-doped GaAs. As was first observed by Cronin and Haisty [18], the semi-insulating properties of bulk grown GaAs:Cr are remarkably independent of the Cr concentration added to the melt. This behavior is typically explained [11] by assuming that the deep acceptor level(s) of Cr_{Ga} pin the Fermi level close to the center of the gap. Excess Cr can then precipitate [18].

We suggest the following compensation mechanism: At the high bulk-growth temperatures the residual donors D_{As} are chemically compensated by Cr through the formation of the isoelectronic complex $(Cr_{Ga}D_{As})^{\circ}$. The excess Cr is in the

form of isolated Cr_{Ga} and Cr_i. As the ingot is cooled the Cr_i donors flush out because of limited solubility and large diffusion constant. Since the acceptors and the mobile Cr_i donors are oppositely charged, electrostatic attraction between the two species is expected. This will enhance the formation of (Cr_iA) complexes and contribute to good compensation.

In addition to giving an alternative interpretation of the semi-insulating properties of GaAs doped with Cr during bulk-growth, this offers an explanation of the enhanced apparent activation of Si in the presence of Cr. Si is amphoteric and the Si-acceptors can be neutralized by rapidly diffusing Cr_i-donors. The same effect can explain the increase of Cr concentration with increasing Si concentration that was observed by Brozel et al. [11] even locally.

The compensation mechanism gives a first hint to an understanding of the redistribution properties of Cr in GaAs since we no longer can expect Cr incorporated during high-temperature bulk growth to redistribute in the same way as Cr introduced into the crystal at lower temperatures. The rest of this paper will be devoted to the redistribution problem.

5.5 REDISTRIBUTION MECHANISM

The foregoing discussion suggests that the problem of Cr redistribution in GaAs is quite complicated. Cr apparently occurs in several different forms: isolated interstitial Cr_i, isolated substitutional Cr_{Ga}, complexed interstitial (Cr_iA), and complexed substitutional $(Cr_{Ga}D_{As})$. Furthermore, there are a number of mechanisms involved in the redistribution: diffusion in concentration gradients, drift of Cr ions in a built-in electric field, quasi-chemical reactions, and gettering in the strain fields of surfaces and dislocations. We expect the following reactions to be dominant:

$$Cr_i + V_{Ga} \rightleftarrows Cr_{Ga}, \tag{1}$$

$$Cr_i + V_{Ga} + D_{As} \rightleftarrows (Cr_{Ga}D_{As}), \tag{2}$$

and

$$Cr_i + A \rightleftarrows (Cr_iA). \tag{3}$$

Three assumptions appear physically well motivated:

1. The actual transport of Cr occurs interstitially. The diffusion and drift of the substitutional and complexed Cr are negligible. This is typically assumed for

interstitial-substitutional diffusion.

2. At the usually relatively low processing temperatures there is no formation of ($Cr_{Ga}D_{As}$) complexes since this is a third order process and seems very unlikely to occur after the original formation of the crystal.
3. The complexes are considerably more strongly bound than the substitutional Cr ions to their sites.

The major technological problem with Cr doped substrates is their apparent irreproducibility. Capless anneal sometimes leads to surface build-up [1h,9], at other times not [1h,19], depending on temperature and As overpressure. Capped anneal generally leads to thin surface pile-up [3,9,16]. Apart from the surface behavior, however, the different results do not appear too dissimilar; i.e., they are characterized by a thin (1-2μm) surface depletion of Cr, while the bulk concentration remains unaffected. The really astonishing deviation from most of these results is reported in the experiments conducted by Tuck and coworkers [7,14]. They observed a remarkable penetration and diffusion of Cr in GaAs leading to a uniform Cr concentration throughout hundreds of microns, and a thick (10-20μm) surface pile-up on both indiffusion and anneal. The uniform bulk concentration was observed to vary exponentially in time. In this section we will focus on this apparent inconsistency.

As was mentioned in the last section, our model indicates that the redistribution depends strongly on how the Cr was incorporated. We will therefore study the two cases of post-growth incorporated Cr as represented by the data of Tuck and coworkers, and Cr incorporated during high temperature bulk growth as represented by the data of Kasahara and Watanabe. The latter are typical of the behavior usually encountered. The results lack the surface build-up, presumably due to stable conditions set by the As overpressure and temperature. In both cases the vacancies will affect the redistribution, and we will therefore discuss the expected vacancy concentration profiles in GaAs. In the analysis we will ignore the drift of Cr in electric and strain fields. This means that we do not model the immediate vicinity of the surface. However we will begin by giving a separate qualitative discussion of the drift of Cr_i in electric fields due to dopant gradients in the bulk.

5.5.1 Interstitial Drift

Drift in built-in electric fields can typically be neglected except at surfaces and interfaces. At free surfaces it is difficult to distinguish between field induced and strain induced build-up. However at an interface between two doping regions in a structurally homogeneous crystal, an anomaly in the Cr distribution is more likely to be caused by the electric field.

It has been observed [20] that Cr outdiffusing during epitaxy from a semi-insulating GaAs:Cr substrate, through an undoped GaAs buffer layer, into a n-GaAs active layer (electron concentration n), piles up at the buffer layer side of the interface between the epitaxial layers for $n=10^{17}cm^{-3}$, but not for $n=5x10^{16}cm^{-3}$. At the growth temperature of $750^{o}C$ the intrinsic concentration has been measured [21] to be $6x10^{16}cm^{-3}$. That means that for the case where pile-up is observed there is an electric field in the interfacial region between the active layer and the buffer layer. This is mostly confined to the undoped buffer layer and is directed into this. The interfacial pile-up of Cr resembles those of charged impurities reported in [22]. These were caused by the electric field due to doping gradients. The observed Cr pile-up is such that the mobile Cr would have to be positively charged. It is therefore likely that the interstitial Cr actually is a donor as was argued above. The Cr profiles observed by Linh et al. [1i] in MBE layers conform qualitatively with this assignment.

5.5.2 Vacancy Profiles

In the redistribution model we have outlined, the vacancies play an important role primarily through reaction (1). One possible mechanism for Ga vacancy production is the process,

$$Ga_{Ga} + I \rightleftarrows V_{Ga} + Ga_i, \tag{4}$$

where I is an interstitial site. A similar reaction would apply to As vacancies. It is also conceivable to have vacancy production at dislocations. In either case the continuity equation for the vacancy concentration C_v can be written (neglecting possible drift),

$$\frac{\partial C_v}{\partial t} = D_v \frac{\partial^2 C_v}{\partial x^2} - \beta C_v + \alpha, \tag{5}$$

where D_v is the diffusion coefficient. It is not clear what the diffusion mechanism is, but it seems likely that it is similar to that suggested by Swalin [23] for vacancy diffusion in group IV semiconductors. The mechanism would then involve transfer of an atom to a nearby vacancy (for III-V semiconductors, at a next-nearest neighbor site). $\alpha-\beta C$ is the net generation of vacancies by the dominant mechanism. At the surface the concentration of vacancies need not be the same as in the bulk since it can be more readily influenced, for instance, by the As overpressure. In the steady state the vacancy concentration profile is

$$C_v^{(o)}(x) = C_v^{(b)} + [C_v^{(s)} - C_v^{(b)}] \exp(-x/L_v), \tag{6}$$

where $C_v^{(s)}$ is the surface concentration, $C_v^{(b)}$ the bulk concentration, and L_v the vacancy diffusion length given by

$$L_v = \sqrt{D_v/\beta} \,. \qquad (7)$$

5.5.3 Radiotracer Diffusion

We believe that Tuck, Adegboyega and coworkers [7,14] have reported some of the few experiments that involve essentially only reaction (1). In these experiments radiotracer Cr was diffused into bulk grown GaAs (Cr-doped or n-type) at temperatures well below the growth temperature. Under these circumstances, reaction (2) is not expected to go to the right, and reaction (3) is secondary due to the small number of isolated acceptors. The indiffusing Cr, which is the only Cr that is detected, is thus not expected to interact strongly with the residual impurities.

Tuck and Adegboyega (TA) account for the observed exponential time dependence of the uniform bulk concentration by means of a fairly simple model [14] involving the non-equilibrium chemistry of substitutional and interstitial Cr and of Ga vacancies. The width of the surface peak permits them to estimate the diffusion constant of Ga vacancies. It is assumed that Cr can exist in GaAs as a highly mobile interstitial species Cr_i, or substitutionally on Ga sites as immobile Cr_s. The reaction converting each species into the other is reaction (1). Only Cr_s is incorporated or desorbed at the surface. For Cr to penetrate to the interior, it must first be converted by

reaction (1) to Cr_i. It then diffuses rapidly and can again react with V_{Ga} to form Cr_s. The limit chosen by TA to interpret the experiments assumes that the surface incorporation and conversion reactions are in equilibrium, that the interstitial diffusion is extremely rapid (in effect, instantaneous on the time scale considered), and that the bulk conversion is slow. In addition it is assumed that no vacancies are generated or annihilated in the bulk except through reaction (1). The surface concentration gradients are qualitatively accounted for by the diffusion of V_{Ga}. This vacancy concentration, depleted by reaction (1) during indiffusion of Cr, is replaced by diffusion from the surface, resulting in a surface Cr peak, as observed. In the outdiffusion experiment from a homogeneously vacancy-depleted sample, vacancies also diffuse in from the surface, "pulling" Cr from the interior to supply reaction (1), and again resulting in a surface peak.

We adopt a similar model but with a substantially modified picture of the vacancy dynamics. Unlike TA, we assume that the vacancy concentration is always able to reach its steady state, on the time scale of the experiments under study, leading to the vacancy concentration profile (6). This appears to us more consistent with a rather large vacancy diffusion constant, as inferred by TA, than the large departure from equilibrium implied by their interpretation. We could

indeed adopt TA's viewpoint and generalize it to .

$$C_v(x,t) = C_v^{(o)}(x) - [C_s(x,t) - C_s(x,0)], \qquad (8)$$

where we assume equilibrium initial distribution $C_v(x,0)=C_v^{(o)}(x)$, but we find this less plausible. Either approach, however, permits us to extend the validity of the treatment closer to the surface, and we are able to estimate the Ga vacancy diffusion length from TA's data. We start by examining rapid diffusion and find that we can deduce a condition on the diffusion constant necessary to keep the concentration uniform. From this we can estimate the lower limit of the diffusion constant for interstitial Cr, again using TA's data. We study the limit considered by TA and also the limit where the surface conversion reaction is the bottleneck. TA's indiffusion data, which exhibit a large constant surface concentration on indiffusion, indicate incorporation equilibrium, so this must be discarded as a possible bottleneck. The entire process of incorporation, surface conversion of Cr_s into Cr_i, diffusion of Cr_i, generation of Ga vacancies, and conversion between Cr_i and Cr_s in the bulk is illustrated in Figure 1.

5.5.3.1 Rapid Diffusion Leading to Uniform Concentration

We study an atomic species that redistributes in a sample of thickness ℓ by a simple diffusion mechanism. The

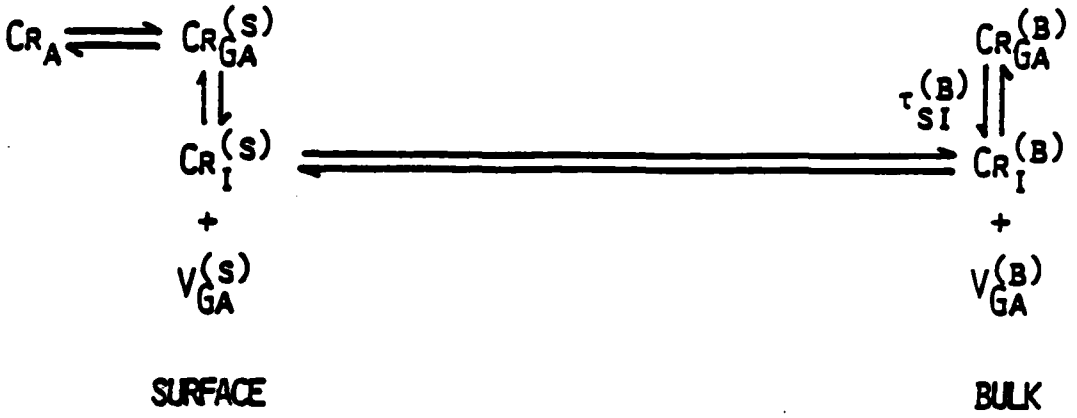

Figure 1. Reactions involved in the redistribution of Cr introduced after bulk growth.

continuity equation is then

$$\frac{\partial C}{\partial t} = D\frac{\partial^2 C}{\partial x^2}, \tag{9}$$

with boundary conditions set by the surface flux,

$$J(0,t) = -D\frac{\partial C}{\partial x}(0,t) = v[kC_a - C(0,t)], \tag{10a}$$

and

$$J(\ell,t) = -D\frac{\partial C}{\partial x}(\ell,t) = -v[kC_a - C(\ell,t)]. \tag{10b}$$

In these equations $C(x,t)$ and C_a are the concentrations in the sample and in the ambient atmosphere respectively, D is the atomic diffusion constant, k the segregation coefficient and v the surface diffusion velocity. We wish to determine the condition on D that will keep the concentration practically uniform at all times,

$$C(x,t) = C'(t), \tag{11}$$

assuming the consistent initial condition

$$C(x,0) = C'(0). \tag{12}$$

With these initial and boundary conditions, the solution of

the diffusion equation is [24]

$$C(x,t)-kC_a = [C'(0)-kC_a]\left[\cos\alpha_1 x+\frac{v}{\alpha_1 D}\sin\alpha_1 x\right]\exp(-D\alpha_1^2 t), \quad (13)$$

where α_1 is the first positive root of

$$\tan\alpha\ell = \frac{2\alpha(v/D)}{\alpha^2-(v/D)^2}. \quad (14)$$

For $C(x,t)$ to be considered independent of x we must have $\alpha_1\ell \ll 1$ and $v/\alpha_1 D \ll 1$. If these conditions are fulfilled, (13) becomes

$$C'(t) = kC_a+[C'(0)-kC_a]\exp(-t/\tau), \quad (15)$$

where

$$\frac{1}{\tau} = \alpha_1^2 D \ll \frac{D}{\ell^2} \quad (16)$$

and $\alpha_1^2 = 2v/D\ell$ so that $1/\tau = 2v/\ell$.

Thus, if the concentration is observed to relax uniformly with the characteristic time τ, (16) sets a lower limit on the diffusion constant,

$$D \gg \ell^2/\tau. \quad (17)$$

5.5.3.2 Bulk Cr Concentration

The continuity equation for the Cr_i concentration C_i is not as simple as (9) since Cr_i is also involved in reaction (1). The diffusion of Cr_i is assumed to be fast enough to maintain a uniform concentration and much faster than the rate of the reaction. Under these conditions, the continuity equation becomes

$$\frac{\partial C_i}{\partial t} = D_i \frac{\partial^2 C_i}{\partial x^2} - \frac{\overline{\partial C_s}}{\partial t}, \tag{18}$$

where the bar indicates the spacial average $(1/\ell)\int dx$. That is, because of the fast diffusion of Cr_i, it is only the global effect of the reaction that matters.

Neglecting diffusion of Cr_s, the continuity equation for the Cr_s concentration C_s is governed entirely by the rate of the reaction (1),

$$\frac{\partial C_s}{\partial t} = -\frac{C_s}{\tau_{si}^{(b)}} + \frac{\kappa_{is}^{(b)}}{\tau_{si}^{(b)}} C_v^{(o)}(x) C_i(t). \tag{19}$$

This is an alternative to and an extention of TA's continuity equation where we adopt the equilibrium vacancy picture (6), allow for the time dependence of the Cr_i concentration, and superscribe the relaxation time τ_{si} and the equilibrium constant κ_{is} with "b" for "bulk". This is done to distinguish these quantities from those associated with the formally identical surface conversion reaction,

for which the parameters may be different. This equation will lead to an "outer" solution [25], which does not satisfy the boundary condition that C_s be constant at the surface. At the surface there is a boundary layer in which the outer solution connects with an "inner" solution which falls off rapidly due to finite substitutional diffusion and effects due to strain and fields. This will be neglected here but kept in mind when we estimate the vacancy diffusion length later.

The boundary condition for the Cr_i concentration is prescribed by the flux as in the last section. This flux equals the net surface production of Cr_i by the surface conversion reaction. There is a surface generation $\sigma_s/\tau_{si}^{(s)}$ of Cr_i, where σ_s is the surface concentration of Cr_s and $\tau_{si}^{(s)}$ is the relaxation time analogous to $\tau_{si}^{(b)}$ in (19) but with superscript "s" referring to the surface. σ_s is constant since we have assumed incorporation equilibrium. Thus,

$$\sigma_s = k_s C_a d_a, \tag{20}$$

where k_s is the segregation constant for Cr_s, C_a is the Cr concentration in the ambient atmosphere, and d_a is the thickness of an effective surface layer. There is also surface annihilation of Cr_i; i.e., Cr_i becomes Cr_s. This process is described by a similar relaxation term,

$C_i(t)d_i/\tau_{is}^{(s)}$, where d_i is analogous to d_a and $\tau_{is}^{(s)}$ is the relaxation time for this process. We find then

$$J(0,t) = -J(\ell,t) = v[k_i C_a - C_i(t)], \tag{21}$$

where we have defined the surface diffusion velocity v and segregation constant k_i for Cr_i as

$$v = \frac{d_i}{\tau_{is}^{(s)}}, \tag{22}$$

and

$$k_i = k_s \frac{d_a}{d_i} \frac{\tau_{is}^{(s)}}{\tau_{si}^{(s)}}, \tag{23}$$

to point out the similarity with the boundary conditions (10) for the problem in the last section. Any direct incorporation of Cr will just add to v in (22) and k_i in (23).

Equation (18) in its present form is not similar to equation (9), but it will be in the following two limiting cases:

1. Bulk conversion bottleneck: If conversion from Cr_i to Cr_s in the bulk is so slow that we can neglect $\frac{\partial C}{\partial t}s$ in (18), it becomes identical with (9) by putting $D=D_i$. The estimate (17) of D_i is

$$D_i >> \ell^2/\tau_i. \tag{24}$$

However, the observed time constant is presumably $\tau_{si}^{(b)}$ which is associated with the slow bulk conversion reaction. Thus, $\tau_i << \tau_{si}^{(b)}$ and the estimate of the required magnitude of D_i tends to get larger. On the experimental time scale then,

$$C_i(t) = k_i C_a = C_{io}, \tag{25}$$

and the solution to (19) is

$$C_s(x,t) = \kappa_{is}^{(b)} C_{io} C_v^{(o)}(x) + \\ + [C_s(x,0) - \kappa_{is}^{(b)} C_{io} C_v^{(o)}(x)] \exp(-t/\tau_{si}^{(b)}). \tag{26}$$

The total Cr concentration is

$$C(x,t) = C_{io} + C_s(x,t). \tag{27}$$

2. Surface conversion bottleneck: The bulk conversion is assumed to be in equilibrium,

$$C_s(x,t) = \kappa_{is}^{(b)} C_v^{(o)}(x) C_i(t), \tag{28}$$

and the space average is

$$\overline{C_s}(t) = \kappa_{is}^{(b)} \overline{C_v^{(o)}} C_i(t). \tag{29}$$

Equation (18) then becomes,

$$\frac{\partial C_i}{\partial t} = \frac{D_i}{1+\kappa_{is}^{(b)} \overline{C_v^{(o)}}} \frac{\partial^2 C_i}{\partial x^2}, \tag{30}$$

and for uniform C_i

$$\frac{D_i}{1+\kappa_{is}^{(b)} \overline{C_v^{(o)}}} >> \frac{\ell^2}{\tau_i}. \tag{31}$$

In this case the observed relaxation time is τ_i but one usually expects $\kappa_{is}^{(b)} \overline{C_v^{(o)}}$ to be much larger than unity since it is essentially the ratio of C_s to C_i. So again the estimate of D_i would tend to get larger than that associated with the observed time constant. The concentration of Cr_i becomes

$$C_i(t) = k_i C_a + [C_i(0) - k_i C_a] \exp(-t/\tau_i), \tag{32}$$

and the total Cr concentration is

$$C(x,t) = C_i(t)[1+\kappa_{is}^{(b)} C_v^{(o)}(x)]. \tag{33}$$

5.5.3.3 Estimate of Ga Vacancy Diffusion Length

No matter which of the conversion reactions is the bottleneck, a plot of $\ln[C(x,t)-C(\infty,t)]$ vs. x of TA's data

should yield a straight line with a slope $-L_v^{-1}$. If the assumption of vacancy equilibrium is correct the slopes should be independent of time t. The data for such a plot from TA's Figures 1, 3, 4 and 6 are displayed in our Figure 2. From this it is apparent that the data points for x>10μm can be fitted with straight lines except possibly for the data recorded with the 900°C, 4 hour indiffusion (line g). The 750°C, 1 hour outdiffusion data (line i) fall on a straight line all the way to the surface. This is not surprising since there is no large Cr_s surface concentration producing a large gradient in a boundary layer. All the lines except e and f yield roughly the same value of L_v,

$$L_v(Ga) = (11 \pm 3)\mu m. \qquad (34)$$

The two cases e and f are responsible for effectively the entire standard deviation of 3μm. It may be argued that this value of L_v is not precise. However, there are two important points to be made:

1. L_v is essentially time independent (lines a,b,c,d and e); and
2. L_v is essentially temperature independent (lines b,f,g and h).

The time independence supports the assumption of vacancy equilibrium. The temperature independence is not unexpected

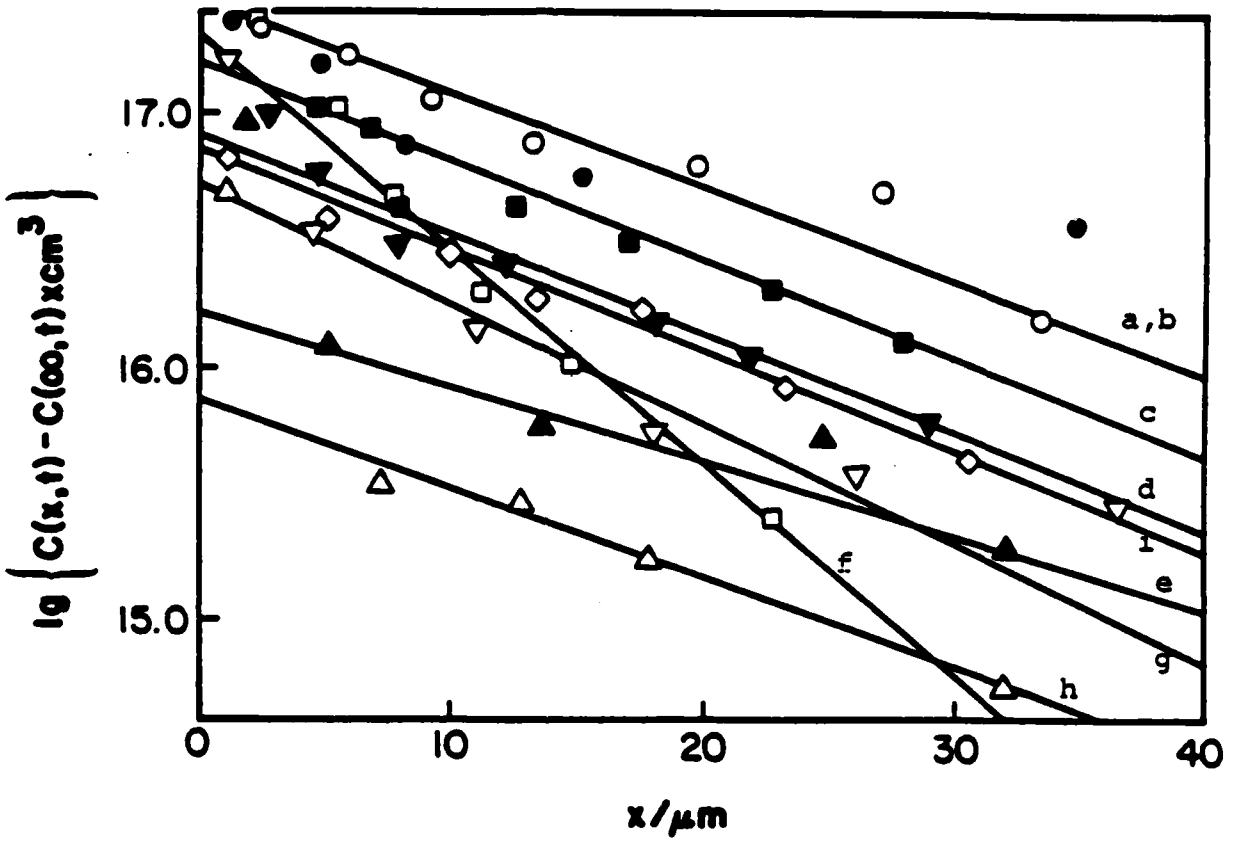

Figure 2. Some of TA's diffusion data replotted in order to estimate the Ga vacancy diffusion length. The numbers in parenthesis refer to the figures in [14] used.

a. ● 10h, 1100°C, L_v=11.7μm (4)
b. ○ 4h, 1100°C, L_v=11.7μm (1,4)
c. ■ 3h, 1100°C, L_v=11.1μm (4)
d. ▼ 2h, 1100°C, L_v=11.1μm (4)
e. ▲ 1h, 1100°C, L_v=14.7μm (4)
f. □ 4h, 1000°C, L_v=5.1μm (1)
g. ▽ 4h, 900°C, L_v=9.1μm (1)
h. △ 4h, 800°C, L_v=12.2μm (1)
i. ◇ 1h, 750°C, L_v=10.9μm (6)

if one considers the vacancy production to occur through the reaction (4), and the diffusion mechanism to be of the Swalin kind as discussed earlier. In this case both D_v and β in expression (7) for L_v contain an exponential of the activation energy to remove an atom from its substitutional site. If an additional vacancy production mechanism were present, for instance due to a high dislocation density, one would expect L_v to decrease (β increase). We would also expect temperature dependence and some time dependence since the properties of dislocations can change, for instance by motion. This may be a reason for the anomalous cases.

5.5.3.4 Estimate of Interstitial Cr Diffusion Constant

During indiffusion we have

$$C(x,t) = C(x,\infty)[1-\exp(-t/\tau)], \tag{35}$$

where the timeconstant τ is $\tau_{si}^{(b)}$ if the bulk conversion is the bottleneck and τ_i if the surface conversion is the bottleneck. In the former case we have neglected the concentration of Cr_i compared to the equilibrium concentration of Cr_s. The condition on D_i is

$$D_i >> \ell^2/\tau, \tag{36}$$

Plotting $\ln[1-C(x,t)/C(x,\infty)]$ vs. t should yield a straight

line with slope $-\tau^{-1}$. In Figure 3 we show such a plot for $x=\infty$, i.e., in the uniform bulk, where the fit is expected to be best. We used TA's Figure 4 for indiffusion at 1100°C. The estimated straight line to fit the data points has been drawn, keeping in mind that the relative errors increase as $C(\infty,t)$ approaches $C(\infty,\infty)$. It yields $\tau=2.1\times10^{4}$s. In TA's work $\ell=0.05$ cm so $\ell^2/\tau \approx 10^{-7}$cm^2/s. A rough lower limit for D_i would be

$$D_i(1100^{\circ}C) \geq 10^{-5}\text{cm}^2/\text{s}. \qquad (37)$$

It is interesting to compare this with the largest conceivable diffusion constant. This occurs when the diffusion is driven by optical phonons with a jump frequency equal to the phonon frequency. For interstitial diffusion in GaAs the optical phonon frequency is $f=8\times10^{12}\text{s}^{-1}$. The interstitial jump distance is $\sqrt{3}\,a/4$, where a is the lattice constant (5.65 Å), and

$$D_i(\text{max}) = a^2 f/8 \approx 3\times10^{-3}\text{cm}^2/\text{s}. \qquad (38)$$

The Cr_i diffusion constant is, thus, very large and appears to be quite close to the phonon-driven limit. It is interesting at this point to recall the theory developed by Weiser [26] for interstitial diffusion in the diamond lattice. He found that one would expect some ions of

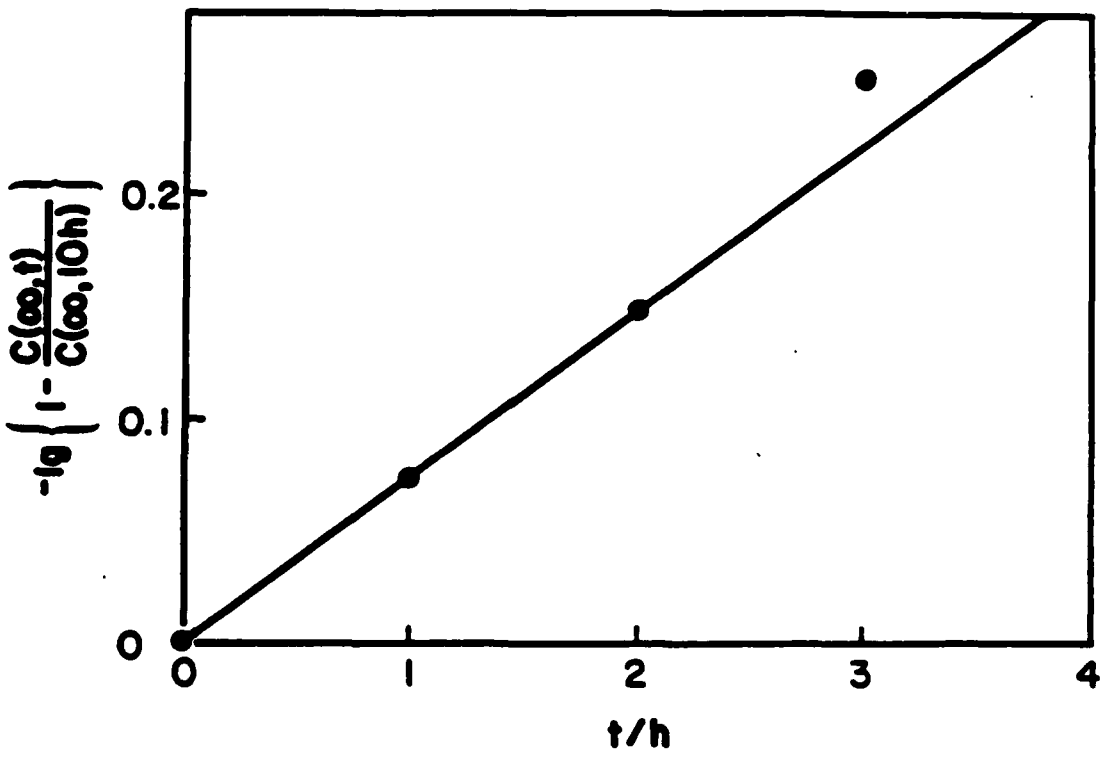

Figure 3. TA's 1100°C bulk concentration ([14] Figure 4) plotted as a function of time in order to estimate the associated time constant.

intermediate size to diffuse interstitially, virtually without any potential barrier between sites. He proposed that this may be the case for Cu in GaAs which would explain its diffusion behavior.

5.5.4 Bulk Growth Outdiffusion

The contrasting experimental results that we set out to study are those represented by the data of Kasahara and Watanabe (KW) [19]. These authors perform annealing experiments and study the outdiffusion of Cr from the sample. They model the result assuming substitutional diffusion and a finite surface diffusion velocity. They get good fit far from the surface with an increasing discrepancy between theory and experiment as the surface is approached.

The present model offers an alternative explanation which appears capable of accounting for the results closer to the surface. In the experiments the measured Cr was incorporated during bulk growth. That means that most of the Cr is presumably bound in relatively strong complexes, mostly as $(Cr_{Ga}D_{As})$. We suggest that the dominant redistribution mechanism is the dissociation of these complexes. Note that there is no uniform reduction of the Cr concentration. If the dissociation had occurred throughout the sample, one would expect, in view of the fast diffusion of Cr_i inferred in the last section, that the reduction of the Cr concentration would extend further

into the sample. The dissociation appears to be catalyzed close to the surface. The defect responsible for this is likely to be native to the GaAs crystal since the surface depletion appears in a variety of samples. The region of the outdiffusion is much thinner than the Cr peak in TA's data, which indicates that Ga vacancies are not directly involved. We therefore suggest that the arsenic vacancies are responsible for the catalysis. An As vacancy adjacent to a $(Cr_{Ga}D_{As})$ complex could very well increase the probability of dissociation which would then be described by

$$(Cr_{Ga}D_{As}) + V_{As} \rightleftarrows Cr_i + D_{As} + V_{Ga} + V_{As}. \qquad (39)$$

By a technique similar to the one used to analyse TA's data, we can estimate the As vacancy diffusion length from KW's data. We assume that the As vacancy equilibrium is maintained. This appears reasonable since no V_{As} are consumed in the reaction (with the possible exception of the formation of divacancies). We will approximate the equilibrium vacancy profile (6) by

$$c_v^{(o)} = c_v^{(s)} \exp(-x/L_v), \qquad (40)$$

since the surface is typically very V_{As} rich. In view of

the rapid diffusion of Cr_i, the Cr_i formed will "immediately" result in a uniform distribution. The concentration of Cr_i will be exceedingly small and we can neglect this and the capture by V_{Ga}. With these premises the continuity equation for the total Cr concentration will be

$$\frac{\partial C}{\partial t} = -\gamma(x)C, \tag{41}$$

where $\gamma(x)$ is proportional to the As vacancy concentration. With a uniform initial concentration C_o the solution is

$$C(x,t) = C_o \exp(-\gamma(x)t), \tag{42}$$

with approximation (40) for the As vacancy concentration.

A plot of $\ln[(\ln C(x,t)-\ln C_o)/t]$ vs. x should yield a straight line with slope $-L_v^{-1}$. For different times the lines should coincide; i.e., the position and slope should be time independent. We plot the data of KW's Figure 2 in the described manner in our Figure 4. In each case (different t) a straight line fits the points very well and we can calculate the average estimated diffusion length and the standard deviation,

$$L_v(As) = (0.5 \pm 0.1)\mu m. \tag{43}$$

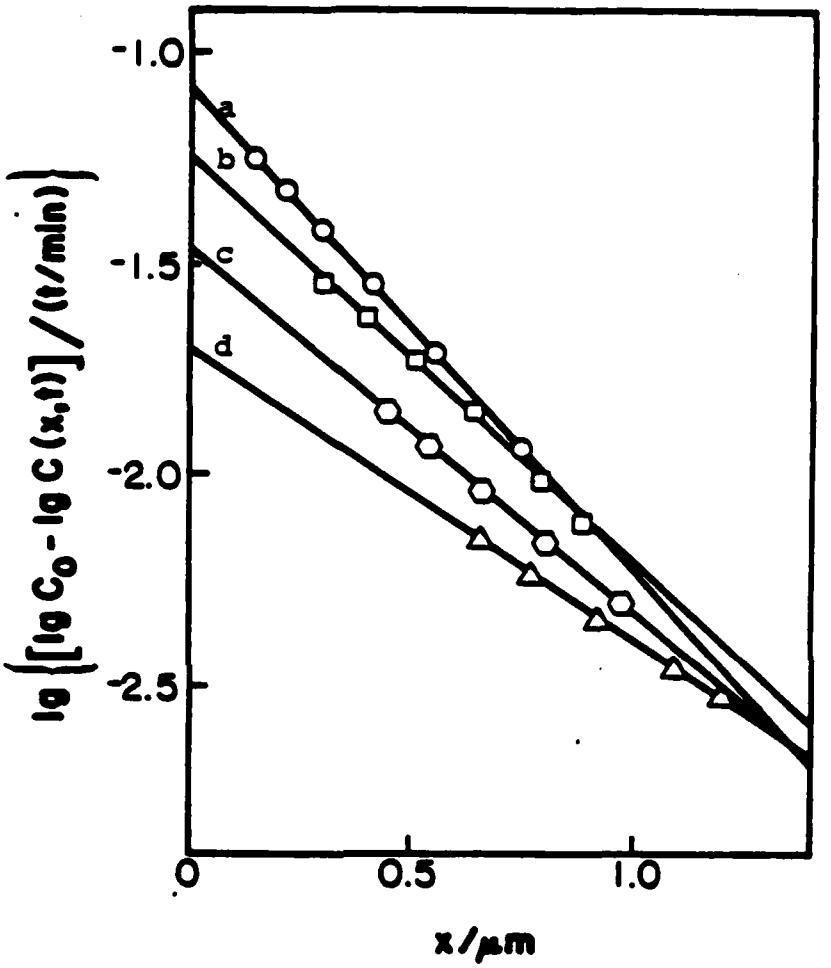

Figure 4. KW's 850°C anneal data ([19] Figure 2) replotted in order to estimate the As vacancy diffusion length.
a. ○ 15 min, L_v=0.38 μm
b. □ 30 min, L_v=0.45 μm
c. ⬡ 60 min, L_v=0.50 μm
d. △ 120 min, L_v=0.63 μm

The standard deviation represents a reasonable error. The drift of slope and intercept may indicate the extent to which the vacancy equilibrium fails to be maintained.

5.6 CONCLUSIONS

We have proposed a model for Cr impurities in GaAs that is consistent with a wide variety of experimental observations, including spectroscopic, redistribution and diffusion, and electrical data. This model does not appear to be in conflict with any reported experiments. In particular, we can account in detail for the excellent compensation that is achieved with Cr doping, and we can reconcile the apparently incompatible but equally reliable diffusion and annealing data that have been reported by different workers. It is also capable of interpreting the observed Cr redistribution about implants during annealing.

By using this model to reinterpret experimental work reported in the literature, we have also established new estimates of several useful parameters for both the impurity and the host crystal.

We hope that the model also will be helpful in analyzing other experimental data on Cr in GaAs, such as thermal conversion of GaAs:Cr substrates and surface Cr pile-up during heat treatment, and those associated with Cr outdiffusion into epitaxial layers.

5.7 REFERENCES

1. G.J. Rees (Ed.), Semi-Insulating III-V Materials, Nottingham 1980, Shiva Publishing Limited.

   a. A.M. White, p. 3.

   b. L. Eaves, T. Englert, T. Instone, C. Uihlein, P.J. Williams and H.C. Wright, p. 145.

   c. N. Killoran, B.C. Cavenett and W.E. Hagston, p. 190.

   d. G. Picoli, B. Deveaud and D. Galland, p. 254.

   e. P.N. Favennec and H. L'Haridon, p. 130.

   f. F. Simondet, C. Venger, G.M. Martin and J. Chaumont, p. 100.

   g. C.A. Evans, Jr., C.G. Hopkins, J.C. Norberg, V.R. Deline, R.J. Blattner, R.G. Wilson, D.M. Jamba and Y.S. Park, p. 138.

   h. T. Udagawa, M. Higashiura, T. Nakanisi, p. 108.

   i. N.T. Linh, A.M. Huber, P. Etienne, G. Morillot, P. Duchemin and M. Bonnet, p. 206.

2. P.N. Favennec, M. Gauneau, H. L'Haridon, B. Deveaud, C.A. Evans,Jr. and R.J. Blattner, Appl. Phys. Lett. 38, 271 (1981).

3. P.N. Favennec and H. L'Haridon, Appl. Phys. Lett. 35, 699 (1979).

4. P.M. Asbeck, J. Tandon, B.M. Welch, C.A. Evans, Jr. and V.R. Deline, IEEE Electron. Device Lett. EDL-1, 35 (1980).

5. C.A. Evans, Jr., V.R. Deline, T.W. Sigmon and A. Lidow, Appl. Phys. Lett. 35, 291 (1979).

6. T.J. Magee, R.D. Ormond, C.A. Evans, Jr., R.J. Blattner, R.M. Malbon, D.S. Day and R. Sankaran, Appl. Phys. Lett. 38, 559 (1981).

7. B. Tuck, G.A. Adegboyega, P.R. Jay and M.J. Cardwell, Inst. Phys. Conf. Ser. No. 45, p. 114 (1979).

8. J.B. Clegg, G.B. Scott, J. Hallais and A. Mircea-Roussel, J. Appl. Phys. 52, 1110 (1981).

9. V. Eu, M. Feng, W.B. Henderson, H.B. Kim and J.M. Whelan, Appl. Phys. Lett. 37, 473 (1980).

AD-A122 217 IMPURITY AND DEFECT INTERACTIONS IN GAAS(U) WASHINGTON 2/3
UNIV ST LOUIS MO SEMICONDUCTOR RESEARCH LAB
C M WOLFE ET AL. 30 SEP 82 WU/SRL-64422-10
UNCLASSIFIED N00014-80-C-0762 F/G 20/2 NL

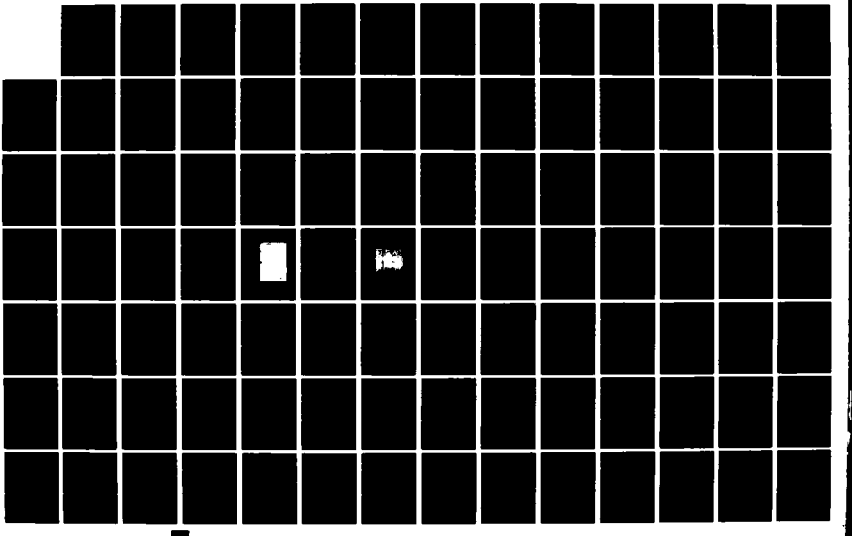

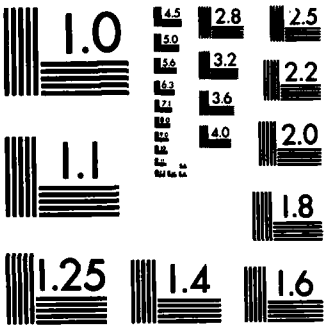

MICROCOPY RESOLUTION TEST CHART
NATIONAL BUREAU OF STANDARDS-1963-A

10. J.B. Mullin, D.J. Ashen, G.G. Roberts and A. Ashby, Inst. Phys. Conf. Ser. No. 33a, p. 91 (1977).

11. M.R. Brozel, J. Butler, R.C. Newman, A. Ritson, D.J. Stirland and C. Whitehead, J. Phys. C. 11, 1857 (1978).

12. H.M. Hobgood, Graeme W. Eldridge, Donovan L. Barrett and R. Noel Thomas, IEEE Trans. Electron. Devices ED-28, 140 (1981).

13. R.F. Broom, J. Appl. Phys. 38, 3483 (1967).

14. Brian Tuck and G.A. Adegboyega, J. Phys. D. 12, 1895 (1979).

15. B. Deveaud and P.N. Favennec, Solid State Commun. 24, 473 (1977).

16. A.M. Huber, G. Morillot, N.T. Linh, P.N. Favennec, B. Deveaud and B. Toulouse, Appl. Phys. Lett. 34, 858 (1979).

17. E. Andre and J.M. Le Duc, Mat. Res. Bull. 4, 149 (1969).

18. G.R. Cronin and R.W. Haisty, J. Elechochem. Soc. 111, 874 (1964).

19. Jiro Kasahara and Naozo Watanabe, Jap. J. Appl. Phys. 19, L151 (1980).

20. M.J. Cardwell, private communication.

21. K.H. Nichols, Camellia M.L. Yee and C.M. Wolfe, Solid State Electron. 23, 109 (1980).

22. H. Rohdin, M.W. Muller and C.M. Wolfe, J. Electron. Mater. 11, 517 (1982).

23. R.A. Swalin, in D. Shaw (Ed.), Atomic Diffusion in Semiconductors, Plenum Press, London and New York, 1973, p. 65.

24. H.S. Carslaw and J.C. Jaeger, Conduction of Heat in Solids, 2nd ed., Oxford University Press, 1959, p. 114.

25. C.M. Bender and S.A. Orszag, Advanced Mathematical Methods for Scientists and Engineers, McGraw-Hill, 1978, chapter 9.

26. K. Weiser, Physical Review 126, 1427 (1962).

6. Cr SURFACE REDISTRIBUTION DURING ANNEALING

There has been considerable recent interest in the redistribution of Cr in GaAs during annealing processes. A prominent feature of this redistribution is often an accumulation of Cr at the surface. This pileup has been observed under a variety of conditions, and attributed to As vacancies[1-3] or encapsulant strains[1,4-9]. To examine these possibilities it is useful to consider the characteristic lengths associated with Cr buildup. In many cases the cause of a physical phenomenon can be determined from the various length scales associated with different mechanisms. For example, the estimated diffusion length of As vacancies is about 0.5μm[10]. Although the characteristic lengths associated with surface strain can change with conditions, it is also a long range phenomenon compared to the smaller regions of Cr pileup observed at the surface. In this paper we examine the shortest length scale associated with Cr accumulation, which is apparently due to the electrostatic field caused by surface states.

6.1 CHARACTERISTIC LENGTHS

The characteristic lengths associated with surface Cr buildup as determined from SIMS data in recent literature[6-9,11-14] and from our own annealing experiments are plotted in Fig. 1 as a function of annealing temperature. The characteristic lengths, L_i, were extracted from the SIMS data with the expression[15],

$$N(r) = n_i \coth^2 \left(\frac{r}{L_i} + \alpha\right), \qquad (1)$$

where $N(r)$ is the impurity profile, n_i is the intrinsic carrier concentration, r is the distance from the surface, and

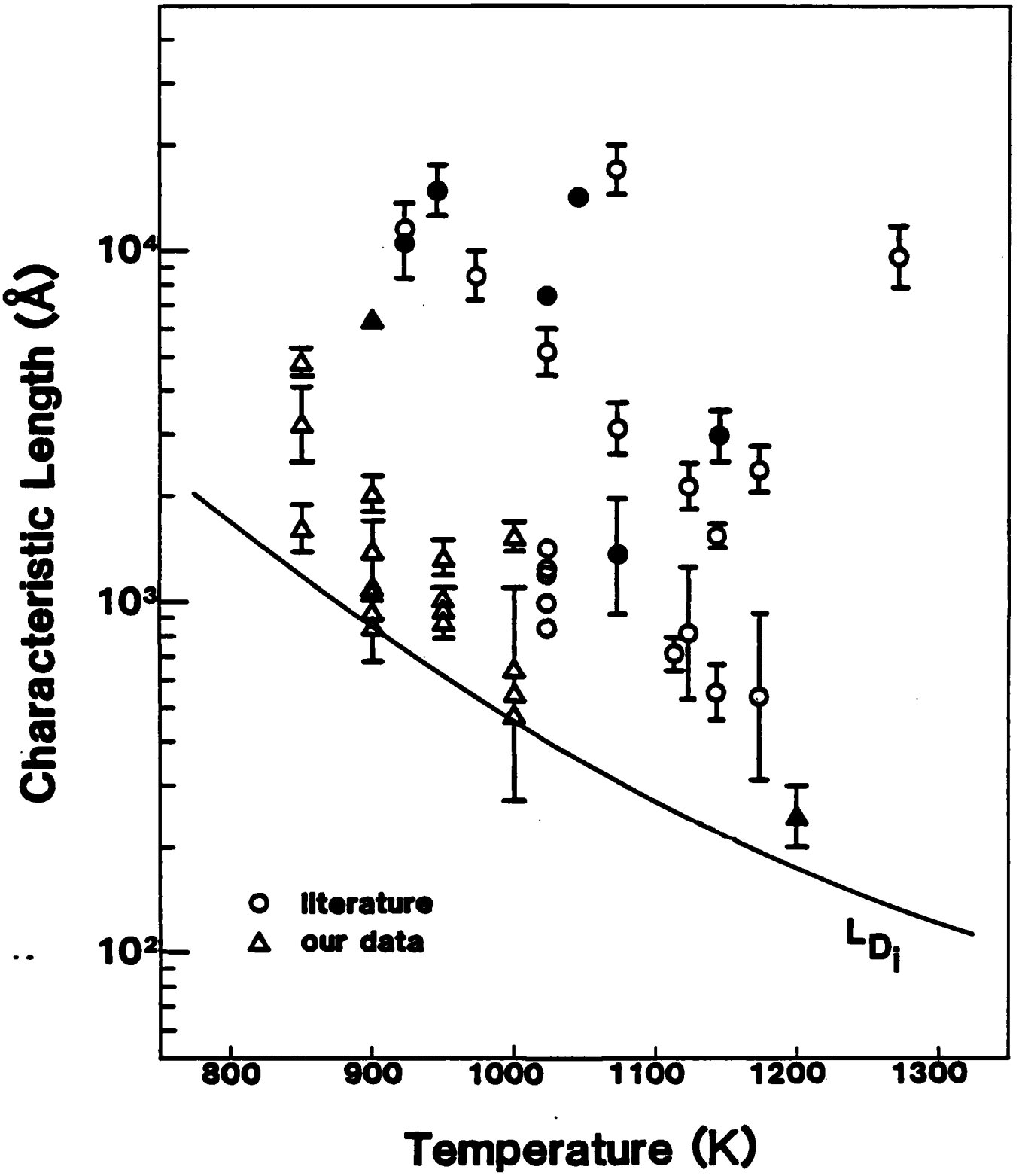

Fig. 1. Comparison of characteristic lengths, L_i, obtained from recent literature[6-9,11-14] and our own experiments with the intrinsic Debye length, L_{D_i}. Open symbols indicate encapsulated samples and closed symbols indicate unencapsulated samples.

$$\alpha = \coth^{-1}\sqrt{\frac{n(0)}{n_i}} \quad . \tag{2}$$

This is the equilibrium profile expected[16] for positively charged impurities in the presence of an electric field due to surface states. Since Cr doped substrates are nearly intrinsic at typical annealing temperatures[17], the intrinsic Debye length, L_{D_i}, was also plotted as a function of temperature for comparison. As can be seen in Fig. 1, all the data points lie above or near the intrinsic Debye length curve. This suggested to us that electric fields due to surface states is the limiting factor in the redistribution of Cr near the surface.

6.2 THERMODYNAMIC MODEL

To examine this possibility in more detail, an equilibrium thermodynamic model was developed for the behavior of Cr near the surface. Basically, this model consists of a fixed surface charge and charged Cr species that can redistribute. Space charge neutrality is assumed so that the surface charge is exactly compensated by the net charge within the crystal. We also assume a surface area that is large with respect to the sample thickness, so that the problem is one dimensional. The free energy of the system is then minimized to produce an equilibrium distribution of Cr.

We first consider the case of only one mobile positively charged Cr ion. The equation for the Helmholtz free energy, F, of the system is given by,

$$F = -\int V(r)N^+(r)dr + 1/2 \int [N^+(r)-N_o^+]\, v(r-r')\, [N^+(r')-N_o^+]\, dr'dr + kT \int N^+(r)\ln N^+(r)dr + \int \mu N^+(r)dr, \tag{3}$$

where V is the potential due to surface states, v is the coulomb potential, μ is the chemical potential, r is the distance from the surface, $N^+(r)$ is the concentration of positive Cr ions, and N_o^+ is the bulk concentration of positive Cr ions. The first integral on the right hand side of Eq. (3) is the energy due to surface states, while the second term corresponds to the coulomb interaction among all charges. The third integral is the entropy contribution to the free energy, and the last term is the chemical potential energy.

To determine the equilibrium situation, Eq. (3) for the free energy was minimized everywhere. This resulted in a nonlinear differential equation which has an exact solution,

$$t = \frac{1}{2} \int_{x}^{x_o} \frac{dy}{y\sqrt{y-1-\ln y}} , \tag{4}$$

where

$$t = \frac{r}{\sqrt{2}\, L_{D_i}} \tag{5}$$

is the normalized distance from the surface,

$$x = \frac{N^+(r)}{N_o^+} \tag{6}$$

is the normalized Cr concentration, and

$$x_o = x(0) \tag{7}$$

is the normalized surface Cr concentration.

The free energy of a system with two Cr charged species capable of redistributing was also examined and is given by,

$$F = -\int V(r)[N^+(r) - N^-(r)]\,dr + 1/2 \int \{[N^+(r) - N_o^+] - [N^-(r)-N_o^-]\}v(r-r')\{[N^+(r')-N_o^+] - [N^-(r')- N_o^-]\}\cdot dr'dr + kT\int[N^+(r)\ln N^+(r) + N^-(r)\ln N^-(r)]dr + \int \mu[N^+(r) + N^-(r)]\,dr, \quad (8)$$

where $N^-(r)$ is the concentration of negative Cr ions. The terms in this equation have the same meaning as in Eq. (3). The solution for Eq. (8) is,

$$t = \frac{1}{2}\int_x^{x_o} \frac{dy}{\sqrt{y^3+(R-1)y^2\ln y+Ry-(R+1)y^2}}, \quad (9)$$

where

$$R = \frac{N_o^+}{N_o^-}. \quad (10)$$

Equations (4) and (9) were solved numerically with the results indicated in Fig. 2. The solution for two Cr ions is shown for R = 0.10. As can be seen, in both cases there is a pileup of $N^+(r)$ at the surface. The profile for two Cr ions, however, has a dip in total concentration due to the depletion of $N^-(r)$ near the surface.

6.3 ANNEALING EXPERIMENTS

To determine how well this model corresponds to an experimental situation, unencapsulated GaAs substrates were annealed in an As overpressure using a boat of InAs held at the same temperature upstream. The InAs has about an order of magnitude

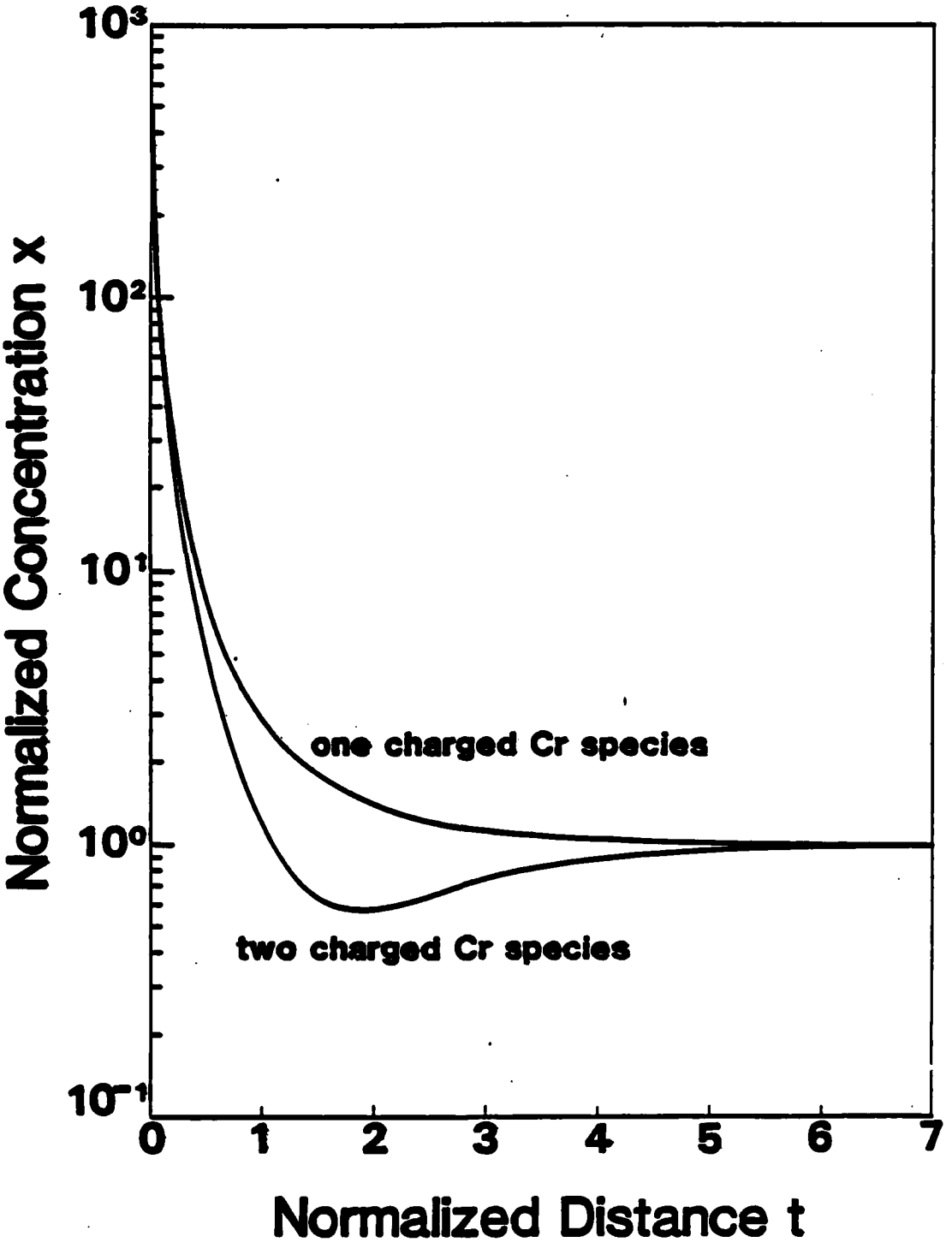

Fig. 2. Comparison of the models for one charged Cr species and two charged Cr species.

higher dissociation pressure than GaAs and has been previously used[18] to stabilize the GaAs surface during annealing. SIMS analyses done on two of these samples are shown in Fig. 3. One of the interesting features of this experimental data is that the characteristic length at 900K is much larger than that at 1200K. This behavior is opposite to that expected for As vacancies or surface strain, but in agreement with the temperature dependence of the intrinsic Debye length. The characteristic length at 900K, however, is about a factor of seven too large. Both samples show a dip below the bulk level in their profiles which is in qualitative agreement with the behavior for two Cr ions as indicated in Fig. 2. The total depletion in the 1200K data, however, is too large to be explained by surface states alone.

The dashed lines in Fig. 3 indicate an attempt to fit Eq. (9) to the experimental data. The ratio R in the model determines the magnitude of the dip when only two charged Cr species are present. If there are neutral Cr atoms, N^0, in the system, however, they will tend to mask the dip since SIMS analysis shows the total Cr concentration. The presence of neutral Cr would have no effect in Eq. (9), since it acts only as an added amount of Cr distributed evenly over the sample. It does give us, however, an added parameter that can be adjusted to fit the experimental data. Also, the condition of charge neutrality allows us to determine the surface charge density, N_s. The fit shown in Fig. 3 for the 900K SIMS data corresponds to an R of 5.8×10^{-4}, a surface charge density, N_s, of $2.8 \times 10^{12} cm^{-2}$, and a neutral Cr concentration, N^0, of

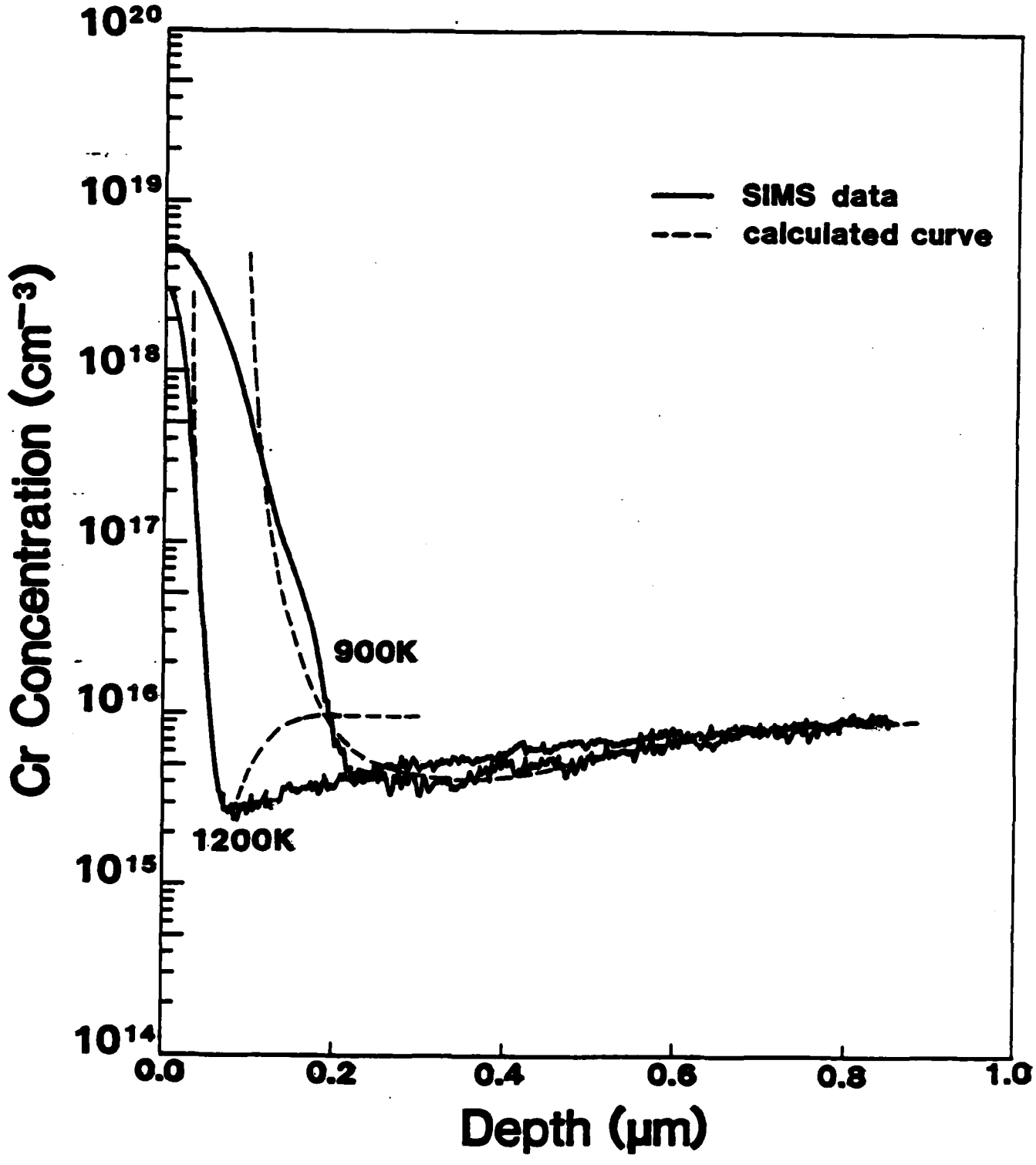

Fig. 3. SIMS data for 900K and 1200K curve fitted to the two charged species model.

$5.9 \times 10^{15} cm^{-3}$. The fit for the 1200K SIMS data corresponds to an R of 2.0×10^{-4}, an N_s of $5.5 \times 10^{11} cm^{-2}$, and an N^0 of $7.4 \times 10^{15} cm^{-3}$. The values of N_s obtained in this process can be compared to a previously determined[15] value at 1000K of $5.1 \times 10^{11} cm^{-2}$.

As shown in Fig. 3 the agreement between the model and the experimental data is only qualitative. The reference point used for the curve fitting process was located at the point where the Cr concentration equaled that of the bulk. The calculated curve obtained by this method indicates that the surface on both samples should begin further in the material. This difference in surface location could be due to the presence of an oxide layer on these samples. The presence of surface artifacts is known to cause matrix effects that affect the accuracy of SIMS analysis near the surface[19,20]. Part of the cleaning process for these samples involved a 5:1:1 H_2SO_4:H_2O_2:H_2O etch, which invariably leaves a thin oxide layer on GaAs surfaces. To support this conjecture, the data indicate a thinner oxide layer for the sample annealed at 1200K which could be explained by greater oxide reduction in a H_2 ambient at higher temperatures.

6.4 APPLIED VOLTAGES

To investigate further the role that electric fields play in the redistribution of Cr at the GaAs surface, samples were annealed with different applied voltages. Due to the surface states present there is a built-in potential at the surface which causes band bending. By applying a voltage to the surface, the built-in electric field can be altered and the amount

of band bending reduced or increased accordingly. If Cr redistribution is electric field dependent, then larger electric fields and band bending due to negative bias should cause larger positively-charged Cr pileups at the surface. Conversely, positive applied voltage should reduce the amount of Cr pileup.

For this purpose an MOS structure was used to apply various voltages to different areas of the substrate during annealing. Anneals were performed from 800 to 1000K for two different time periods at each temperature. The SIMS data shown in Fig. 4 are typical of the results obtained. As can be seen, a negative bias on the MOS structure produced a larger build up of Cr near the surface, while a positive bias reduced the build up of Cr. This behavior is in agreement with the expected behavior for positively-charged Cr. In all the samples, however, the Cr depletion beyond the surface is larger than can be attributed to the effect of surface states.

In conclusion, our results indicate that the electric field caused by surface states is a limiting factor in the redistribution of Cr at the GaAs surface. This is supported by the following observations: (1) The lower limit on the characteristic lengths of the surface regions is very close to the intrinsic Debye length. (2) A thermodynamic model for the redistribution of Cr in the presence of surface states predicts the general shape of the Cr profile. (3) The application of electric fields to the surfaces during annealing changes the magnitude of the Cr build up.

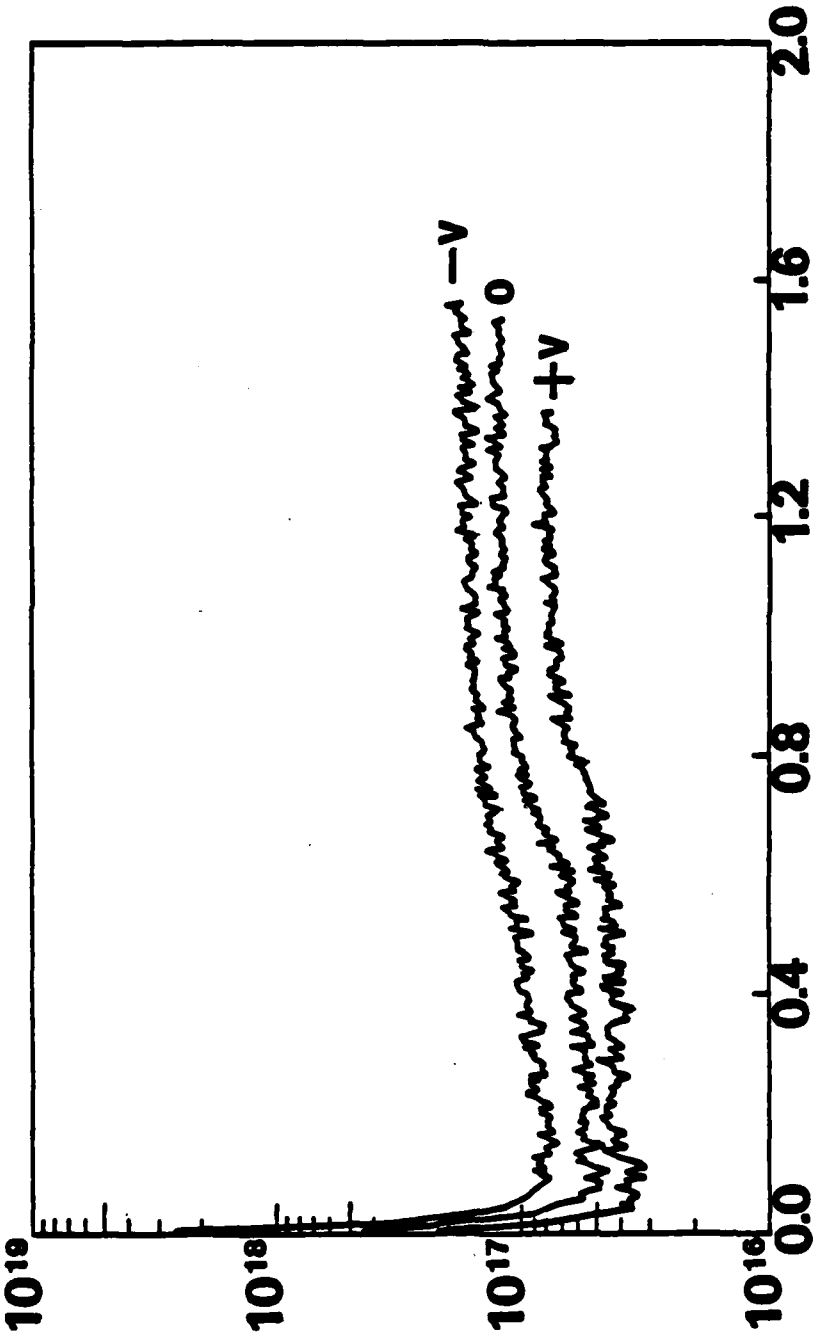

Fig. 4. Cr redistribution as a function of applied voltage.

6.5 REFERENCES

1. V. Eu, M. Feng, W.B. Henderson, and H.B. Kim, Appl. Phys. Lett. 37, 473 (1980).
2. J.B. Clegg, G.B. Scott, J. Hallais, and A. Mircea-Roussel, J. Appl. Phys. 52, 1110 (1981).
3. T.J. Magee, K.S. Lee, R. Ormond, C.A. Evans, Jr., R.J. Blattner, and C. Hopkins, Appl. Phys. Lett. 37, 635 (1980).
4. M. Feng, S.P. Kwok, V. Eu, and B.W. Henderson, J. Appl. Phys. 52, 2990 (1981).
5. A.M. Huber, G. Morillot, N.T. Linh, P.N. Favennec, B. Deveaud, and B. Toulouse, Appl. Phys. Lett. 34, 858 (1979).
6. C.A. Evans, Jr., V.R. Deline, T.W. Sigmon, and A. Lidow, Appl. Phys. Lett. 35, 291 (1979).
7. T.J. Magee, K.S. Lee, R. Ormond, R.J. Blattner, and C.A. Evans, Appl. Phys. Lett. 37, 447 (1980).
8. C.A. Evans, Jr., C.G. Hopkins, J.C. Norberg, V.R. Deline, R.J. Blattner, R.G. Wilson, D.M. Jamba, and Y.S. Park, Semi-Insulating III-V Materials, (Shiva, Orpington, 1980) p. 138.
9. F. Simondet, C. Venger, G.M. Martin, and J. Chaumont, Semi-Insulating III-V Materials, (Shiva, Orpington, 1980) p. 100.
10. H. Rohdin, M.W. Muller, and C.M. Wolfe, J. Phys. Chem. Solids (to be published).
11. Y.S. Park, unpublished data.
12. P.K. Vasudev, R.G. Wilson, and C.A. Evans, Jr., Appl. Phys. Lett. 37, 308 (1980).

13. T.J. Magee, R.D. Ormond, C.A. Evans, Jr., R.J. Blattner, R.M. Malbon, D.S. Day, and R. Sankaran, Appl. Phys. Lett. 38, 559 (1981).

14. P.N. Favennec, M. Gauneau, H. L'Haridon, B. Deveaud, C.A. Evans, Jr., and R.J. Blattner, Appl. Phys. Lett. 38, 271 (1981).

15. K.H. Nichols, R.E. Goldwasser, and C.M. Wolfe, Appl. Phys. Lett. 36, 601 (1980).

16. C.M. Wolfe and K.H. Nichols, Appl. Phys. Lett. 31, 356 (1977).

17. K.H. Nichols, Doctoral Thesis, Washington University, 1979 (unpublished).

18. J. Woodall, H. Rupprecht, C. Ransome, T.I. Chappel, and G. Wicks (unpublished).

19. J.W. Coburn and Eric Kay, Crit. Rev. Solid State Sci. 4, 561 (1974)..

20. Richard E. Honig, Thin Solid Films 31, 89 (1976).

7. CHARGED IMPURITY REDISTRIBUTION DURING EPITAXIAL GROWTH

The incorporation of impurities in epitaxially grown layers of semiconductors and their subsequent redistribution often leads to impurity and and carrier density profiles that are unforeseen and that may be unfavorable for certain applications. Examples are: the formation of high resistance or inverted polarity layers in Gunn devices and the occurence of high conductivity layers close to the semi-insulating substrate in FET's and IC's.

A model has been proposed by Wolfe and Nichols [1,2] to account for some of these effects. In this model the impurities redistribute by diffusion in concentration gradients, drift in the built-in electric field due to surface states and the doping discontinuity at the layer-substrate interface, and finally due to the growth itself. In Figure 1 the geometry of simple planar epitaxial growth is shown. The incorporation and redistribution of impurities are indicated.

In order to model these processes analytically it was necessary to make several restrictive assumptions, some of which were known to be unrealistic.

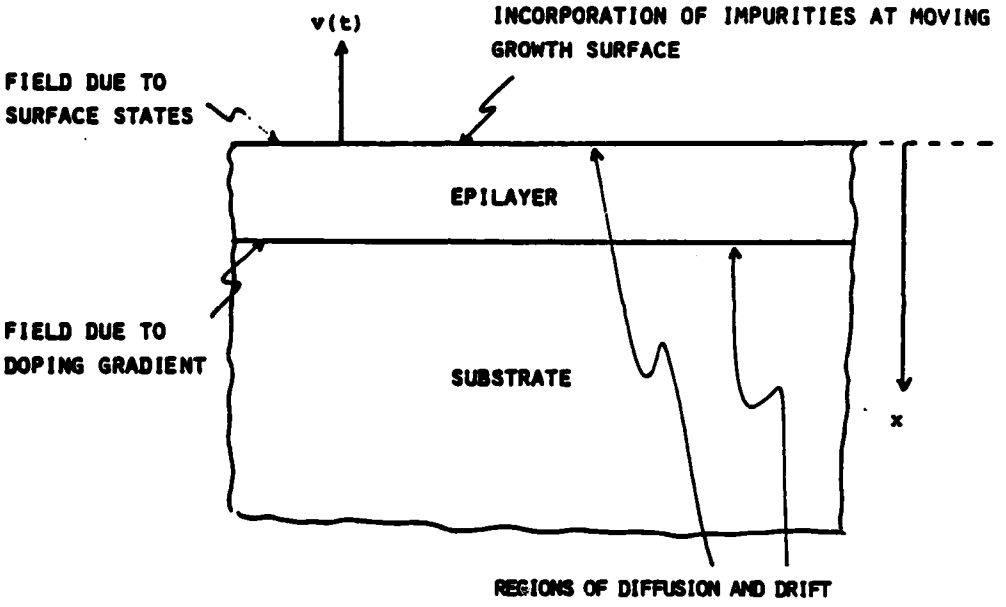

Figure 1 Geometry of an epitaxial layer growing with a velocity v(t) on a thick substrate.

In particular, it was assumed that the impurity distributions were stationary, that no impurity transport crossed the substrate-epitaxial layer interface, and calculation was restricted to epitaxial layer impurity concentrations so small as not to affect the interfacial electric fields. Therefore, although insight could be gained, especially into the usually neglected effect of the field, no quantitative conclusions could be drawn. In the present work we improve the model, renounce the less realistic assumptions and provide for the simulation of a greater variety of growth conditions.

7.1 NONEQUILIBRIUM MODEL

With typical ionic diffusion constants and mobilities, and with epitaxial growth rates of technological importance, the impurity distribution does not reach a steady state during epitaxy. Transport of impurities across the epitaxial layer-substrate interface can be an important, even dominant feature of impurity redistribution. If the doping of the epitaxial layer exceeds the intrinsic carrier concentration, redistribution affects the field. These points are accommodated in the new model. Moreover, although the specific simulations we have carried out assume constant initial and intentional doping and uniform growth rate, the model is designed to accommodate arbitrary nonuniformities in both space and time.

7.1.1 Assumptions

The following assumptions are made:

1. The material is structurally homogeneous (homoepitaxy).
2. The material is nondegenerate, and the electrons and holes are in thermal equilibrium. This implies that the electron and hole concentrations (n and p respectively) satisfy

$$np = n_i^2, \tag{1}$$

where n_i is the intrinsic carrier concentration. From the absence of carrier current, the electron concentration and electric field E are related by

$$E = -\frac{kT}{q}\frac{d}{dx}\ln(n). \tag{2}$$

3. The substrate is effectively semi-infinite, and the potential and field deep in the substrate go to zero.
4. The growth surface is characterized by a fixed surface state concentration. These states are always fully ionized and the field at the surface (x=0) is constant, and determined by the surface charge density σ_s;

$$\varepsilon E(0,t) = \sigma_s, \tag{3}$$

where ϵ is the total dielectric constant.

5. The ambient phase is ideally stirred, so that there is no diffusive impurity flow there.
6. There are no temperature gradients.
7. All impurities are fully ionized. This means that the total doping Q is

$$Q = \sum_k z_k N_k, \tag{4}$$

where N_k is the concentration of the k^{th} impurity I_k, and z_k the number of elementary charges it carries. z_k is +1 for a simple donor and -1 for a simple acceptor.

8. The impurities diffuse by a simple non-reactive mechanism. This implies that the flow J_k of I_k is

$$J_k = -D_k \frac{\partial N_k}{\partial x} + \mu_k E N_k, \tag{5}$$

where the ionic mobility for I_k is given by the Einstein relation;

$$\mu_k = B_k \frac{z_k q}{kT} D_k. \tag{6}$$

B_k is a numerical factor which depends on the diffusion mechanism; it is 1 for interstitial diffusion and 1.27 for a vacancy mechanism [3]. The

continuity equation for I_k is

$$\frac{\partial N_k}{\partial t} = -\frac{\partial J_k}{\partial x}, \tag{7}$$

without generation or recombination terms.

9. The surface conductance, or diffusion velocity, which determines the outdiffusion from the growth surface [4], is much smaller than the growth velocity. The implications of this assumption will be discussed in the next section.
10. The high temperature impurity distribution is frozen in upon cooling.

7.1.2 Incorporation of Impurities at the Growth Surface

We will adopt a simple kinetic model for the incorporation of impurities. The values of the different parameters will depend on the detailed chemistry of the incorporation.

At the interface between the semiconductor and the ambient phase (a gas or a liquid) there is a dynamical process in which atoms leave the solid and go into the ambient, and vice versa. Here we are interested in impurity atoms. We will describe the situation by two opposite flows as illustrated in Figure 2. $N(x,t)$ is the concentration of the impurity in the solid, and $N_a(t)$ the concentration of the impurity in the ambient phase (for the present purpose we leave out the subscript for

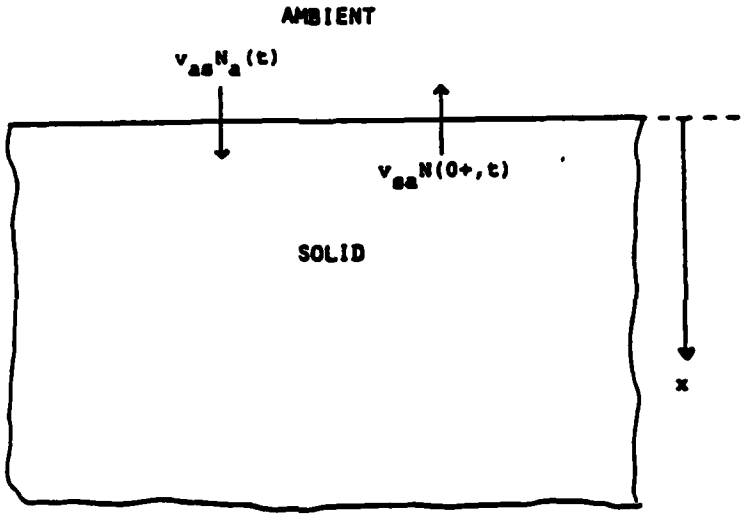

Figure 2 Incorporation of impurities modeled by two opposite flows at the solid-ambient interface.

the impurity type). N_a is assumed to be uniform (assumption 5) due to good stirring. This is really an equivalent concentration, since impurity atoms can be tied up in molecules in the ambient phase. The chemistry of the incorporation is compounded in the flow $v_{as}N_a(t)$. The opposite flow is given by $v_{sa}N(0+,t)$. v_{as} and v_{sa} are surface diffusion velocities, related by the distribution coefficient k; $v_{as}=kv_{sa}$. The net flow just outside the solid is

$$J(0-,t) = v_{as}N_a(t) - v_{sa}N(0+,t). \tag{8}$$

Just inside the solid the flow is due to diffusion and drift;

$$J(0+,t) = -D\frac{\partial N}{\partial x}(0+,t) + \mu E(0+,t)N(0+,t). \tag{9}$$

If the boundary is moving with a velocity v in the -x direction due to growth, and we fix our frame of reference in the moving boundary, we have to add a term $vN_a(t)$ to the right hand side of (8) and a term $vN(0+,t)$ to the right hand side of (9). The current must be continous at x=0, so the boundary condition becomes

$$-D\frac{\partial N}{\partial x}(0,t) + [\mu E(0,t)+v(t)+v_{sa}]N(0,t) = \\ = [v(t)+v_{as}]N_a(t). \tag{10}$$

If there is no diffusion or drift in the solid either, $v(t)=v$, $N(x,t)=N_s$ and $N_a(t)=N_a$, independent of time and position, and (2.10) simplifies to

$$\frac{N_s}{N_a} = \frac{v_{as}+v}{v_{sa}+v}. \tag{11}$$

This is one of the expressions for the effective distribution coefficient k_{eff} reviewed by Kroger [5] in connection with purification. In the case of sufficiently fast growth (assumption 9), we can neglect v_{as} and v_{sa}, and k_{eff} approaches 1.

7.1.3 Critique of the Assumptions

For some of the assumptions the validity is determined by how the growth situation is set up; for others by what types of impurities are used. Most electronically useful materials are nondegenerate especially at growth temperatures. Also, many impurities are fully ionized, even at room temperature. During growth this is true for an even larger class of impurities. If the chemistry of any reactive diffusion mechanism present were well understood, the model could be extended to include this as will be discussed below.

The assumption of constant surface field is an approximation. In principle one should fix neither the potential nor the field at at the surface, but instead seek a self-consistent solution taking into account the

energy dependence of the surface state density, a quantity about which little is known at growth temperature. We shall see below that for common growth conditions the choice of boundary condition made here is not critical.

There is very little information on the surface conductance (or diffusion velocity) of impurities in GaAs. It is known to be very small for Sb diffusing in Ge [4], and a tentative analysis of more recent data on the outdiffusion of Cr from GaAs [6] yields a value of 1μm/h, consistent with our assumption under typical growth conditions.

In most instances the combination of diffusion constants, their temperature dependence, and rapid cooling rate will make the last assumption a very good one.

In summary, the assumptions made here are not very restrictive, and the model should be useful to simulate a wide variety of growth processes. It is to be understood, as indicated in Figure 1, that we model only planar growth. Lateral growth and edge effects are excluded from consideration.

7.1.4 Governing Equations

We make the following normalizations:

1. The position x is expressed in terms of the intrinsic Debye length;

$$L_{Di} = \sqrt{\frac{\varepsilon kT}{q^2 n_i}} . \qquad (12)$$

2. The potential ψ is expressed in terms of the thermal voltage;

$$V_T = \frac{kT}{q}. \tag{13}$$

3. The electric field E is expressed in terms of

$$E_T = \frac{V_T}{L_{Di}}. \tag{14}$$

4. The concentrations n, p, N and Q are expressed in terms of the intrinsic carrier concentration n_i.
5. The time t is expressed in some convenient unit t_o.
6. A diffusion constant D_k is expressed in terms of

$$D_o = \frac{L_{Di}^2}{t_o}. \tag{15}$$

7. The growth velocity v is expressed in terms of

$$v_o = \frac{D_o}{L_{Di}}. \tag{16}$$

8. An impurity flow J_k is expressed in terms of

$$J_o = n_i v_o. \tag{17}$$

9. The conductivity σ associated with the mobile carriers is expressed in terms of

$$\sigma_o = q\mu_n n_i. \tag{18}$$

The electrostatic potential is obtained by solving Poisson's equation, which for a one dimensional nondegenerate semiconductor with the mobile carriers in thermal equilibrium reads [7]

$$\frac{\partial^2 \psi}{\partial x^2} = 2\sinh(\psi_o+\psi)-Q. \tag{19}$$

This will be referred to as the Shockley-Poisson equation. It has been written with partial derivatives although it is, strictly, only valid for a static situation. However, the change in time of the total net doping Q is so slow that an electrostatic approach is valid. The electric field is

$$E = -\frac{\partial \psi}{\partial x}. \tag{20}$$

The boundary conditions for our semi-infinite case are

$$\frac{\partial \psi}{\partial x}(0,t) = -\frac{\sigma_s}{\varepsilon E_T}, \tag{21a}$$

and

$$\psi(\infty,t) = 0. \tag{21b}$$

The constant ψ_o is given by

$$\psi_o = \sinh^{-1}(Q_o/2), \tag{22}$$

where $Q_o=Q(\infty,t)$, independent of time.

From the potential the electron and hole concentrations can be obtained from the relations

$$n = n(\infty)\exp(\psi); \quad p = 1/n. \tag{23}$$

The conductivity is given by

$$\sigma = n+(\mu_p/\mu_n)p. \tag{24}$$

Since we put the origin (x=0) at the moving growth surface the impurity flow is

$$J_k = -D_k\frac{\partial N_k}{\partial x} + z_kB_kD_kEN_k + vN_k. \tag{25}$$

The continuity equation (7) can be written

$$\frac{\partial N_k}{\partial t} = D_k\frac{\partial^2 N_k}{\partial x^2} - z_kB_kD_k\frac{\partial}{\partial x}[EN_k] - v\frac{\partial N_k}{\partial x}. \tag{26}$$

There is an initial condition;

$$N_k(x,0) = N_{k0}(x). \tag{27}$$

The boundary conditions are

$$N_k(\infty,t) = N_k(\infty,0) = N_{k0}(\infty), \qquad (28)$$

and (10) with v_{as} and v_{sa} neglected, and subscript "k" for impurity type reintroduced.

The electric field problem and the redistribution problem constitute a system of two coupled second order differential equations, the former ordinary and intrinsically very nonlinear, the latter partial and nonlinear in the sense that the field depends in a complicated way on all the impurity concentrations. Without making simplifications this calls for numerical treatment. The results will be interpreted analytically in Section 7.3.

7.2 HIGH TEMPERATURE RESULTS

We have chosen, as an initial application of the model, to simulate two epitaxial growth processes in which the effect of interfacial fields might be significant. They are:

1. Growth of lightly doped n-type GaAs on a heavily doped n-type substrate; and
2. Growth of moderately doped n-type GaAs on a compensated semi-insulating substrate.

These processes are interesting because they are representative, respectively, of the technologies for fabricating Gunn effect devices and MESFET material. We have chosen realistic values of initial impurity concentrations and of growth velocity, and what we believe are reasonable estimates of ionic mobilities and diffusion constants [8]. The resulting impurity profiles show some striking inhomogeneities in the distribution of minority species. In the two runs we have simulated in detail the redistribution does not generate harmful conductivity regions. It is possible, however, to recognize combinations of parameters that may prove troublesome in applications as we will give an example of later.

Before discussing the numerical simulations in detail, we can point out some features that they have in common. We assume a high temperature acceptor-like surface state density as calculated by Wolfe and Nichols [2] of $N = 6.3 \times 10^{11} cm^{-2}$. The surface electric field associated with the corresponding charge density is $E = -8.6 \times 10^{4} V/cm$. In Figures 3 to 16 all concentrations are given in units of the measured [9] 1000K intrinsic carrier concentration of $n_i = 6 \times 10^{16} cm^{-3}$, distances in units of the intrinsic Debye length $L_{Di} = 3.2 \times 10^{-2} \mu m$, potential in units of the thermal voltage $V_T = 86.2$ mV, electric field in units of $E_T = 2.66 \times 10^{4} V/cm$, and time in minutes. The resulting

units of diffusion constant and velocity are, respectively, $D_o=1.75x10^{-13}cm^2/s$ and $v_o=1.94\mu m/h$.

We find that, for any reasonable growth velocity, the growth surface rather quickly outruns any effects associated with the layer-substrate interface. This means that the interfacial field rapidly divides into two regions. The chief effect of the field region associated with the growth surface, after the initial growth stage, is to establish a surface concentration profile. If, as is usual, the growth rate is held constant, this profile does not change. At the interface the field will have different effects on minority and majority species. The two regions will be discussed in detail in section 7.3

The separation of the two interfacial field regions has another interesting, and not <u>a priori</u> obvious bearing on the growth surface boundary condition. We have assumed a fixed surface field, and we find that, after the initial stage, the surface potential remains effectively constant (Figures 3 and 11). Obviously the converse would be true as well. Thus, knowledge of the actual and poorly understood high temperature surface state energy distribution which determines the relation between the surface field and potential, is not essential for a realistic simulation.

For some of the impurity profiles ripples occur close to the layer-substrate interface. These are numerical artifacts and are discussed in Chapter 3.

7.2.1 Growth on n^+ Substrate (Table 1)

When the n-type substrate is more heavily doped than the epitaxial layer, the interfacial field points from the substrate to the epitaxial layer (Figures 3 and 4). The substrate is partially compensated, its donors (Figure 5) experience a force pulling them out of the substrate, its acceptors (Figure 6) a force pushing them back. Hence the electric force increases the concentration gradient for the donors while decreasing it for the acceptors. If the diffusion constant for the two species are roughly equal, this means that the outdiffusion of the acceptors lags behind that of the donors, as can be seen in Figure 10. If the acceptors are an order of magnitude more mobile than the donors, we find (Figure 9) that very little charge separation occurs.

The opposite effect is experienced by the donors (Figure 7) and acceptors (Figure 8) grown into the epitaxial layer. Here interfacial field and concentration gradient drive the acceptors in the same, the donors in the opposite directions. The somewhat surprising concentration profiles of Figures 7 and 8 result from this interaction. These profiles can be understood when it is realized that the field is mostly confined in the

Table 1 First n-GaAs growth simulation: Lightly doped epitaxial layer on heavily doped substrate. v=10μm/h.

Impurity No.	Type	Intended/Initial Concentration (cm^{-3})	D (cm^2/s)	B
1	substrate donor	$1x10^{18}$	$1x10^{-14}$	1.27
2	substrate acceptor	$5x10^{17}$	$1x10^{-13}$	1.27
3	incorporated donor	$1x10^{15}$	$1x10^{-14}$	1.27
4	incorporated acceptor	$2.5x10^{14}$	$1x10^{-13}$	1.27

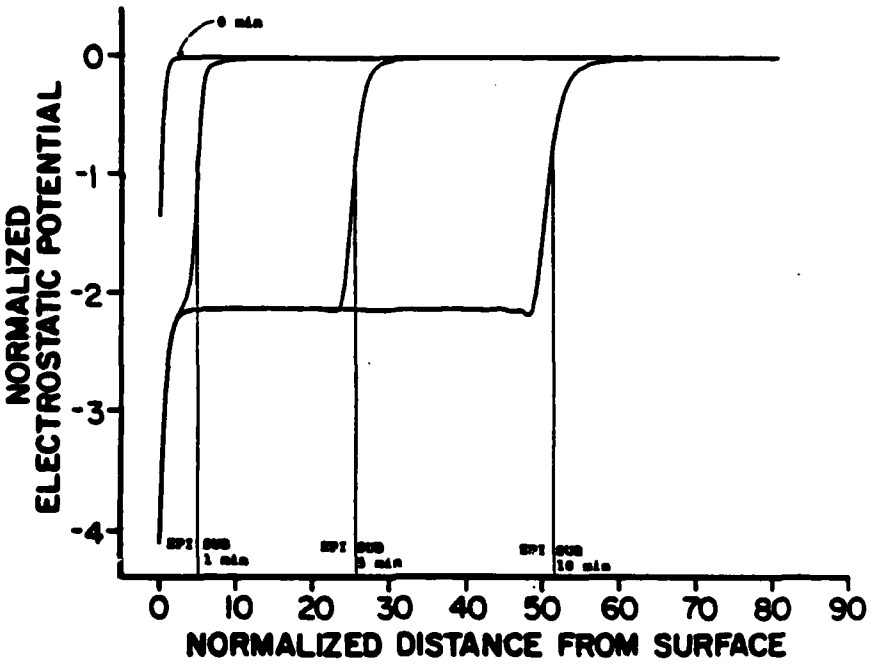

Figure 3 The electrostatic potential for the growth case listed in Table 1, after 0, 1, 5 and 10 minutes of growth.

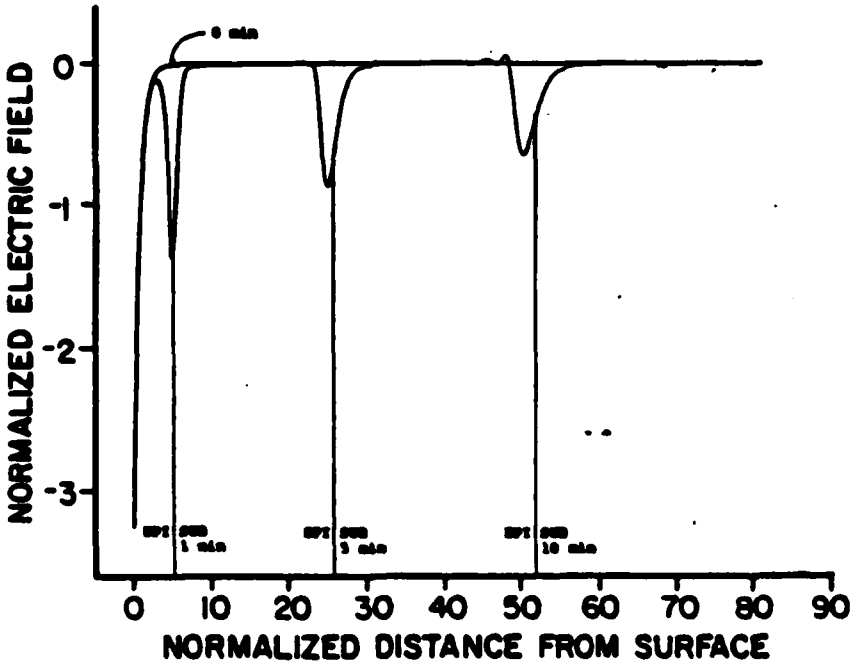

Figure 4 The electric field for the growth case listed in Table 1, after 0, 1, 5 and 10 minutes of growth.

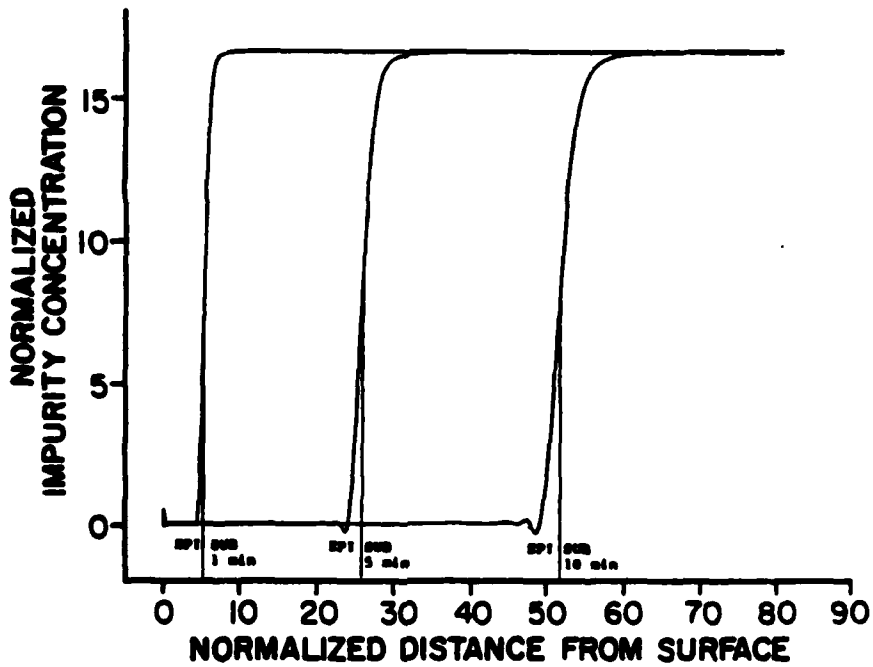

Figure 5 The distribution of impurity 1 for the growth case listed in Table 1, after 1, 5, and 10 minutes.

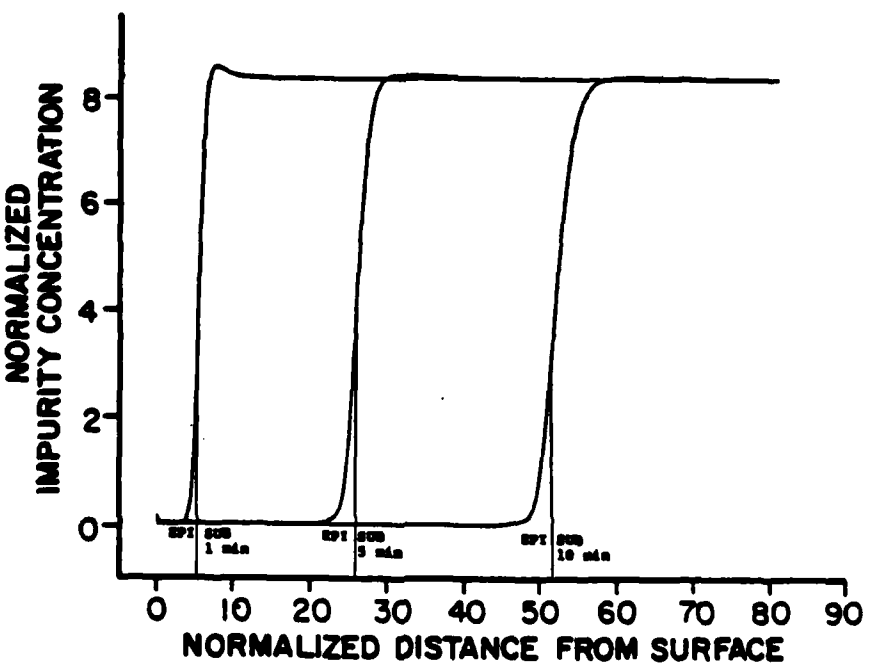

Figure 6 The distribution of impurity 2 for the growth case listed in Table 1, after 1, 5 and 10 minutes.

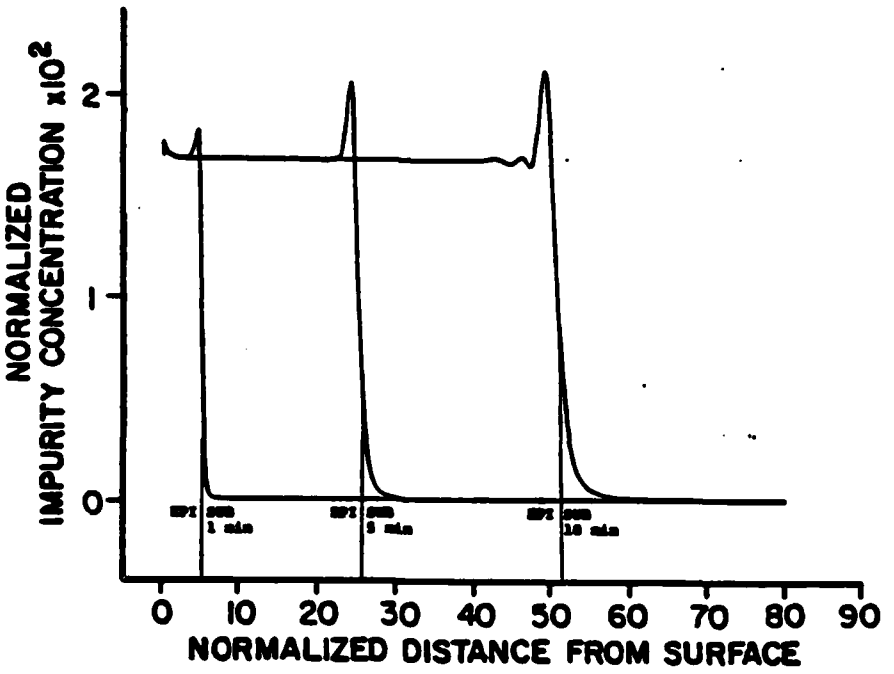

Figure 7 The distribution of impurity 3 for the growth case listed in Table 1, after 1, 5, and 10 minutes.

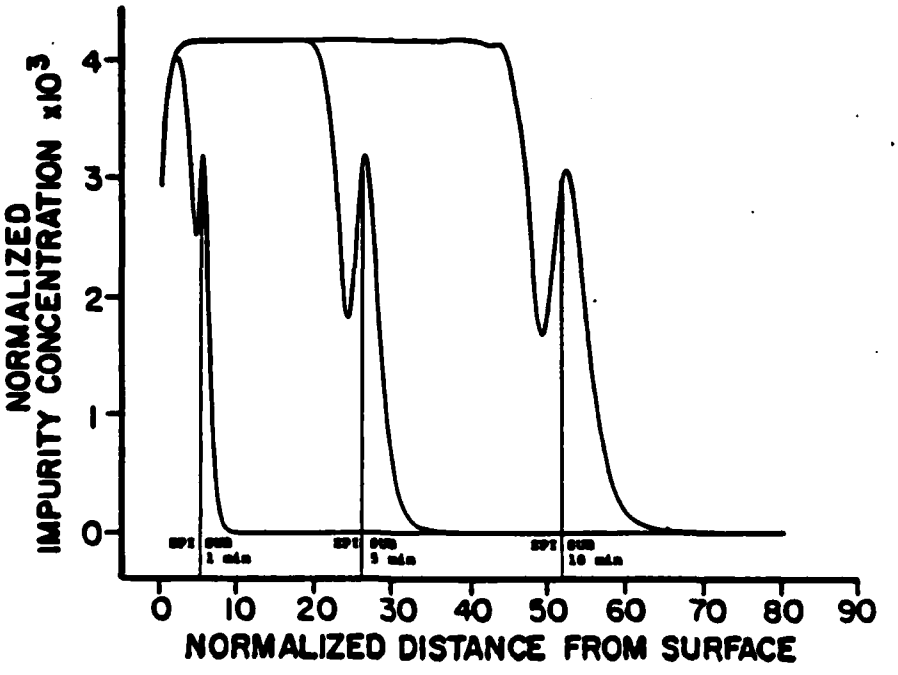

Figure 8 The distribution of impurity 4 for the growth case listed in Table 1, after 1, 5 and 10 minutes.

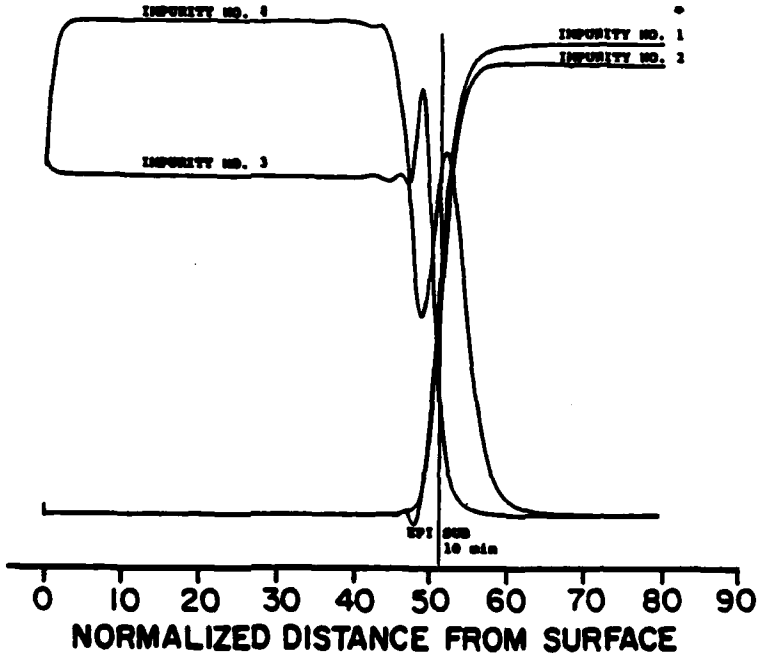

Figure 9 Superposition of the impurity profiles after 10 minutes for the growth case listed in Table 1. (The impurity concentrations are plotted to different scale).

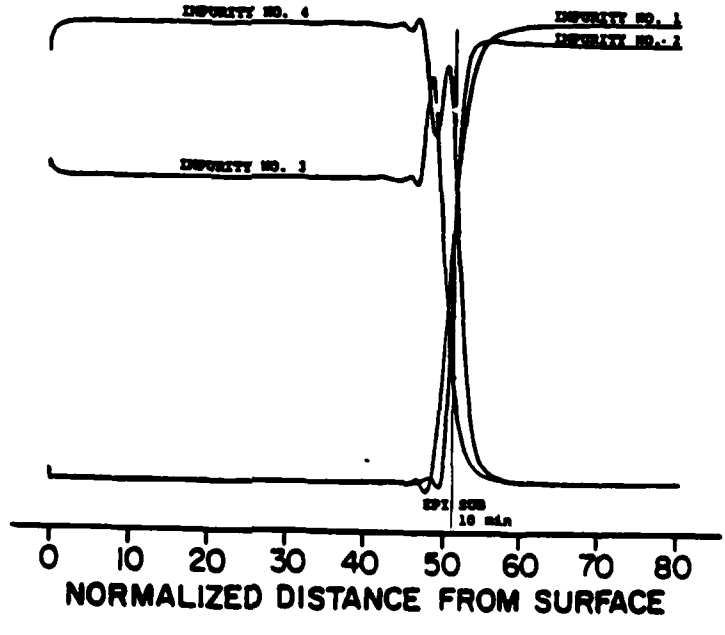

Figure 10 Same as Figure 9 but for a slightly different growth case with $D_1=D_2=D_3=D_4=10^{-14}cm^2/s$.

more lightly doped epitaxial region. Hence, while it influences only the edge of the substrate impurity profiles, it can cause a pile-up of donors, and "eat a hole" into the distribution of acceptors in the epitaxial layer. It is the fact that these impurities are minority species that allows the non-diffusion-like profiles to occur, as we will see in section 7.3.

The dominant effect in this simulation is the field-enhanced outdiffusion of donors from the substrate. Since this species has a concentration from one to three orders of magnitude greater than any other, it blots out the variation of all the minority species, so far as the room temperature carrier concentration is concerned. The effect posited by Wolfe and Nichols [1,2] to account for an interfacial high resistivity layer would be expected to occur if the substrate donors were effectively immobile. Then, outdiffusion of partially compensating acceptors could produce a thin nearly intrinsic or polarization reversed layer. This will be discussed in more detail below.

7.2.2 Growth on a Compensated Semi-Insulating Substrate (Table 2)

We have attempted to model a Cr-compensated substrate as follows: A concentration of $8 \times 10^{16} cm^{-3}$ slowly diffusing ($D=10^{-14} cm^2/s$) residual donors (for example Si) is compensated by $1 \times 10^{17} cm^{-3}$ Cr of which 90% are totally

Table 2 Second n-GaAs growth simulation: Moderately doped epitaxial layer on semi-insulating substrate. v=10μm/h. The substrate is initially perfectly compensated by 9×10^{16} cm^{-3} Cr acceptors which are treated as fixed.

No.	Impurity Type	Intended/Initial Concentration (cm^{-3})	D (cm^2/s)	B
1	substrate donor	8×10^{16}	1×10^{-14}	1.27
2	substrate donor	1×10^{16}	1×10^{-12}	1.00
3	incorporated donor	1×10^{17}	1×10^{-14}	1.27
4	incorporated acceptor	2.5×10^{16}	1×10^{-13}	1.27

immobile substitutional acceptors, 10% mobile ($D=10^{-12}cm^2/s$) interstitial donors. This is not a complete model since, for instance, conversion between interstitial and substitutional Cr is neglected. It will, however, illustrate the effect of, particularly, the surface field on the redistribution of interstitial Cr. In Section 5 a more elaborate and and comprehensive model of Cr in GaAs is presented. The epitaxial layer grown on this substrate incorporates $1x10^{17}cm^{-3}$ slowly diffusing ($D=10^{-14}cm^2/s$) donors and $2.5x10^{16}cm^{-3}$ an order of magnitude more mobile acceptors, giving a net n-type doping of $7.5x10^{16}cm^{-3}$. With this concentration, barely in excess of the intrinsic carrier concentration of $6x10^{16}cm^{-3}$ at 1000K, the epitaxial layer-substrate interfacial potential (Figure 11) and field (Figure 12) are quite small and modify the diffusion only slightly. The chief effect of the impurity redistribution comes from the outdiffusion of Cr-donors (Figure 14) and the preferential indiffusion of acceptors into the substrate (Figure 16), which turn the substrate slightly p-type near the surface. As a result, upon cooling to room temperature, the Debye shielding length is reduced below what it would be without redistribution, and the carrier concentration falls off considerably more steeply as will be illustrated below.

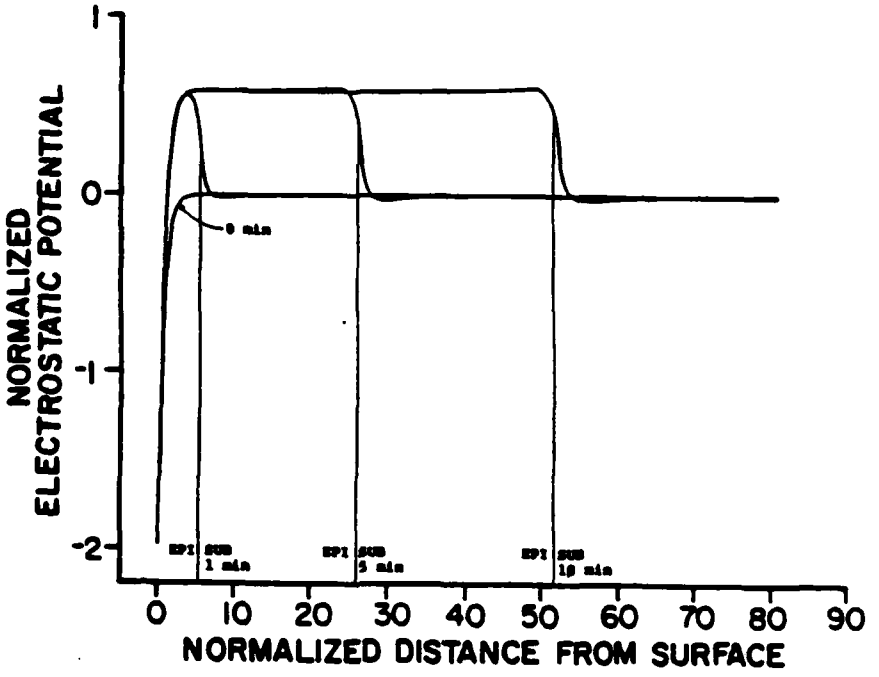

Figure 11 The electrostatic potential for the growth case listed in Table 2, after 0, 1, 5 and 10 minutes of growth.

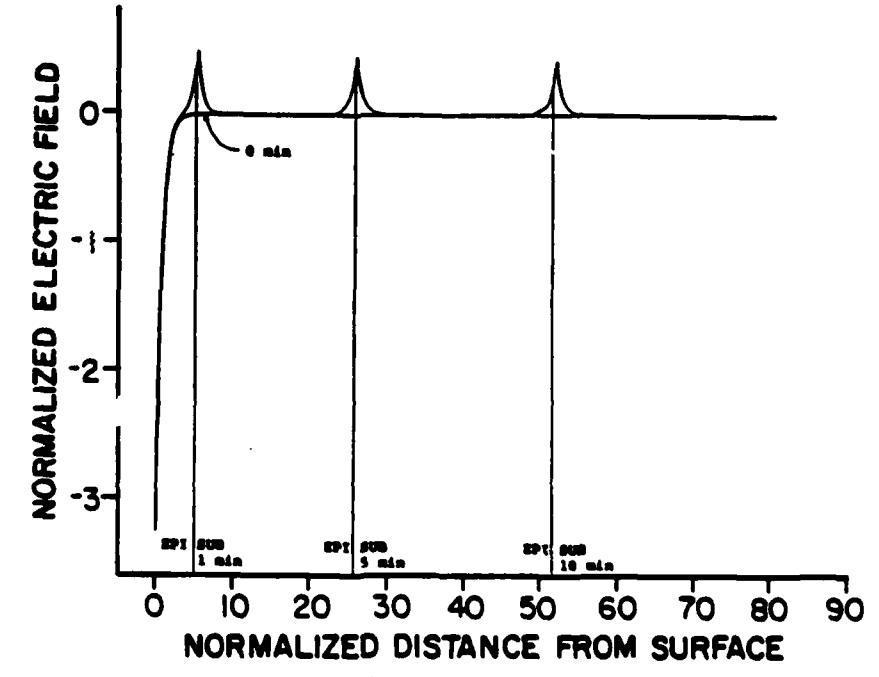

Figure 12 The electric field for the growth case listed in Table 2, after 0, 1, 5 and 10 minutes of growth.

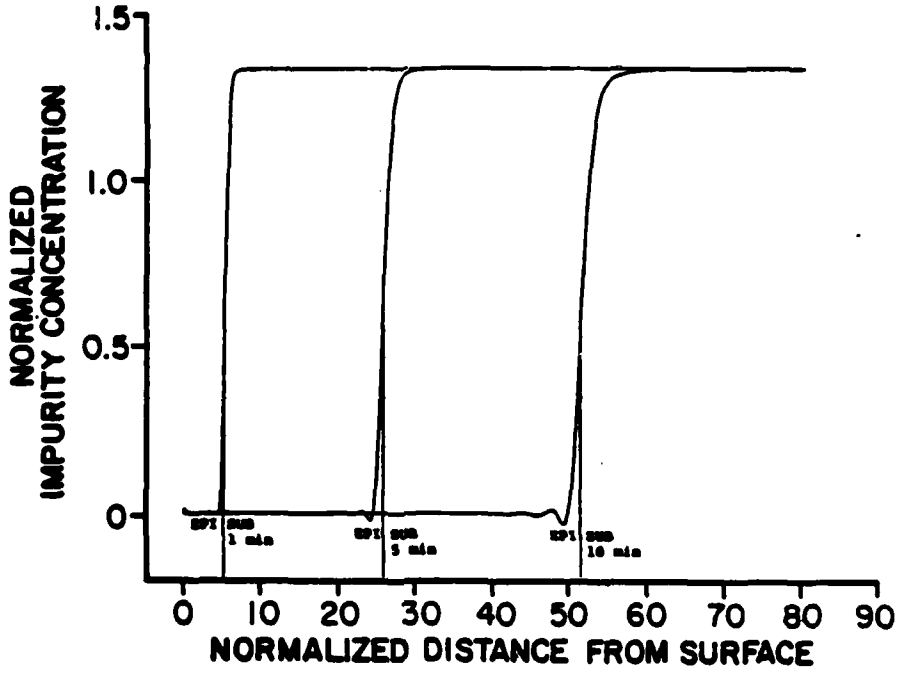

Figure 13 The distribution of impurity 1 for the growth case listed in Table 2, after 1, 5, and 10 minutes.

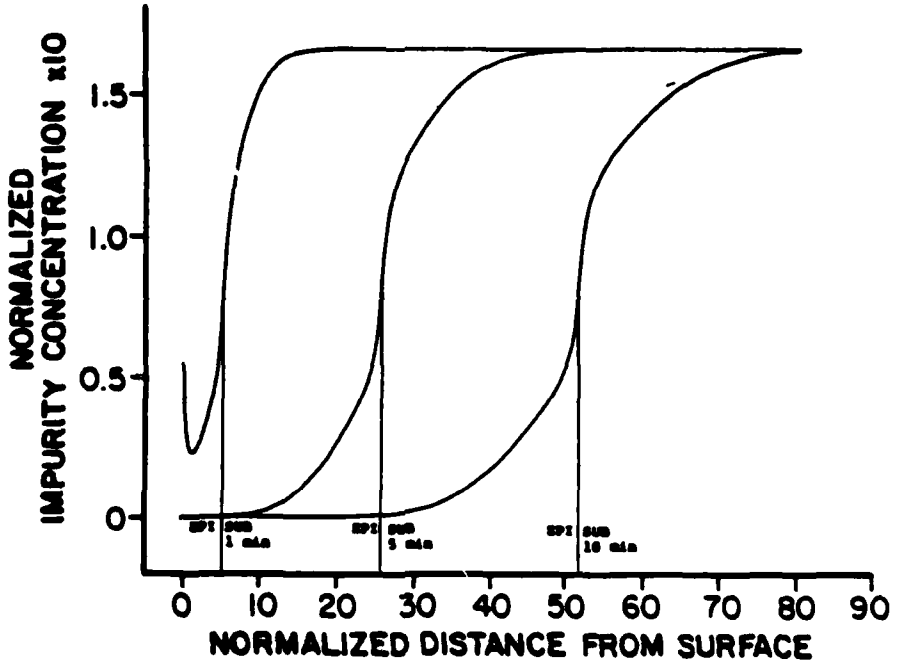

Figure 14 The distribution of impurity 2 for the growth case listed in Table 2, after 1, 5 and 10 minutes.

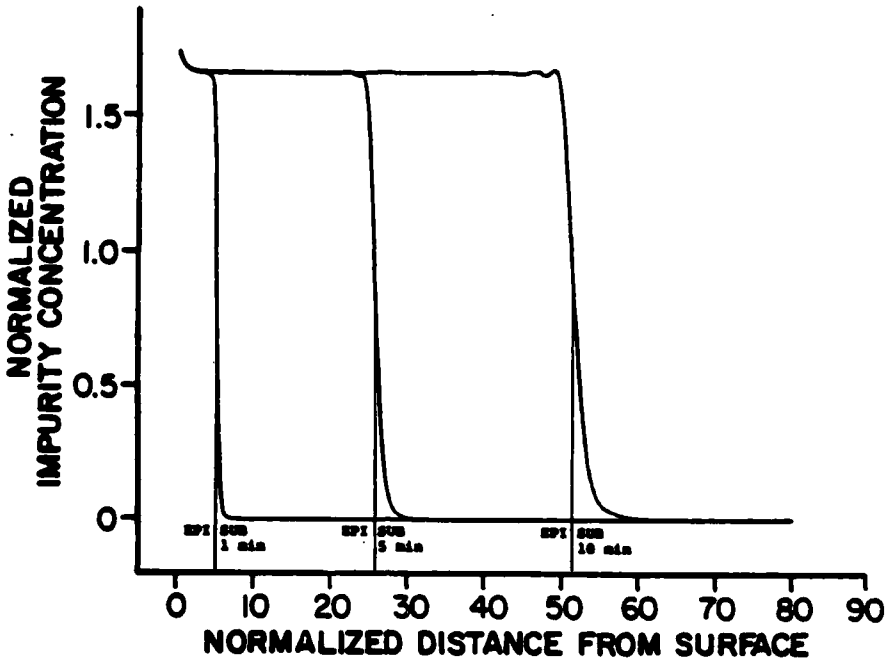

Figure 15 The distribution of impurity 3 for the growth case listed in Table 2, after 1, 5, and 10 minutes.

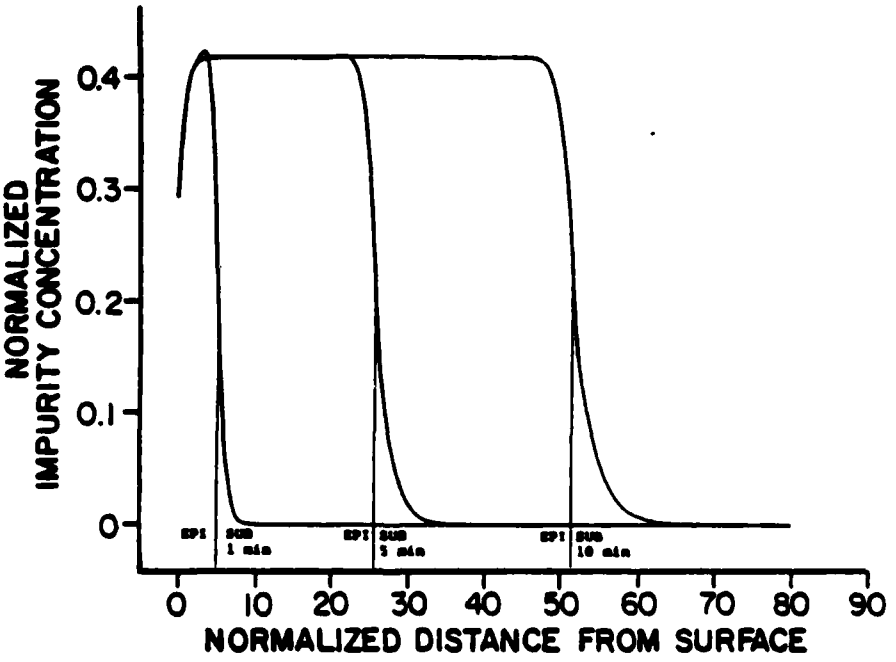

Figure 16 The distribution of impurity 4 for the growth case listed in Table 2, after 1, 5 and 10 minutes.

The epitaxial material for use in MESFET's and IC's is frequently one to two orders of magnitude more lightly doped than our numerical example. Such epitaxial layers are intrinsic at 1000K, and their growth on semi-insulating substrates would occur without an interfacial field. Under these conditions preferential diffusion [10] of donors from a heavily compensated substrate, as shown in Figure 13 could produce a high conductivity layer at the interface.

7.2.3 Room Temperature Potential and Carrier Concentration

As mentioned, neither of the two growth simulations result in any harmful conductivity regions. In the second case the redistribution actually makes the electron concentration in the substrate fall off even faster than without redistribution, as we will see in this section.

We calculate the potential distribution at room temperature (300K) after the high temperature (1000K) redistribution that we studied for 10 minutes in the last two sections. Our interest is to see how the redistribution itself affects the potential $\psi(x)$, and thus the electron and hole concentrations (23). We therefore set the surface field to zero (no charged surface states). We use normalized units as before but now using the room temperature values; position x is expressed in terms of $L_{Di}(300K)=0.34cm$, potential in terms of $V_T(300K)=26mV$,

and concentrations in terms of the intrinsic carrier concentration $n_i(300K)=1.6x10^6cm^{-3}$.

In the first growth case we do not get any harmful conductivity regions since the substrate donors and acceptors redistribute in a similar fashion. However, we also calculate the potential that would result if the substrate donors were fixed but the rest of the impurities had the diffusion properties listed in Table 1. We do not recalculate the redistribution. Instead we use the final distribution of the other impurities computed during the simulation, but assume a fixed substrate donor distribution. This is of course not quite correct since a fixed majority dopant concentration would result in a practically constant field at the interface as opposed to the first simulation, where the peak field decreases (Figure 4). This would, for instance, cause less outdiffusion of the substrate acceptors. Nevertheless, it will give an idea of the result of a rigorous calculation. The result is shown in Figure 17. The material does not become p-type, but there is a considerable lowering of the potential due to the outdiffusion of acceptors from the substrate, and thus an even larger (about four orders of magnitude) lowering of the electron concentration and conductivity in quite a wide region. A rigorous calculation would make the effect less pronounced.

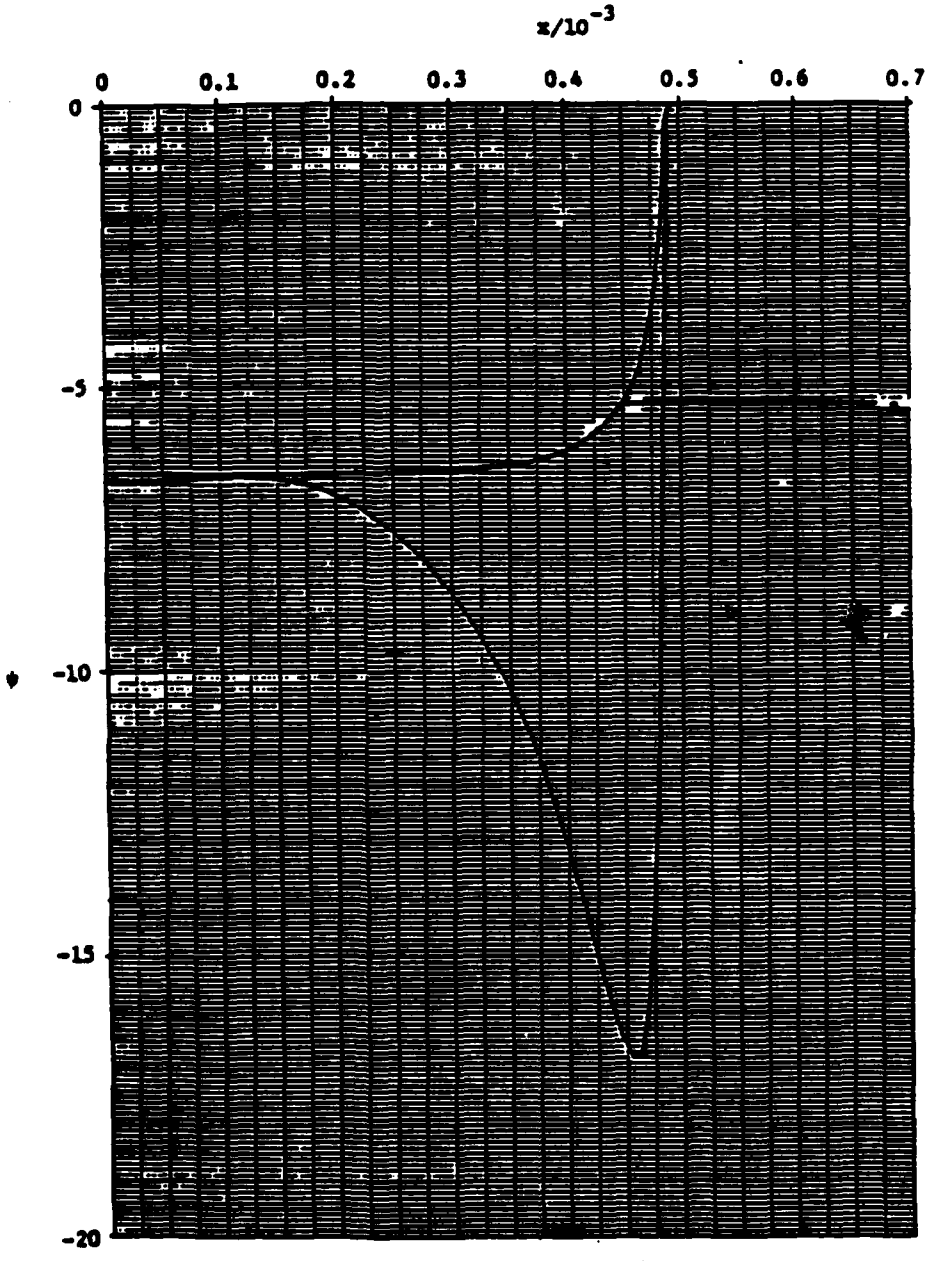

Figure 17 Room temperature potential ψ as a function of the distance x from the growth surface resulting from the first growth simulation (Table 1). The material would be intrinsic for ψ=-26.
a. with no redistribution.
b. after redistribution.

When we do the calculation for the potential at room temperature resulting from the second growth simulation we get the peculiar result shown as curve b in Figure 18. Curve a is the potential for no redistribution and this falls off very slowly (note that the abscissae is lg(x). In the relatively moderately doped epitaxial layer (lg(x)<-3.31), where the fast outdiffusion of donors does not affect the total doping, curve a and b coincide as expected. For -3.3<lg(x)<-3.1 curve b falls off much faster than curve a due to the uncovered acceptors in the substrate. This means that the conductivity falls off faster than "expected" which is advantageous in this case. Beyond lg(x)=-3.1 the result is incorrect due to errors in the concentrations that we have allowed in the simulation. For lg(x)<-3.04 the total net doping should be practically zero since at lg(x)=-3.04 the total net doping ceases to be negative. However, the numerical treatment produces a small positive doping in the region -3.04<lg(x)<-2.70 and a small negative doping in the region -2.70<lg(x)<-1.41. At room temperature these errors get effectively much larger since we measure the concentrations relative to the intrinsic one. The reason that similar effects do not occur in the first simulation is that there the material is more heavily doped, and the errors in potential are essentially inversely proportional to the doping

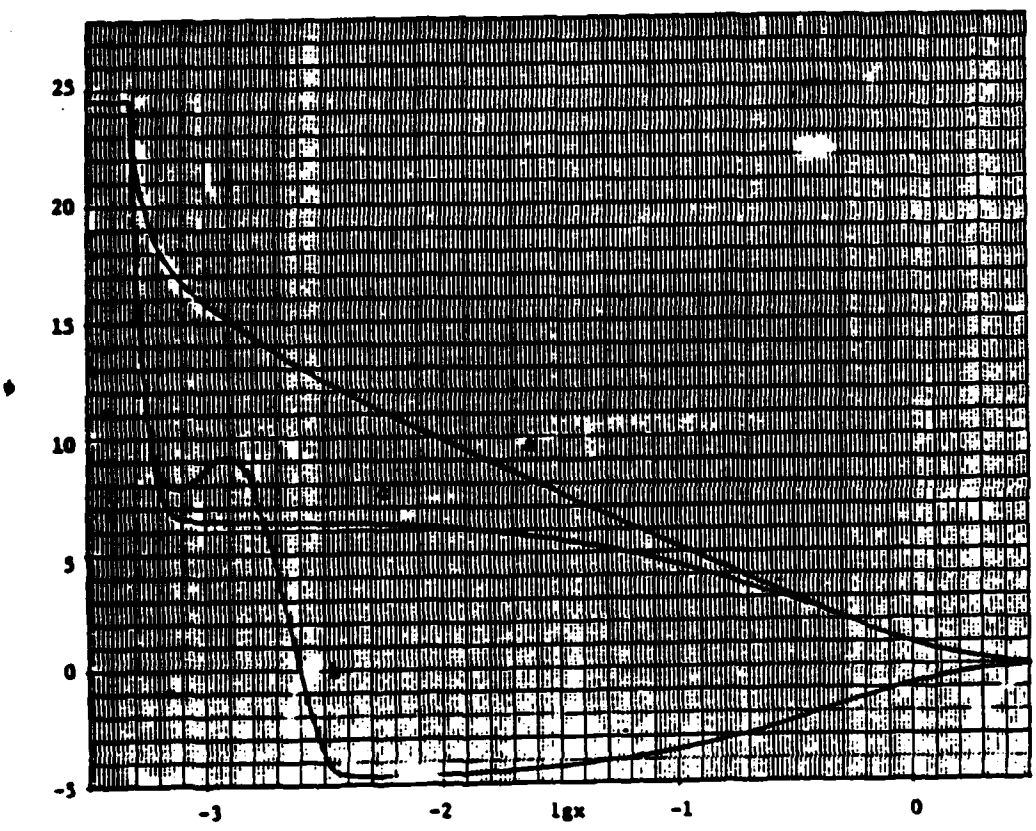

Figure 18 Room temperature potential ψ as a function of the distance x from the growth surface resulting from the second growth simulation (Table 2). The material is intrinsic for $\psi=0$.

a. with no redistribution.
b. after redistribution. Net doping set to zero for lgx>-2.70.
c. after redistribution. Net doping set to zero for lgx>-3.04.

Curve c shows the result when we require the doping to be zero beyond the point lg(x)=-3.04, where the simulation says that the doping becomes positive (which it should not). This curve looks more realistic; it coincides with curve b in the substrate close to the interface, where the p-conversion is most pronounced, while coinciding with curve a deep in the substrate far away from the region of redistribution. The region where curve b and c coincide shows that the potential actually falls off much faster than it would in the case of no redistribution.

7.3 QUALITATIVE ANALYTICAL INTERPRETATION

The numerical results clearly illustrate that the problem separates into two practically independent pieces, one associated with the surface and the other with the layer-substrate interface. In this section we attempt an analytical interpretation of the results based on this observation.

7.3.1 Surface Impurity Profiles

In the simulations presented, using a constant growth velocity, the surface profiles very quickly become stationary. The choice of growth velocity, ionic mobility and surface electric field allows us to solve the stationary problem approximately. Assuming steady state and applying the boundary condition (10), again neglecting v_{as} and v_{sa}, the continuity equation (26)

becomes (suppressing subscripts for the impurity type)

$$\frac{dN}{dx} - [zBE+\frac{v}{D}]N = -\frac{v}{D}N_a. \tag{29}$$

The solution of this is straightforward;

$$N(x) = N_a e^{-zB\psi(x)} \int_0^\infty e^{-\xi} e^{zB\psi(x+\frac{D}{v}\xi)} d\xi. \tag{30}$$

Here we have used the fact that the surface profile is practically independent of the interfacial impurity profile by extending the upper limit of integration to infinity. $zB\psi(x+(D/v)\xi)$ goes to zero exponentially as ξ becomes large. The largest contribution to the integral comes from small ξ. We make the approximation

$$\psi(x+\frac{D}{v}\xi) \approx \psi(x) - E(x)\frac{D}{v}\xi, \tag{31}$$

which is expected to be better the smaller $zBDE(x)/v$ is compared to 1. With this approximation we get

$$N(x) \approx N_a[1+\frac{zBE(x)}{v}]^{-1}. \tag{32}$$

This is the same result as the zeroth order approximation in a perturbation scheme of (29), in which dN/dx is considered the perturbation. In Figures 19 and 20 the surface profiles of the incorporated donors and acceptors

(impurity 3 and 4 in Table 1, respectively) are plotted together with the prediction of equation (32) using the numerical results for the electric field. This is therefore also a check of the consistency. The agreement is good in both cases exept for the donors in an extremely thin surface layer. Mathematically this is real (a so called boundary layer [11]), but it is of no physical importance in this case since it is only about a lattice parameter thick.

The treatment here is basically the same as in [1], but we use the boundary condition (10), and make the approximation (31) which appears to be valid for large growth velocity.

7.3.2 Interfacial Region

After the interface has separated from the surface it can be treated as a moving interface between two semi-infinite regions, in which case it makes more sense to fix the frame of reference at the interface. The continuity equation then reads

$$\frac{\partial N}{\partial t} = D\frac{\partial^2 N}{\partial x^2} - zBD\frac{\partial}{\partial x}[EN]. \qquad (33)$$

If N describes the concentration of the majority species, and charge neutrality is assumed so that

$$E = -z[4+N^2]^{-\frac{1}{2}}\frac{\partial N}{\partial x}, \qquad (34)$$

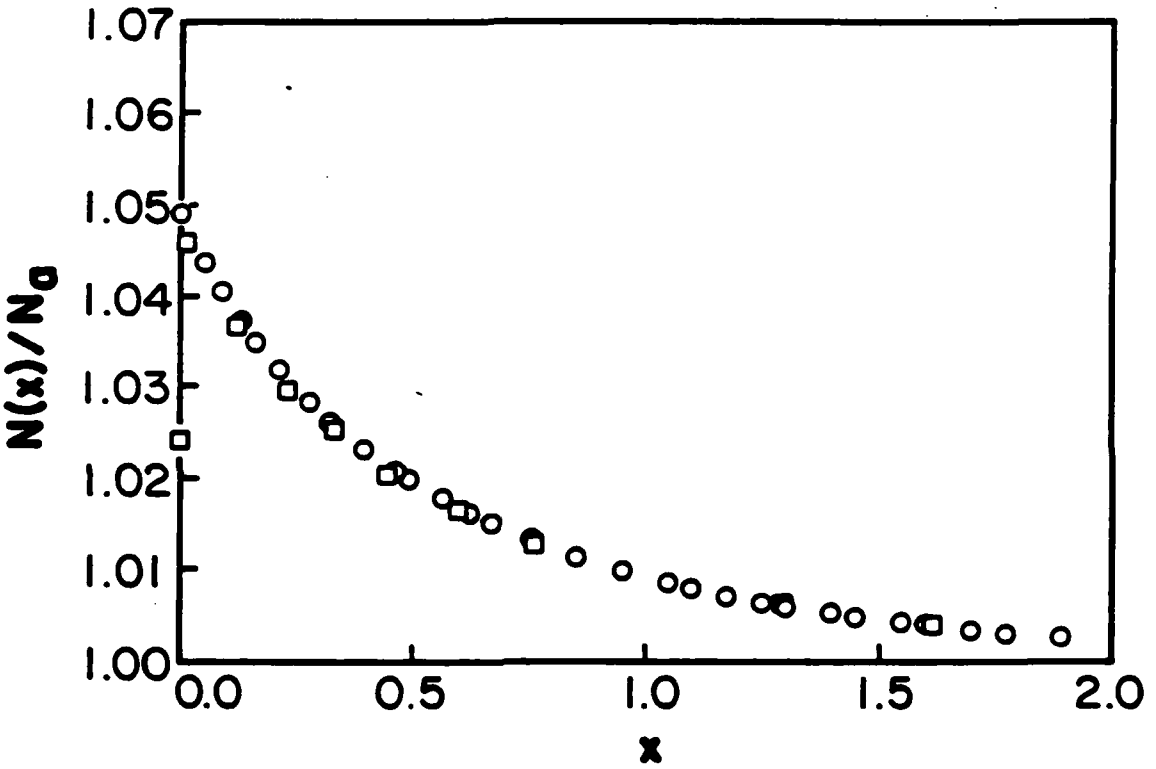

Figure 19 Surface profile of impurity 3 for the growth case listed in Table 1.
□ numerical result for the concentration.
○ (32) using the numerical result for the electric field.

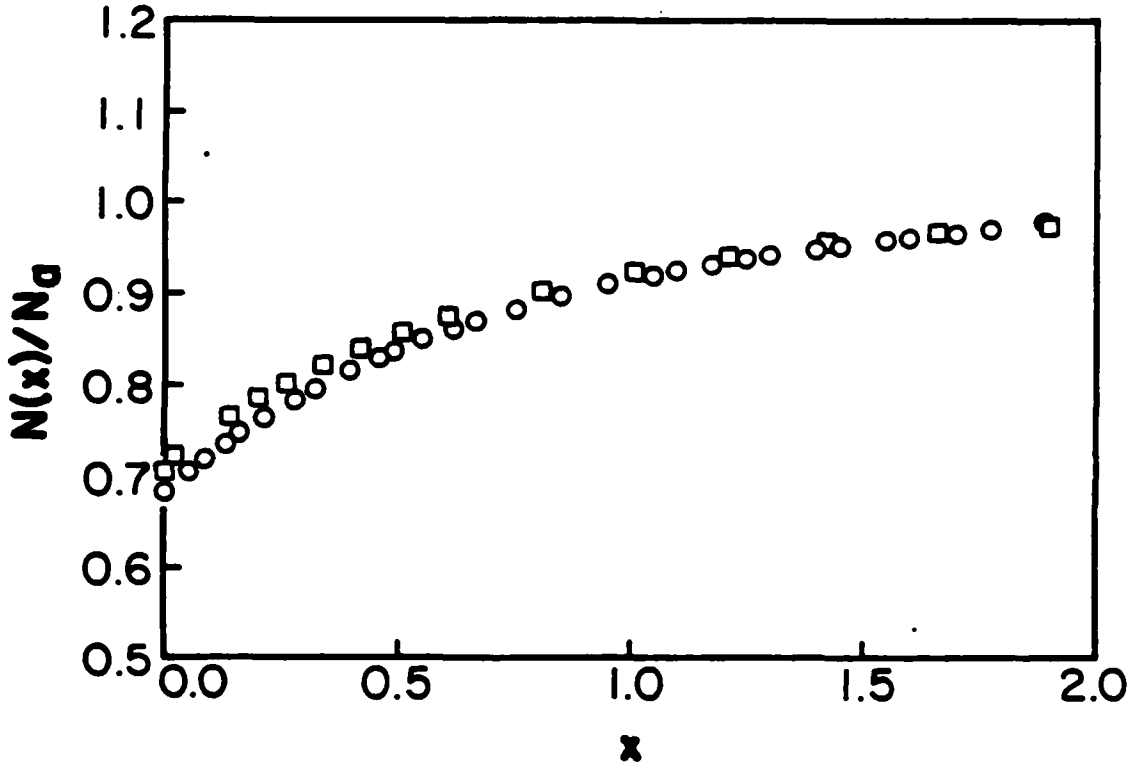

Figure 20 Surface profile of impurity 4 for the growth case listed in Table 1.
▫ numerical result for the concentration.
o (32) using the numerical result for the electric field.

one can [12] rewrite (33) as a diffusion equation;

$$\frac{\partial N}{\partial t} = \frac{\partial}{\partial x}[D'(N)\frac{\partial N}{\partial x}], \tag{35}$$

with the concentration dependent diffusion constant

$$D'(N) = D[1+z^2BN(4+N^2)^{-\frac{1}{2}}]. \tag{36}$$

We see that the diffusion constant is smaller for smaller concentration. This is observed in Figure 5 as the concentration gradient being steeper in regions of lower concentration.

If N describes a minority species, the field is practically independent of N and is determined by other species. We could treat the drift term in (33) as a perturbation. Assuming constant initial doping N_s in the substrate ($x>0$) and constant intentional doping N_e of the epitaxial layer ($x<0$), the zeroth order solution is [13]

$$N_0(x,t) = \frac{1}{2}[N_s+N_e] + \frac{1}{2}[N_s-N_e]\mathrm{erf}(\frac{x}{2\sqrt{(Dt)}}). \tag{37}$$

The first order correction N_1 is obtained by solving the equation

$$\frac{\partial N_1}{\partial t} = D\frac{\partial^2 N_1}{\partial x^2} - zBD\frac{\partial}{\partial x}[EN_0]. \tag{38}$$

Just by looking at the structure of this equation, some information can be extracted. (38) is a diffusion equation for N_1 with a known generation term $-zBD(\partial(EN_0)/\partial x)$. For the donors in Figure 7 it will act as a source, while for the acceptors in Figure 8 it will act as a sink on the epitaxial layer side of the interface, leading to the observed interfacial structure.

The separation of the problem observed in our numerical treatment suggests that one would get a good picture of the redistribution if one treated the surface and interface problem separately when the situation is one of sufficiently fast growth and constant intentional doping of the epitaxial layer. This is certainly a common situation and would allow a substantial reduction in excecution time due to the absence of moving boundaries in such an approach.

7.4 QUASI-CHEMICAL REACTIONS

It is well known that many impurities participate in reactions which greatly influence the redistribution. Since GaAs is of particular interest to us, a good example is Zn, which diffuses interstitially, but can get captured by Ga vacancies. If the reactions are in local equilibrium the analysis is simplified since the mass action laws give relations between impurity concentrations that are valid locally. Zn diffusion has been analysed rather successfully in this way [8], leading to a

concentration-dependent diffusion constant. However, if the reactions are not in equilibrium, we have to solve the continuity equations with proper generation and recombination terms included. This will enhance the coupling between the redistribution of the different species that already exists in our model through the electric field. Nonlinearities will be introduced which will necessitate a less-than-implicit numerical scheme.

Extension of our model would, in principle, be straightforward, but it is conceivable that in practice one might run into problems with stability and convergence in the numerical implementation. The primary problem, however, is to model what reactions go on, and at what rate. In an attempt to do so, we started out to study the diffusion of Cr in GaAs. This system is of technological importance since it can produce semi-insulating material useful as substrates for IC's. It is particularly interesting since Cr exhibits remarkable redistribution behavior in GaAs, unlikely to be accounted for by a simple diffusion mechanism. The problem proved to be a complicated one, and is at this point not sufficiently well understood to be studied by our general numerical redistribution model.

7.5 CONCLUSIONS

In this work some aspects of impurity redistribution in semiconductors during processing at elevated temperatures has been discussed.

We have presented a general nonequilibrium model for the field-assisted diffusion during epitaxy and annealing. It was demonstrated that even under very simple epitaxial growth conditions, ionic redistribution can produce fairly complicated impurity concentration profiles, particularly for minority species. We also discussed how harmful conductivity regions could come about as a result of outdiffusion *from* the substrate. The model should prove useful in simulating a wide variety of situations since the numerical implementation contains options such as inhomogeneous substrate doping, depletion of the ambient and changes of growth rate. In addition, it appears straightforward to include reactions, which would be particularly interesting when trying to simulate redistribution during post-implantation annealing. Under some simple epitaxial conditions, improved execution speed could be accomplished by treating the surface and interface regions separately.

7.6 REFERENCES

1. C.M. Wolfe and K.H. Nichols, "Impurity Gradients Caused by Surface States and Substrate Doping in Epitaxial GaAs", Applied Physics Letters 31, 356 (1977).

2. C.M. Wolfe and K.H. Nichols, "Impurity and Defect Behaviour in High-Purity Epitaxial GaAs", Final Scientific Report No. 59356-6, Washington University, St. Louis, 1979.

3. L.A. Girifalco, Atomic Migration in Crystals, Blaisdell Publishing Company, New York, Toronto, London, 1964, pp. 92.

4. R.C. Miller and F.M. Smits, "Diffusion of Antimony Out of Germanium and Some Properties of the Antimony-Germanium System", Physical Review 107, 65 (1957).

5. F.A. Kroger, The Chemistry of Imperfect Crystals, 2nd ed., Vol. 1, North-Holland, Amsterdam, 1973.

6. Jiro Kasahara and Naozo Watanabe, "Redistribution of Cr in Capless-Annealed GaAs under Arsenic Pressure", Japanese Journal of Applied Physics 19, L151 (1980).

7. William Shockley, Electrons and Holes in Semiconductors, Van Nostrand, Toronto, New York, London, 1950, p. 306.

8. H.C. Casey, Jr., "Diffusion in the III-V Compound Semiconductors", in D. Shaw (ed.), Atomic Diffusion in Semiconductors, Plenum Press, London and New York, 1973, p. 351.

9. K.H. Nichols, Camellia M.L. Yee and C.M. Wolfe, "High-Temperature Carrier Transport in n-Type Epitaxial GaAs", Solid-State Electronics 23, 109 (1980).

10. C.M. Wolfe, A.G. Foyt and W.T. Lindley, "Epitaxial Gallium Arsenide for High-Efficiency Gunn Oscillators", Electrochemical Technology 6, 208 (1968).

11. Carl M. Bender and Steven A. Orszag, Advanced Mathematical Methods for Scientists and Engineers, McGraw-Hill, New York, 1978, Chapter 9.

12. Alan H. Marshak and Ritu Shrivastava, "Calculation of the Electric Field Enhancement for a Degenerate Diffusion Process", Solid-State Electronics 25, 151 (1982).

13. H.S. Carslaw and J.C. Jaeger, "Conduction of Heat in Solids", 2nd ed., Clarendon Press, Oxford, 1959.

8. INCORPORATION OF AMPHOTERIC IMPURITIES

The Group IV impurities, namely C, Si, Ge, Sn, and Pb, are expected to behave either as donors or acceptors in GaAs, depending on whether they substitute on Ga or As sites. It is well known that the relative incorporation as donors and acceptors is different for different elements, growth techniques, and growth conditions (e.g. growth temperature, III/V ratio, etc.) Much of this information has come from doping experiments which rely on Hall effect data and the tacit assumption that only changes in dopant incorporation are important in determining changes in carrier concentration and 77 K mobility. The direct measurement of the concentrations of individual impurity species would afford a clearer picture of impurity incorporation, particularly at low concentrations. To this end, photothermal ionization spectroscopy (described in detail by Stillman et al. (1977)), and low temperature photoluminescence have been used to measure the concentrations of donors and acceptors, respectively, in high purity GaAs prepared by a wide variety of growth techniques. The relative donor concentrations were determined from the 1s-2p(m=-1) peak amplitudes at high magnetic fields using the identifications of Wolfe et al. (1976) for Pb, Sn, Se, and of Low et al. (1982 a and b) and Ozeki et al. (1977) for X_1=Si, X_2=S, and X_3=Ge. The relative acceptor concentrations were estimated from the relative amplitudes of the (D°-A°) peaks at 2 K under 1 mW excitation from an Ar^+ laser, using the identifications in Ashen et al. (1975). Absolute donor and acceptor concentrations could then be determined using the total N_D and N_A calculated, under the assumption that the shallow impurities dominate the ionized impurity scattering, from the 77 K Hall effect data by the method of Wolfe et al. (1970).

8.1 LIQUID PHASE EPITAXY

The residual shallow impurities in high purity undoped LPE samples from seven different sources were measured (see Skromme et al. 1983a). The photothermal ionization and photoluminescence spectra for the Hewlett Packard sample are shown in Fig. 1 (a) and (b), and are typical of the spectra of the other samples measured. The characteristic LPE residual donors, Pb, X_1=Si, Sn, and X_2=S are present at concentrations of 0.28, 0.22, 0.12 and 1.54 x10^{14}cm^{-3} respectively. The dominance of X_2=S is usual for both graphite (Skromme et al. 1983a) and silica (Cooke et al. 1978) boat grown LPE GaAs. The characteristic LPE residual shallow acceptors, C, Mg, Si and Ge are present at approximate concentrations of 0.13, 0.18, 1.0 and 0.03 x10^{14}cm^{-3} respectively.

The photothermal ionization and photoluminescence data for the LPE samples measured consistently indicates that the Group IV impurities Pb and Sn incorporate preferentially as donors while Si, Ge, and C incorporate preferentially as acceptors. The incorporation of Pb in GaAs grown by $AsCl_3$-VPE is small (Wolfe et al. 1976a) and although Pb doping experiments have associated Pb with a peak coincident with that of Mn deep acceptors, it seems likely that this can be explained by traces of Mn present in the Pb dopant (Bebb et al 1972), and that Pb may not incorporate as an acceptor in GaAs. It should be noted however that the Mn acceptor peak was observed in most of the LPE samples measured. The Pb and Sn donor peaks were sometimes larger in the spectra of the other LPE samples than that shown in Fig. 1 but were always dominated by sulfur. In the two Cornell LPE samples in which Sn was most prominent (nearly equal in concentration

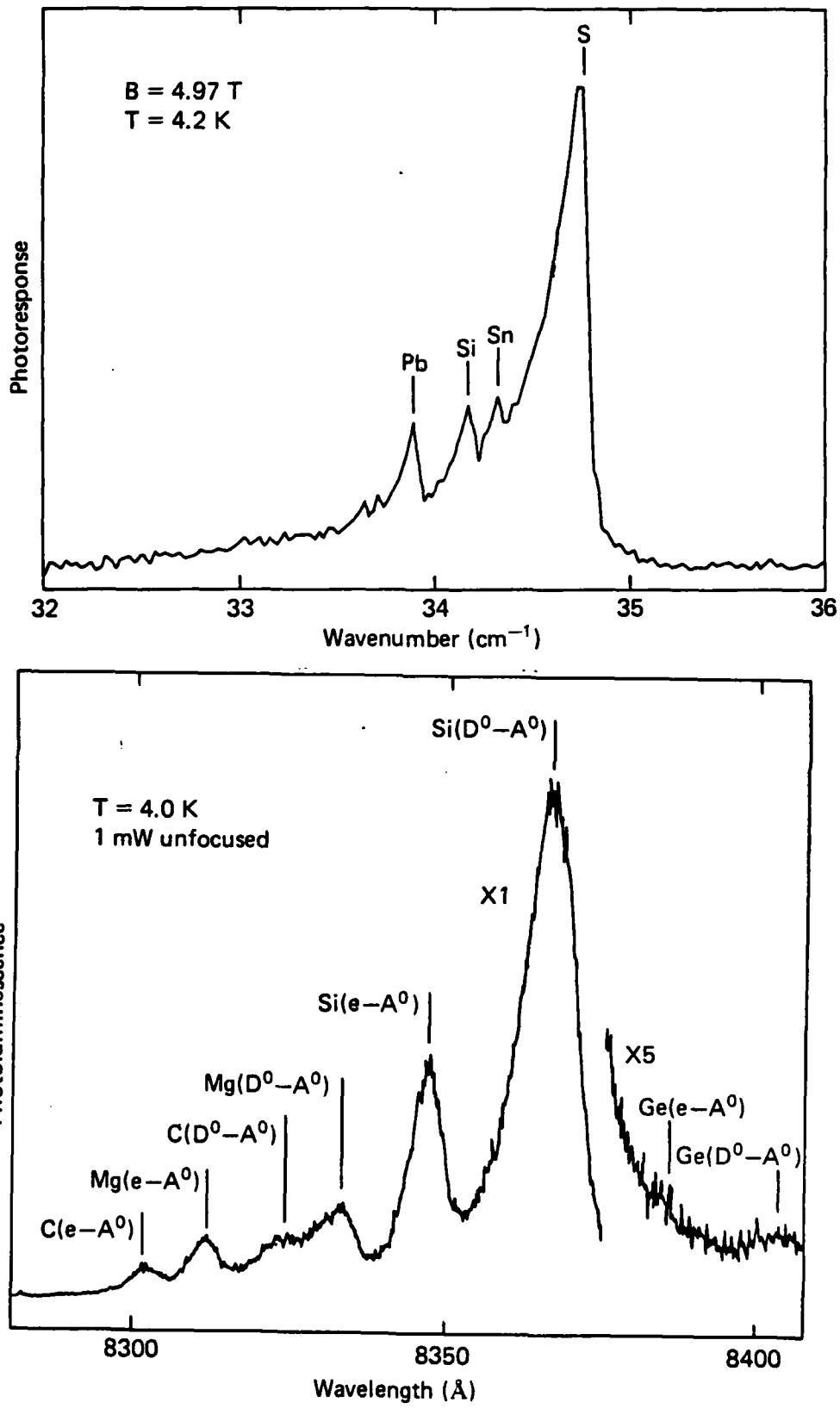

Fig. 1 (a) Photothermal ionization and (b) photoluminescence spectra of Hewlett Packard LPE sample.

to S) traces of Sn acceptors were detected (via the neutral Sn acceptor bound exciton line), but no Sn acceptors could be detected in any of the other LPE samples. It was impossible to determine the Sn acceptor concentration so from this data the incorporation ratio $[Sn_{Ga}]/[Sn_{As}]$ can only be said to be much greater than one. The X_1=Si donor peak was sometimes absent from the photothermal ionization spectra and this correlated with a much smaller level of the usually dominant Si acceptor detected by photoluminescence. In the three samples for which both Si donor and acceptor concentrations could be accurately measured, (each of which was grown at 700°C) incorporation ratios of $[Si_{Ga}]/[Si_{As}]$ = 0.16, 0.19, and 0.22 were determined. The X_3=Ge donor peak has never been observed in LPE GaAs but small concentrations (0.01-0.10 $x10^{14}cm^{-3}$) of Ge acceptors were observed in most of the LPE samples measured. The detection limit for X_3=Ge donors in the sample with the largest Ge acceptor concentration can be estimated as about $0.02x10^{14}$, and so $[Ge_{Ga}]/[Ge_{As}]$ must be less than about 0.2. Early doping experiments suggested that C donors may contribute a photothermal ionization peak coincident with the X_3=Ge peak (Wolfe et al. 1976). There is evidence to suggest that C does not incorporate as a donor at least in $AsCl_3$-VPE GaAs (Ozeki et al. 1977), but even assuming that C donors do contribute such an X_3 peak, the detection limit for X_3 donors together with the largest concentration of C acceptors detected determine an upper bound on $[C_{Ga}]/[C_{As}]$ in LPE GaAs of about 0.02.

These observations of the relative incorporation of the Group IV impurities $[IV_{Ga}]/[IV_{As}]$ are in qualitative agreement with the well established behavior of Si, Ge and Sn as dopants in LPE deduced from Hall

effect data, and have been predicted quantitatively for these impurities in terms of Ga and As activities and the free energy difference $\Delta G^{\circ}_{A/B}$ between IV_{Ga} and IV_{As} site occupation (Teramoto 1972) as:

$$\log ([IV_{Ga}]/[IV_{As}]) = \log (X^{\ell}_{As}/X^{\ell}_{Ga}) + \varepsilon/T$$

where ε is determined by $\Delta G^{\circ}_{A/B}$ and the heats of solution ΔH^{ℓ}_{Ga} and ΔH^{ℓ}_{As}. The melt mole fractions X^{ℓ}_{As} and X^{ℓ}_{Ga} can be determined at a given growth temperature from the liquidus data of Hall (1963). Using the $\Delta G^{\circ}_{A/B}$ values for Si, Ge, and Sn calculated by Teramoto and the typical growth temperature of 700°C we obtain $[Si_{Ga}]/[Si_{As}] = 0.16$, $[Ge_{Ga}]/[Ge_{As}] = 0.034$, and $[Sn_{Ga}]/[Sn_{As}] = 4.7$, which are in good agreement with our observed results above.

Following Teramoto and using the tetrahedral covalent radii of Pauling (1960) one can calculate $\Delta G^{\circ}_{A/B}$ for both C and Pb as +14.75 kcal/mole and -28.33 kcal/mole, respectively. For a growth temperature of 700°C, we obtain incorporation ratios of $[C_{Ga}]/[C_{As}] = 6.4\times10^{-7}$ and $[Pb_{Ga}]/[Pb_{As}] = 3.0\times10^{+3}$. These numbers should be taken as very approximate in view of the inadequacy of equilibrium thermodynamics to describe the non-equilibrium process of crystal growth, and of the way in which $\Delta G^{\circ}_{A/B}$ is calculated and its sensitivity to choice of covalent radii, but they are in agreement with the observation of Pb as exclusively donors and of C exclusively as acceptors in GaAs. The physical interpretation of these results is, since the "size" of the Ga site is larger than that of As, the lattice strain energy contribution to $\Delta G^{\circ}_{A/B}$ then forces the smaller C onto As (acceptor) sites, and forces the larger Pb onto Ga (donor) sites.

8.2 $AsCl_3$ VAPOR PHASE EPITAXY

The residual shallow impurities in several high purity undoped $AsCl_3$-VPE samples from seven different sources were measured. The bottom photothermal ionization spectrum in Fig. 2 for the Motorola sample shows the characteristic $AsCl_3$-VPE residual donors X_1=Si, X_2=S, and X_3=Ge, which are present at concentrations of 0.47, 0.53, and 0.27 $x10^{14}$ cm^{-3} respectively. These same residual donors were observed in the other samples although Si was sometimes more and Ge less prominent. Because of its very high purity the peaks in this sample are extremely well resolved, and so at a given magnetic field it was used as a reference for peak identifications in many of the other samples described in this work. The photoluminescence spectrum for this sample in Fig. 3 shows the typically prominent residual acceptor Zn (0.51 $x10^{14}$ cm^{-3}) and smaller concentrations of C and Ge acceptors (0.17 and 0.10 $x10^{14}$ cm^{-3}). Residual Si acceptors were not detected in this sample but were detected in trace amounts in some of the other samples measured. Residual Ge acceptors were frequently observed at approximately this same concentration and always dominated the traces of Si acceptors when the latter were present. The observed preferential incorporation of Si as donors rather than acceptors is in agreement with the general absence of Si acceptors in the photoluminescence data of Ashen et al. (1975) for undoped $AsCl_3$-VPE GaAs, and is in qualitative agreement with their prediction, under the typical $AsCl_3$-VPE growth conditions of T_G = 750°C and $P(AsCl_3) = 6 \times 10^{-3}$ atm, that $[Si_{Ga}]/[Si_{As}] = 1.6 \times 10^3$. The arguments of Ashen et al. can be extended to the other Group IV impurities, using the $\Delta G^\circ_{A/B}$ values calculated in the manner of Teramoto, giving incorporation ratios which scale

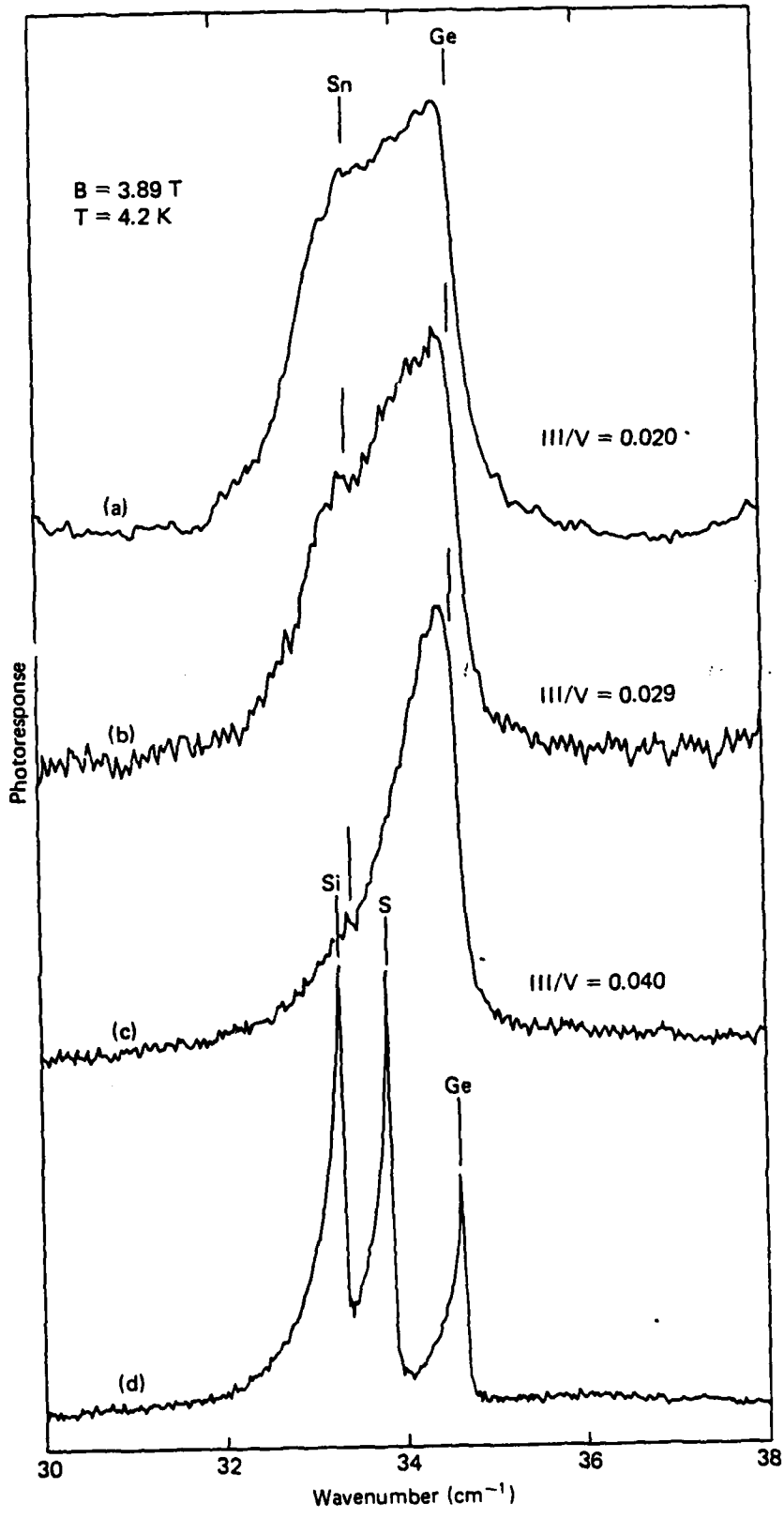

Fig. 2 Photothermal ionization spectra for the Toshiba MOCVD samples (top three plots) in which Sn and Ge donor incorporation was suppressed by increasing the III/V ratio. Lower plot is for the Motorola $AsCl_3$-VPE reference sample.

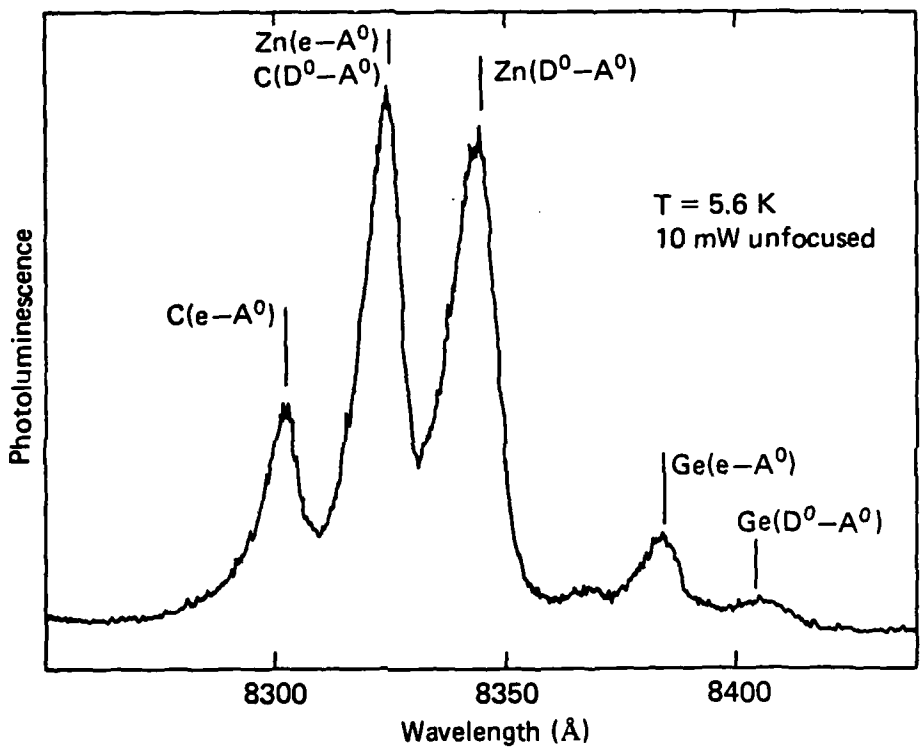

Fig. 3 Photoluminescence spectrum for Motorola $AsCl_3$-VPE sample.

for a given growth temperature with those calculated for LPE. We obtain then $[C_{Ga}]/[C_{As}]=1.2x10^{-2}$, $[Ge_{Ga}]/[Ge_{As}]=3.7x10^{+2}$, $[Sn_{Ga}]/[Sn_{As}]=3.9x10^{+4}$, and $[Pb_{Ga}]/[Pb_{As}] = 1.9x10^{+7}$ for the above $AsCl_3$-VPE growth conditions. The measured concentrations of Si and Ge donors and acceptors indicate that the calculated incorporation ratios for these elements are substantially too large. These ratios correctly predict however, the conduction type (n or p) when Ge, Si, Sn, Pb (Wolfe et al. 1976a) and C (Ozeki et al, 1977) are used as dopants in $AsCl_3$-VPE, and the dominance observed here of Si and Ge donors over acceptors. In the samples measured which have comparable Si and Ge donor concentrations, they also correctly predict the observed dominance of Ge acceptors over Si acceptors.

8.3 AsH_3 VAPOR PHASE EPITAXY

The residual shallow impurities in high purity undoped AsH_3-VPE samples from three different sources were determined and these measurements are discussed in more detail by Skromme et al. (1983b). The three residual donors X_1=Si, X_2=S, and X_3=Ge were observed in the samples from each source with X_2=S always dominant, while C and Zn were the dominant shallow acceptors. Both Si and Ge acceptors were observed at low concentrations in the University of Illinois samples but were absent in all the samples from the other two sources. The most striking behavior with respect to Group IV impurities was observed in the Hanscom AFB samples grown under otherwise similar conditions but varying the III/V ratio (i.e. $P(HCl)/P(AsH_3)$). The photothermal ionization spectra of these samples in Fig. 4 show the steady decrease in Group IV donor incorporation (X_1=Si and X_3=Ge) relative to Group VI donor incorporation (X_2=S) as the III/V ratio is increased, until the Group IV donors are barely detectable at III/V =

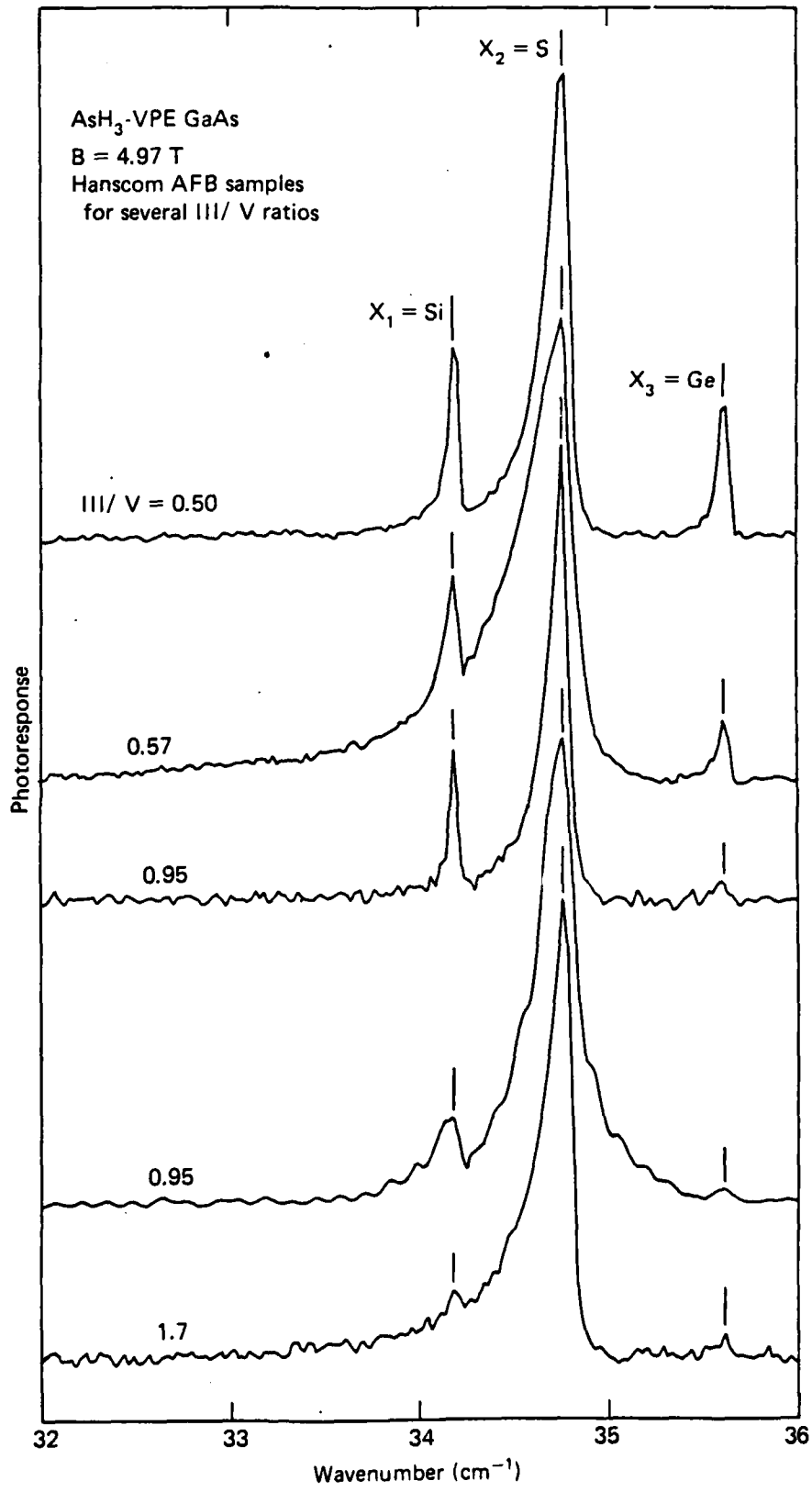

Fig. 4 Photothermal ionization spectra for AsH_3-VPE samples showing suppression of Group IV donors Si and Ge with increasing III/V ratio.

1.7. A similar but less dramatic trend was observed in photoluminescence for the C_{As} to Zn_{Ga} acceptor incorporation ratio. The ratio $[C_{As}]/[Zn_{Ga}]$ varied from 3.8 to 11 as the III/V ratio was increased from 0.50 to 1.7. These data are consistent with the idea that the gas phase stoichiometry influences the relative impurity incorporation through the relative concentrations of Ga and As vacancies (incorporation sites) on the growing surface. Even in the sample grown with the highest III/V ratio, however, neither Si nor Ge acceptors could be detected.

8.4 METAL-ORGANIC CHEMICAL VAPOR DEPOSITION

High purity undoped MOCVD samples from four different sources were measured and some of this data is decribed in more detail by Low et al (1983c). In all the samples measured X_3=Ge was the dominant residual donor while smaller concentrations of X_1=Si, Sn, X_2=S, and rarely Pb donors were also observed. The dominant residual shallow acceptor was usually C, but Zn was usually prominent and occasionally exceeded C in concentration. Traces of Ge acceptors were occasionally detected. The photothermal ionization spectra of three samples from Toshiba, all grown under similar conditions (T_G = 660°C) but with varying III/V ratio (i.e. P(TMGa)/P(AsH_3)) are shown in the upper three curves Fig. 2. The only two residual donors detected in these samples were Sn and Ge, both from Group IV. The N_D values determined from Hall data steadily decreased from 17.3 to 11.2 to 6.6 x10^{14} cm^{-3} (while N_A remained essentially constant at 4.3, 4.4 and 4.1 x10^{14} cm^{-3}) as the III/V ratio increased from 0.020 to 0.029 to 0.040 respectively. This behavior is similar to that observed in the AsH_3-VPE samples in that Group IV donor incorporation is supressed by increasing the gas phase III/V ratio, and might be interpreted in terms of

vacancy incorporation site availability in the same way. It is interesting to note that the Sn donor concentration seems to decrease more rapidly than that of Ge with increasing III/V ratio. No trend was observed in the ratio $[C_{As}]/[Zn_{Ga}]$ (which assumed the values 36, 26, and 38, respectively) as the III/V ratio was increased. Finally, the concentration of Ge acceptors decreased from 6.5×10^{11} cm^{-3} to 3.6×10^{11} cm^{-3} to undetectable as the III/V ratio increased (see Fig. 5) while, consistent with the expected relative vacancy concentrations the $[Ge_{Ga}]/[Ge_{As}]$ ratio increased from 2.3×10^3 to 3.1×10^3 to $\gtrsim 4 \times 10^3$ respectively. The increase in concentration of both Ge donors and acceptors with decreasing III/V ratio (increasing $P(AsH_3)$) is consistent with the suggestion that the source of the residual impurity Ge in MOCVD GaAs may be the AsH_3 (possibly in the form of GeH_4).

8.5 MOLECULAR BEAM EPITAXY

High purity elemental As source grown MBE samples from four sources were measured and some of this data is discussed in more detail by Low et al. (1982 a and d). The dominant and usually the only residual donor detected in these samples was X_2=S but the necessity of using Si or Sn dopants to achieve the n-type conduction required for the photothermal ionization measurements would mask their presence as residuals. No donor peak attributable to C was observed in any of these samples but C was the only shallow acceptor detected (with one exception noted below). Several Si doped samples grown at Bell Labs using various growth temperatures (T_G = 600-650°C) and various Ga to As pressure ratios (P_{As}/P_{Ga} = 15 to 25 with P_{Ga} and P_{Si} held constant) were measured, but no strong trends were observed in impurity incorporation. Figure 6 is a photothermal ionization

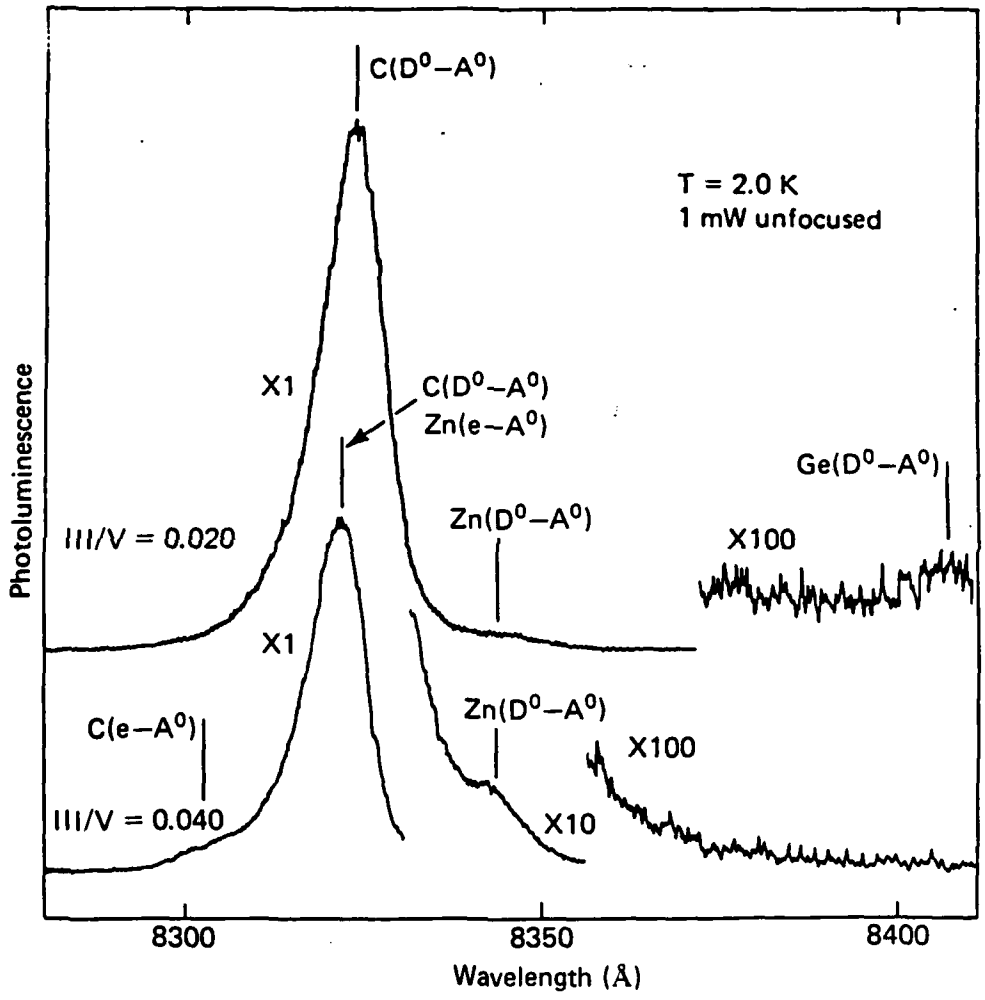

Fig. 5 Photoluminescence spectra for Toshiba MOCVD samples showing decrease of Ge acceptors with increasing III/V ratio.

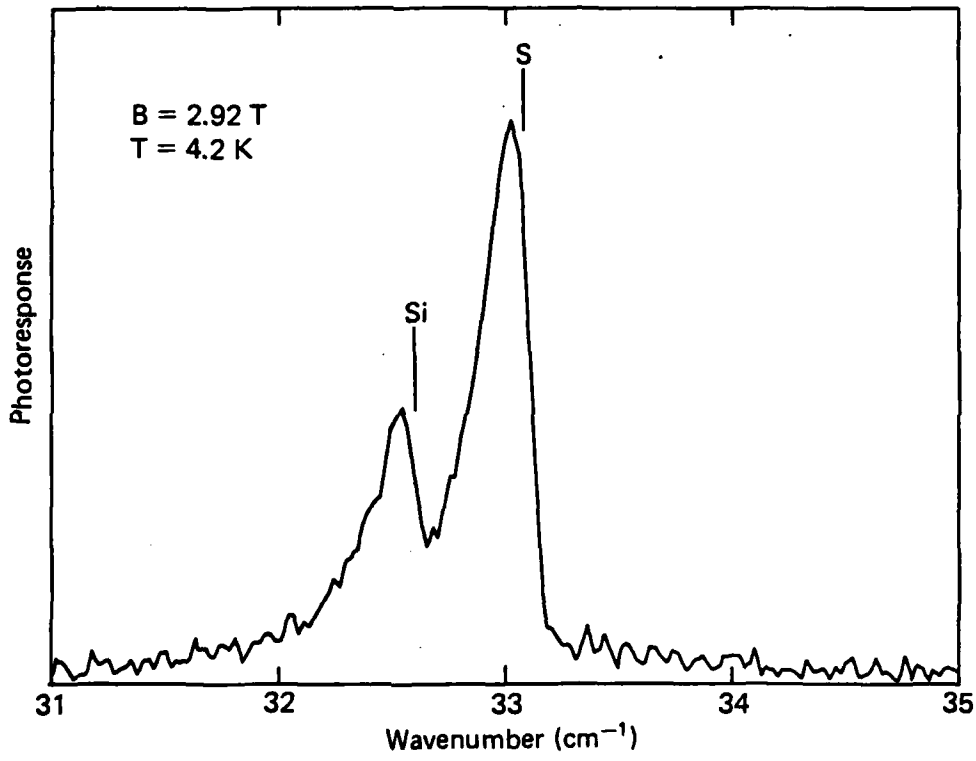

(a)

Fig. 6 Typical photothermal ionization spectrum for the Bell Labs MBE samples (grown with P_{As}/P_{Ga}=15).

spectrum which is typical of these samples. A small peak not visible in the other Bell samples coincident with Si acceptor (D°-A°) (see Fig. 7) recombination was observed in the sample grown with the lowest P_{As}/P_{Ga}, which is consistent with the expected highest As site availability for Si incorporation.

8.6 CONCLUSIONS

In conclusion, the relative incorporation of the Group IV impurities in high purity GaAs prepared by a variety of growth techniques has been measured. The model of Teramoto (1972) for LPE and its extension of $AsCl_3$-VPE by Ashen et al. (1975) are in qualitative agreement with the observations for all the Group IV elements. In particular the large lattice strain energy contributions to $\Delta G^\circ_{A/B}$ for Pb and C are consistent with the failure to conclusively observe C donors or Pb acceptors in epitaxial GaAs grown by any technique. Finally, the III/V ratio dependences of Group IV incorporation for AsH_3-VPE, MOCVD, and MBE are in qualitative agreement with the expected influence on concentrations of Ga and As vacancy sites available for impurity incorporation.

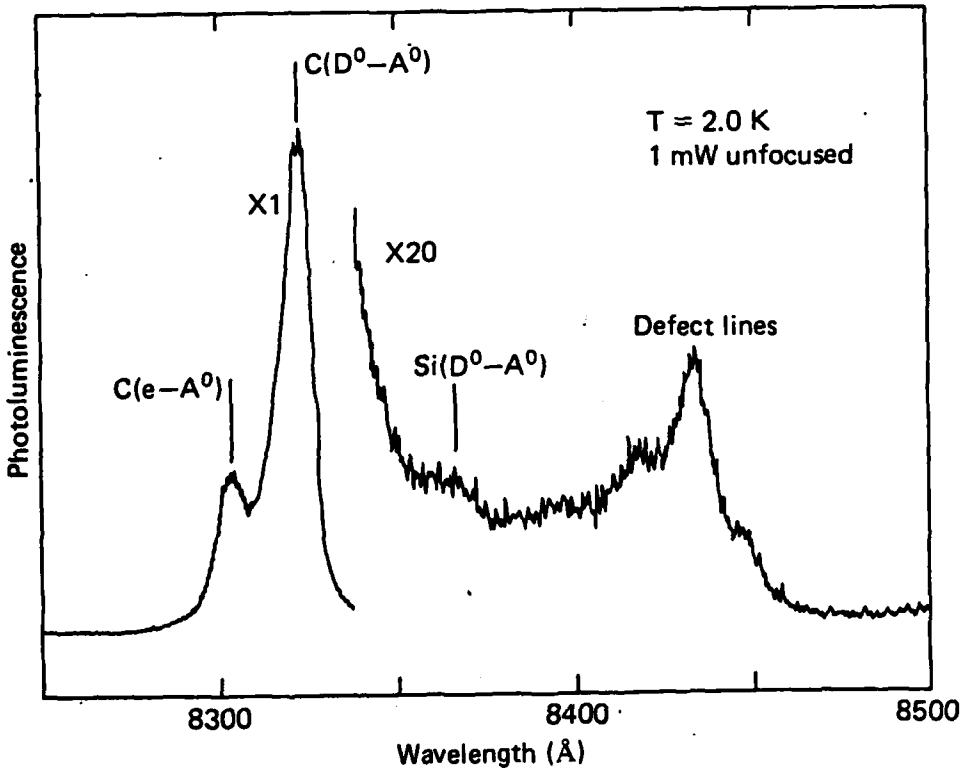

(b)

Fig. 7 Photoluminescence spectrum for Bell Labs MBE sample grown with smallest P_{as}/P_{Ga}=15 showing a trace of Sn acceptors.

8.7 REFERENCES

Ashen D J, Dean P J, Hurle D T J, Mullin J B, White A M, and Greene P D, 1975, J. Phys. Chem Solids 36, pp 1041-1053

Bebb H B and Williams E W in Semiconductors and Semimetals, edited by R K Willardson and A C Beer (Academic Press 1972) Vol 8, pp 321-419

Cooke R A, Hoult R A, Kirkman R K, and Stradling R A, 1978, J. Phys. D. 11, pp 945-953

Hall R N, 1963, J Electrochem. Soc. 110 p 385

Low T S, Stillman G E, Collins D M, Wolfe C M, Tiwari S, and Eastman L F, 1982a, Appl. Phys. Lett. 40, p 1034

Low T S, Stillman G E, Nakanisi T, Udagawa T, Wolfe C M, 1982b, Appl. Phys. Lett. 1982b 41, pp 183-185

Low T S, Skromme B J, Stillman G E, Dapkus P D Hess K L, Manasevit H M, 1983c J. Electronic Materials (to be published)

Low T S, Stillman G E, Morkoç H, Cho A Y, and Calawa A R, 1982d, Appl. Phys. Lett. 40, p 611

Ozeki M, Kitahara K, Nakai K, Shibatomi A, Dazai K, Okawa S, and Ryuzan O, 1977, Jpn. J. Appl. Phys. 16, pp 1617-1622

Pauling L, The Nature of the Chemical Bond 3rd edition (Cornell University Press 1960), p 246

Skromme B J, Low T S, Stillman G E, 1983a, GaAs and Related Compounds, Albuquerque 1982 (Inst. of Physics London 1983) (to be published)

Skromme B J, Low T S, Roth T J, Stillman G E, Abrokwah J K, Kennedy J K, 1983b, J. Electronic Materials (to be published)

Stillman G E, Wolfe C M, and Dimmock J O, in Semiconductors and

Semimetals, edited by R K Willardson and A C Beer (Academic, New York 1977), Vol. 12 pp 169-290

Teramoto I, 1972 J Phys. Chem. Solids 33, pp 2089-2099

Wolfe C M, Stillman G E, and Korn D M, GaAs and Related Compounds, St Louis, 1976, Conf. Ser. No. 33b (Institute of Physics, London, 1977) pp 120-128

Wolfe C M, Stillman G E, and Dimmock J O, 1970, J. Appl. Phys. 41, 504

9. IDENTIFICATION OF Si DONORS

Silicon is widely believed to be an important residual impurity in GaAs prepared by several growth techniques. The results of many experiments on the growth of high purity GaAs have been explained in terms of the influence of various growth parameters on the incorporation of Si. Most such experiments have relied on Hall effect data and on the tacit assumption that only changes in Si incorporation are important in determining changes in the carrier concentration. Since Si is neither the only residual acceptor[1] nor the only residual donor[2] present in high purity GaAs grown by a wide variety of techniques, it is necessary to specifically measure the concentration of electrically active Si in order to assess the role of Si as a residual impurity. Photothermal ionization spectroscopy can detect the donor species present in a high purity semiconductor sample and measure their relative concentrations from the amplitudes of the corresponding spectral peaks. Carefully controlled doping experiments have been performed by several research groups[3-5] to identify various donor species with the associated photothermal ionization peaks. Such experiments are difficult because of the small range of donor concentrations between that of the purest GaAs which can be grown by a given technique and that for which impurity interactions[6] and other effects[7] degrade the spectra by broadening and distorting the spectral peaks. In this report we discuss photothermal ionization measurements made on Si doped GaAs grown by MBE which have resulted in the identification of Si donors with a spectral peak different from that previously associated with Si.[8]

9.1 PHOTOTHERMAL IONIZATION SPECTRA

Si doped samples 1 and 2 were grown at Hewlett-Packard Laboratories on (100) undoped semi-insulating LEC substrates in a Varian GEN/II MBE system equipped with liquid nitrogen cryoshrouds. All source materials were evaporated from pyrolytic boron nitride (PBN) crucibles, contained in high

purity source furnaces in which the heated zones are comprised of only Ta and PBN. An elemental As source was used, and undoped MBE GaAs prepared in this way is generally p-type with $p \approx 10^{14} cm^{-3}$.[9] Doping with elemental Si to produce the n-type samples required for the measurements produces a Si donor concentration which dominates the small background concentration of other donors and acceptors present in undoped material. The only materials other than Ga, As, and Si, which had been previously evaporated in this MBE system were Al, and Be (a p-type dopant). The layers were grown with a substrate temperature of 585°C at a rate of 1 μm/hr. The electrical properties of these samples and the other samples reported in this work, corrected for surface and substrate depletion[10], are shown in Table 1.

Photothermal ionization spectra for samples 1 and 2 and for reference sample 1 are shown in Fig.1. These spectra show the 1s-2p(m=-1) transitions of the various donor species present, and were recorded at precisely the same magnetic field (B=2.92T) by operating the superconducting magnet in the persistent mode. The three peaks in the spectrum of the ultra-pure $AsCl_3$-H_2 grown reference sample 1, labeled X_1, X_2, and X_3, correspond to the three characteristic residual donors present in GaAs grown by this technique. At a given magnetic field, the energies of these peaks provide a reference for identifying the peaks in the spectra of other samples.

The spectra of both Si doped samples 1 and 2 contain two peaks which have the typically observed asymmetric lineshape predicted by Larsen.[6] In both spectra, the large peak corresponds with X_1 in the reference spectrum, while the smaller peak corresponds with X_2. The slight downshift in the peak energies of the MBE spectra with respect to those in the reference spectrum is often observed in samples of this doping level. The dominance of the X_1 peak in the spectra for these Si doped MBE samples by itself strongly suggests the

Table 1 Hall effect data and impurity concentrations derived from spectra and Hall mobility analysis of Wolfe et al.[3].

Impurity Concentrations ($x10^{14} cm^{-3}$)

Sample	N_D(total)	N_A(total)	N_D(Pb)	$N_D(X_1$=Si)	N_D(Sn)	$N_D(X_2)$	$N_D(X_3)$
1	9.7	3.2	----	7.3	----	2.4	----
2	11.3	3.7	----	9.0	----	2.3	----
3	2.8	1.6	$\lesssim$0.1	$\lesssim$0.1	1.3	1.3	----
reference 1	0.89	0.45	----	0.47	----	0.36	0.06
reference 2	0.43	0.13	----	0.8	0.14	0.14	0.08

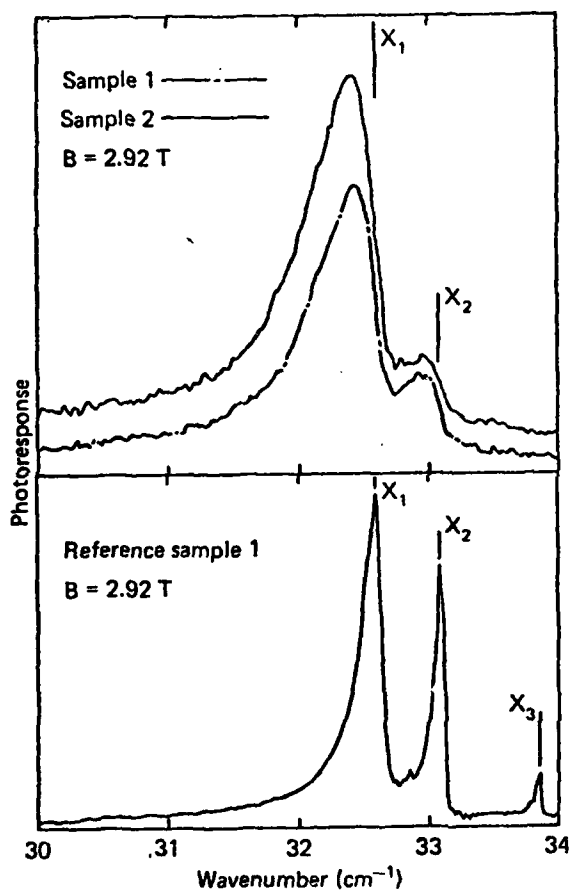

Fig. 1 Photothermal ionization spectra of the $1s$-$2p(m=-1)$ transitions for the Si doped MBE samples 1 and 2, and for reference sample 1.

association of Si donors with the X_1 peak, but further evidence is provided by the absolute donor concentrations in these samples. The relative concentrations of X_1 and X_2 donors were derived from the relative peak amplitudes in the spectra. Absolute concentrations could then be calculated from the total donor concentration using the 77K Hall effect data and the method of Wolfe et al.[11] In the more heavily doped sample 2, the concentration of X_1 donors is 1.23 times larger than in sample 1, but the concentration of X_2 donors is essentially the same in both samples. This is interpreted to mean that the concentration of X_1=Si donors increases with increasing doping while the background of X_2 donors remains constant. It is also interesting to note, in view of the amphoteric nature of Si in GaAs, that the total acceptor concentration in the more heavily doped sample 2 is 1.16 times that of sample 1. The identification of the X_1 peak with Si is consistent with the work of Ozeki et al.[4]

The data which led to the earlier identification of peak X_2 with Si by Wolfe et al.[8] are shown in Fig. 2. In these experiments the photothermal ionization spectrum of a Sn doped $AsCl_3$-H_2 VPE grown GaAs control sample was compared to that of a sample which was prepared identically except that Si was added to the Ga melt. On the basis of the larger amplitude and width of the X_2 peak in the Si doped sample the X_2 peak was identified with Si.

The new identification of Si with X_1 can be reconciled with the data of Wolfe et al.,[8] by examining the region of the spectra of Fig. 2 in the vicinity of X_1. While the X_2 peaks have the typically observed low energy tail predicted by Larsen,[6] the shapes of the X_1 peaks in both spectra are anomalous. The photoresponse drops precipitously for energies less than that of the X_1 peaks, and after a sharp notch, forms the broad wing noted by Wolfe et al.[8] A careful comparison of the original spectra for these samples with a

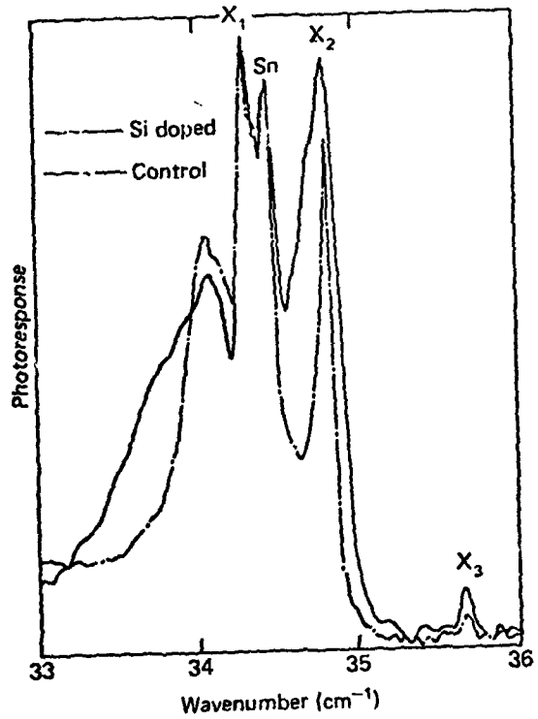

Fig. 2 Photothermal ionization spectra of the 1s-2p(m=-1) transitions for the $AsCl_3$ grown Si doped and control samples of Wolfe et al.[9]. (B=5.00T)

spectrum of reference sample 2, in which all peaks have the typically observed shape, shows that the X_1 peak in the reference spectrum corresponds not with the peaks labeled X_1 in the spectra in Fig.2, but with the notches in the photoresponse just below these peaks. Photothermal ionization peaks having a sharply peaked component slightly above the usual peak energy and a broad wing well below the usual peak energy have been observed previously, particularly for the larger amplitude peaks (i.e. higher concentration donors). Space does not permit a thorough discussion of this effect and related experiments,[12] and the details of the phenomenon are not yet fully understood, but we believe the anomalous peak shape is caused by an absorption by the corresponding (in this case X_1=Si) donors near the substrate-epilayer interface, which does not contribute significantly to the photoconductive response, but reduces the intensity of far infrared light within the sample at the peak energy, so that a sharp notch is observed in the associated photothermal ionization peak. In the absence of this interface absorption, the X_1 peaks in both spectra would have the more typical shape of X_2 and substantially larger amplitudes, indicative of the actual relative concentrations of X_1=Si. The greater width of the X_2 peak in the Si doped sample, as well as that of the broad wing below X_1, which with the present interpretation is the usual low energy tail of X_1 distorted by interface absorption, are the result of additional Stark broadening[6] caused by the additional charged centers (ionized acceptors and compensated donors) introduced by the Si doping.

9.2 RESIDUAL Si DONORS

The identification of Si with X_1 instead of X_2 in photothermal ionization spectra has important implications with regard to the role of Si as a residual donor in GaAs grown by liquid phase epitaxy (LPE). Until recently X_1 was never observed in LPE GaAs, and this led to the suggestion that this peak might be due to a stoichiometric defect.[13] The only residual donor peaks

previously observed in LPE materials were identified as Pb,[3,5,14] Sn,[3,15,16] and X_2, which is often the dominant peak in the spectra, and which has been associated with S.[4,5] The earlier identification of Si with X_2 fit well with the expectation that reduction of hot SiO_2 by H_2 in the LPE reactor would lead to incorporation of Si into the melt, and subsequently into the growing epilayer,[17,18] and that this mechanism was the dominant contribution to residual donors in LPE GaAs. The present identification of Si with X_1, together with the previous photothermal ionization data for LPE GaAs,[2,5,19] indicate not only that Si is not the dominant residual donor, but that it is often present in undetectably small concentrations relative to the other residual donor species. Figure 3 shows the spectrum of the high purity LPE GaAs sample 3, which was grown at Cornell University. Peaks corresponding to the usual Pb, Sn and X_2 donors are clearly visible in this spectrum, but a small peak at the energy of X_1=Si was also reproducibly observed. Most of the photoresponse at the energy of X_1 is due to the low energy tail of the Sn peak and so the relative concentration of X_1 is quite small. The proximity of the X_1 and Sn peaks in energy and the fact that the residual Sn concentration is usually much larger than the concentration of X_1 donors observed here may account for the fact that this is the first report of the X_1 peak in the photothermal ionization spectra of undoped LPE GaAs.

The identification of Si with X_1 instead of X_2 also has implications with regard to the role of Si as a residual donor in GaAs grown by various other techniques. In AsH_3 VPE grown GaAs the residual donors are X_1, X_2, and X_3, as in $AsCl_3$-H_2 VPE, but the concentrations of X_1 and X_3 are lower, and X_2 is dominant[2]. In MBE GaAs grown with an elemental As source and using Sn as the n-type dopant, both X_1 and X_2 are present but the concentration of X_1 is low,[20] while if AsH_3 is cracked in a SiO_2 furnace to provide the As, the

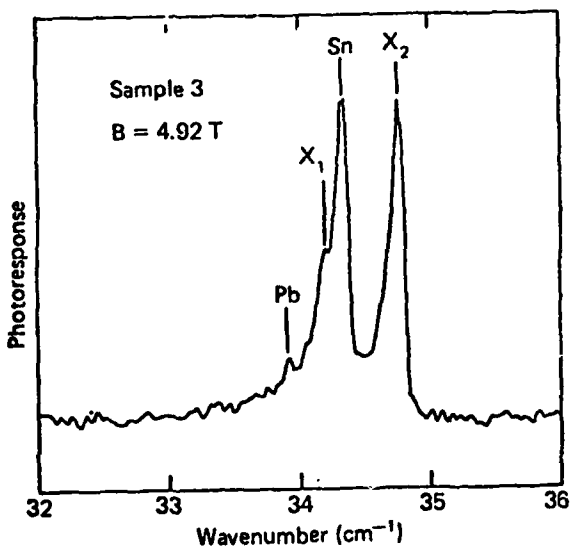

Fig. 3 Photothermal ionization spectrum of the high purity LPE grown sample 3, showing the X_1=Si peak in addition to the usual Pb, Sn, and X_2 peaks.

amplitude of the X_1=Si peak increases with increasing cracking furnace temperature.[20] In MOCVD grown GaAs the relative concentrations of various residual donors including X_1 and X_2 deduced from photothermal ionization measurements have been correlated with various growth parameters and purification techniques from the metalorganics.[21] These results indicate that the residual X_1=Si donor concentration in MOCVD material can be made negligible.

In conclusion, on the basis of photothermal ionization measurements on Si doped MBE GaAs samples, an identification of Si with the spectral peak X_1 has been made. This identification together with previous photothermal ionization data indicate that Si is not an important residual donor in high purity LPE GaAs, and also necessitates a reevaluation of the importance of Si as a residual donor in GaAs grown by a variety of other techniques.

9.3 REFERENCES

1. D.J. Ashen, P.J. Dean, D.T.J. Hurle, J.O. Mullin, A.M. White, and P.D. Greene, J. Phys. Chem. Solids, 36, 1041 (1975).
2. T.S. Low, G.E. Stillman, and C.M. Wolfe, GaAs Conf. Proc. Sym. GaAs and Related Compounds, Oiso, 1981, (to be published).
3. C.M. Wolfe, G.E. Stillman, and D.M. Korn, Inst. Phys. Conf. Ser. No. 33b, 120, (1976).
4. M. Ozeki, K. Kitahara, K. Nakai, A. Shibatomi, K. Dazai, S. Okawa, and O. Ryuzan, Jpn. J. Appl. Phys. 16, #9, 1617 (1977).
5. R.A. Cooke, R.A. Houlte, R.F.Kirkman, and R.A. Stradling, J. Phys. D, 11, 945 (1978).
6. D.M. Larsen, Phys. Rev. B, 13, 1681 (1976).
7. T.S. Low, G.E. Stillman, Camellia M.L. Yee, and C.M. Wolfe, (unpublished).
8. C.M. Wolfe, D.M. Korn, and G.E. Stillman, Appl. Phys. Lett. 24, 78 (1974).
9. H. Morkoç and A.Y. Cho, J. Appl. Phys. 50, 6413 (1979).
10. A. Chandra, C.E.C. Wood, D.W. Woodard, and L.F. Eastman, Solid State Elect, 22, 645 (1979).
11. C.M. Wolfe, G.E. Stillman, and J.O. Dimmock, J. Appl. Phys. 41, 504 (1970).
12. T.S. Low and G.E. Stillman (unpublished).
13. G.E. Stillman, C.M. Wolfe, and D.M. Korn, Proc. 13th Int. Conf. Phys. Semiconductor (Rome 1977) pp. 623-626.
14. R.A. Stradling, private communication (1981).
15. H.R. Fetterman, J. Waldman, C.M. Wolfe, G.E. Stillman, and C.D. Parker, Appl. Phys. Lett. 21, 434 (1972).
16. R.A. Stradling, L. Eaves, R.A. Houlte, N. Miura, P.E. Simmonds, and C.C.

Bradley, Proc. of the Fourth Int. Symp. on GaAs (Inst. of Phys. London, 1973), p65.

17. M.E. Weiner, J. Electrochem. Soc. 119, 496 (1972).

18. H.G.B. Hicks and P.D. Green, Inst. of Phys. Conf. Ser. No. 9, Bristol and London, 92, (1971).

19. H. Morkoç, L.F. Eastman, and D. Woodard, Thin Solid Films, 71, 245 (1980).

20. T.S. Low, G.E. Stillman, H. Morkoç, A.Y. Cho, and A.R. Calawa, to be published Appl. Phys. Lett. (April 1,1982).

21. P.D. Dapkus, H.M. Manasevit, K.L. Hess, T.S. Low, and G.E. Stillman, J. Cryst. Growth 55, 10 (1981).

10. RESIDUAL DONORS IN MOLECULAR BEAM EPITAXY

Molecular beam epitaxy (MBE) of III-V semiconductors is of great interest for semiconductor device applications because of its capability for producing highly uniform layers with precisely controlled thicknesses and doping profiles. For some applications, such as FET buffer layers and undoped layers in high electron mobility transistors, it is also important to be able to grow high purity material. In this report we discuss photothermal ionization measurements of the shallow donor species present in high purity MBE GaAs samples grown in two different laboratories.

Photothermal ionization spectroscopy[1] is a technique which can be used to detect the donor species present and measure their concentrations relative to the total donor concentration in high purity semiconductor samples. The extrinsic photoconductivity spectrum of a high purity n-type GaAs sample consists of sharp peaks at energies corresponding to transition energies of the hydrogenic donors. Because different donor species have slightly different ground state energies but nearly identical excited state energies, each hydrogenic transition has associated with it a closely spaced multiplet of peaks. Each peak in the multiplet corresponds to a hydrogenic transition of a particular donor species. The relative amplitudes of the peaks are a measure of the relative concentrations of the corresponding donor species. The narrow linewidth and large amplitude of the 1s-2p(m=-1) transition at high magnetic fields make it especially suitable for resolving the closely spaced peaks of the individual donor species. The 1s-2p(m=-1) transition energies change substantially with changing magnetic field so, to permit comparison of the peaks observed in a given sample with donor identifications in the literature, the

spectrum of that sample is compared to the spectrum of a well characterized reference sample taken at precisely the same magnetic field. This is accomplished by operating the superconducting magnet in persistent mode while both spectra are recorded. The reference sample used in this work is an ultra pure $AsCl_3$-VPE GaAs sample grown by C.M. Wolfe, which has a liquid nitrogen temperature mobility of μ_{77}=201,000 cm^2/Vs and a carrier concentration of $n_{77}=4.5\times10^{13}$ cm^{-3}.[2] The three peaks present in the spectra of this sample, labeled X_1 X_2 and X_3, correspond to the three characteristic residual donors present in high purity GaAs grown by this technique.[3] Since many of the early donor identification experiments were done using $AsCl_3$-VPE material, the energies of peaks corresponding to different donor species relative to the energies of X_1 X_2 and X_3 are fairly well known.[4,5]

10.1 EPITAXIAL SAMPLES

Hall effect data for the MBE samples described here[6,7] show them to be the highest purity GaAs prepared by this technique which has yet been reported. Sample A-147 was grown by H. Morkoç and A.Y. Cho who reported a liquid nitrogen temperature mobility of 105,000 cm^2/Vs and a carrier concentration of 4×10^{14} cm^{-3} for the 27 μm thick layer.[5] The MBE system used to grow this sample used an elemental As source, and undoped GaAs grown in this way is generally p-type with $p\simeq10^{14}$ cm^{-3}. In order to produce an n-type sample it was necessary to lightly dope the sample with Sn. The details of the substrate preparation, growth procedure and precautions for obtaining high purity have been described elsewhere.[6,8] Samples MBE-91 and MBE-92 were grown by A.R. Calawa[7] in an MBE system which used an AsH_3 cracking furnace in place of the usual effusion cell

As source. Undoped samples grown in this way are n-type and so no intentional doping was required. The details of the cracking furnace and growth procedure for these samples have also been described previously.[7] The liquid nitrogen temperature mobilities, and carrier concentrations corrected for both surface and interface depletion in these 5 μm thick samples are[7,9] μ_{77}=90,000 cm^2/Vs, $n_{77}=2.7x10^{14}$ cm^{-3}, and μ_{77}=110,000 cm^2/Vs, $n_{77}=2.4x10^{14}$ cm^{-3} respectively.

10.2 PHOTOTHERMAL IONIZATION SPECTRA

For extremely pure samples in which the photothermal ionization peaks are separated by more than a linewidth in energy, the relative amplitudes of the peaks are expected to correspond to the relative concentrations of donor species present. In less pure and/or more compensated samples, as the concentration of charged centers (ionized acceptors and compensated donors in an n-type sample) increases, the peaks broaden due to the electric fields and field gradients[10] from these charged centers, until the linewidth becomes comparable to the peak separations. The photoresponse at the energy of a peak of a certain donor species is then no longer simply proportional to the concentration of that species, but is related also to the concentration of donors associated with adjacent peaks. This is the case for the spectrum of MBE-91 in Fig.1(c). Because the photoresponse at the position of the Pb peak is largely due to the contributions of the low energy tails of the Si and Sn peaks, the relative amplitude of the Pb peak is substantially larger than the relative concentration of Pb donors. In order to obtain a quantitative estimate of the concentrations of the various donor species for each sample reported here, a function $f(\varepsilon)$ of the form

$$f(\varepsilon) = \sum_{i=1}^{4} \alpha_i P(\beta[\varepsilon-\varepsilon_i])$$

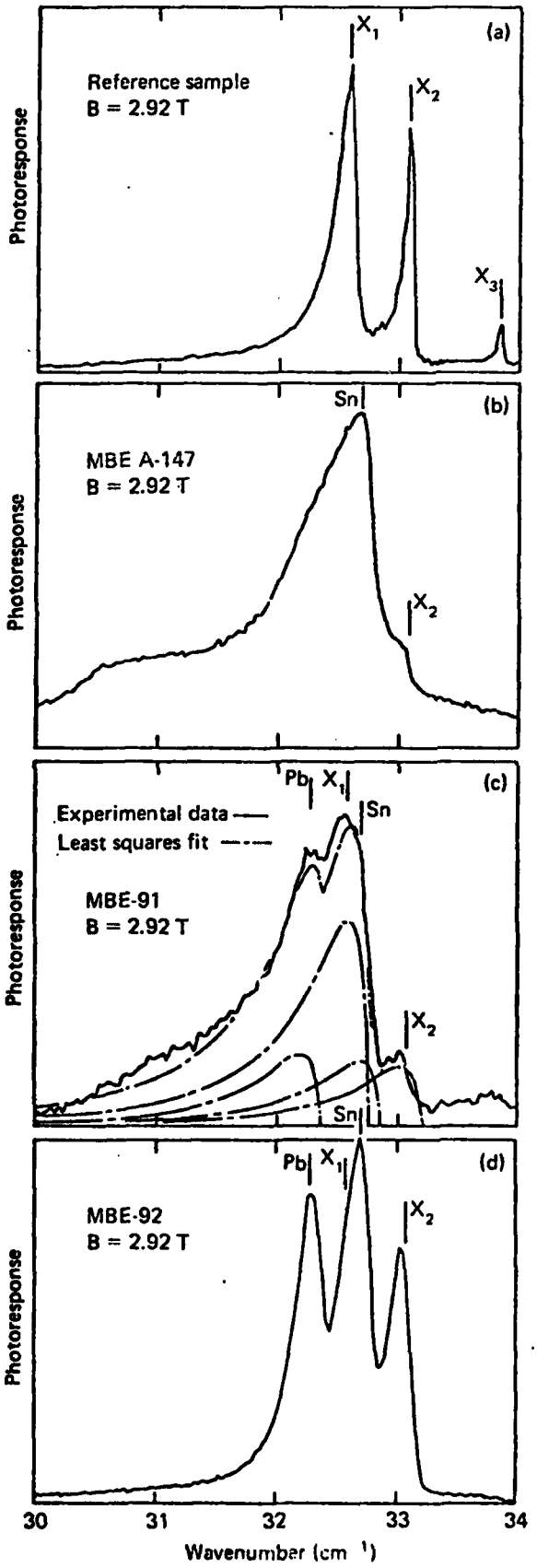

Fig. 1 Photothermal ionization spectra of the 1s-2p(m=-1) transitions for the MBE samples and the reference sample at a magnetic field of 2.92T.

was fitted to the envelope of 1s-2p(m=-1) transitions using a least squares minimization technique. Each term in $f(\varepsilon)$ is a peaked function whose amplitude α_i is interpreted as a relative concentration of the i^{th} donor species. The function $P(\varepsilon)$ was derived from a fit to the 1s-2p(m=-1) lineshape calculation by Larsen.[10] The values of α_i and β were adjusted for a best fit while the peak positions ε_i were determined from the spectra of Fig.1(a) and (d). The width scale β was constrained to be the same for each peak because the inhomogeneous broadening[10] of peaks is expected to be the same for each donor species in a uniformly doped sample, independent of its relative concentration. The resulting best $f(\varepsilon)$ and the individial terms of $f(\varepsilon)$ are plotted for MBE-91 along with the experimental data in Fig.1(c). The total donor and acceptor concentrations for the samples reported here were determined using the Hall mobility analysis of Wolfe et al.[11] The relative concentrations for the various donor species present in each sample could then be expressed as the absolute concentrations shown in Table 1.

Photothermal ionization spectra for sample A-147 and for the reference sample, both recorded at a magnetic field of 4.97 T, are shown in Fig.2. As expected from the intentional Sn doping of this sample, the dominant peaks in its spectrum occurs at an energy which has been previously associated with Sn by Wolfe et al.[4] and Cooke et al.[5] The smaller peak at higher energy corresponds to X_2. The peak X_2 was originally associated with Si by Wolfe et al.[4] but subsequent doping experiments by Ozeki et al.[12] and in our laboratory[13] have indicated that X_1 is Si, while Ozeki et al.[12] have associated X_2 with S. The shoulder on the low energy side of the dominant Sn peak occurs at an energy which has been associated with Pb by Wolfe et al.[4] and Stradling.[14] In a homogeneously doped sample, the ratio of peak width to peak height should be the same for all peaks. This ratio,

Table 1 Impurity concentrations derived from the photothermal ionization spectra and the Hall mobility analysis of Wolfe *et al.*[11].

Sample	N_D(total)	N_A(total)	N_D(Pb)	$N_D(X_1$=Si)	N_D(Sn)	$N_D(X_2)$	$N_D(X_3)$
Reference	0.89	0.45	---	0.47	---	0.36	0.06
A-147	5.8	1.8	$\leq$0.3	$\leq$0.3	3.9	1.3	$\leq$0.1
MBE-91	4.9	3.9	0.9	2.5	0.8	0.7	$\leq$0.2
MBE-92	3.4	2.8	0.8	$\leq$0.15	1.3	1.2	---

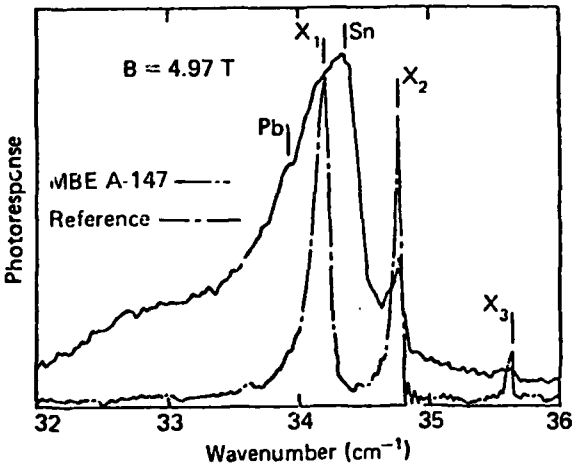

Fig. 2 Photothermal ionization spectrum of the 1s-2p(m=-1) transitions for MBE sample A-147 and the reference sample at a magnetic field of 4.97T.

taken at 75% of the full peak heights, is 1.7 times larger for the Sn peak than the X_2 peak, and this suggests that another unresolved donor (possibly X_1=Si) may be contributing to the low energy tail of the Sn peak.

Photothermal ionization spectra for samples MBE-91, MBE-92, A-147, and the reference sample, recorded at a magnetic field of 2.92 T, are shown in Fig.1. The maximum photoresponse in the spectrum of MBE-91 is at the energy of X_1=Si, but if only Si were present in this sample, the photoresponse would drop off more sharply for energies above that of the maximum. The additional photoresponse on the high energy side of the Si peak is probably due to Sn, especially in view of the presence of a Sn peak in the spectrum of MBE-92. At still higher energy there is a small peak coincident in energy with X_2 and possibly also with X_3, while at lower energy there is a peak at the energy associated with Pb.

The photothermal ionization spectrum for MBE-92 in Fig.1(d) shows the clear presence of Pb Sn and X_2, and the fact that the Sn peak is slightly broader relative to its amplitude than either the Pb or X_2 peak, suggest there may be a slight amount of X_1=Si present. The presence of Sn in the unintentionally doped samples MBE-91 and MBE-92 may be due in part to the previous use of Sn as an n-type dopant in the MBE growth chamber. Several growth runs were made between the use of Sn and the growth of MBE-91 and MBE-92, however, and so passivation of the walls of the growth chamber may have minimized this contribution of Sn. Samples MBE-91 and MBE-92 were grown under identical conditions except for the temperature of the AsH_3 cracking furnace. Calawa[7] correlated an increase in net carrier concentration for samples grown with increasing cracking furnace temperature and attributed it to Si donors provided by the hot quartz walls of the cracking furnace. This idea is substantiated by the donor concentrations derived

AD-A122 217 IMPURITY AND DEFECT INTERACTIONS IN GAAS(U) WASHINGTON 3/3
UNIV ST LOUIS MO SEMICONDUCTOR RESEARCH LAB
C M WOLFE ET AL. 30 SEP 82 WU/SRL-64422-10
UNCLASSIFIED N00014-80-C-0762 F/G 20/2 NL

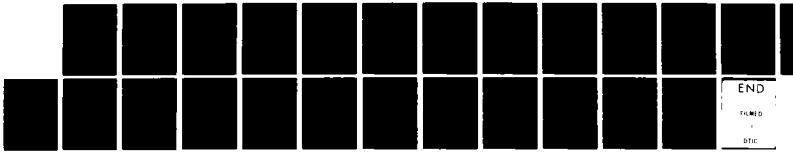

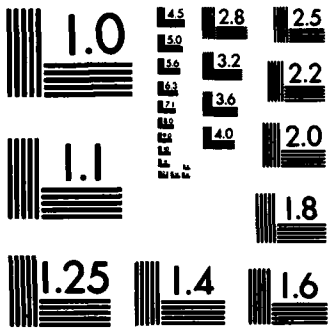

from the fits to the spectra of MBE-91 and MBE-92. In MBE-91, grown with a cracking furnace temperature of 690°C, the concentration of X_1=Si donors is over half of the total donor concentration, while in MBE-92, grown with the lower cracking furnace temperature of 610°C, and having a lower total donor concentration, the presence of X_1=Si donors is barely discernable. The concentrations of Pb, Sn and X_2 donors, however, are similar for both samples (see Table 1.).

10.3 CONCLUSIONS

In conclusion, the photothermal ionization data presented here for high purity MBE GaAs samples grown in different laboratories and using substantially different growth techniques show remarkably similar donor backgrounds. Peaks associated with Pb, Si, Sn, and S are present in each of the MBE samples measured. The X_3 donor, if present at all in these samples, has a concentration at least a factor of 20 smaller than the total donor concentration. The absence of X_3, which has been associated with both C[4] and Ge[15,16] in the literature, is interesting because it is one of the characteristic residual donor species present in $AsCl_3$-H_2 VPE, $AsCl_3$-N_2 VPE, and AsH_3 VPE grown GaAs[3,10] and it is the dominant residual donor species in MOCVD grown GaAs.[3,5,17] In contrast, the Pb donor is absent in unintentionally doped GaAs grown by all of the above techniques except MBE.

10.4 REFERENCES

1. G.E. Stillman, C.M. Wolfe, in Semiconductors and Semimetals Vol. 12, edited by R.K. Willardson and A.C. Beer, (Academic Press 1977), pp. 169-290.
2. C.M. Wolfe, private communication, 1979.
3. T.S. Low, G.E. Stillman, C.M. Wolfe, Proc. Sym. GaAs and Related Compounds, Oiso, 1981, (to be published).
4. C.M. Wolfe, G.E. Stillman, D.M. Korn, *Proc. Sym. GaAs and Related Compounds, St. Louis,* 1976 (Institute of Physics, London) pp. 120-128.
5. R.A. Cooke, R.A. Hoult, R.F. Kirkman, R.A. Stradling, J. Phys. D: Appl. Phys. Vol. 11, 945 (1978).
6. H. Morkoç, A.Y. Cho, J. Appl. Phys. 50, 6413 (1979).
7. A.R. Calawa, Appl. Phys. Lett. 38, 701 (1981).
8. A.Y. Cho, J.R. Arthur, Progess in Solid State Chemistry (Pergamon, New York, 1975) Vol. 10, pp. 157-191.
9. A. Chandra, C.E.C. Wood, D.W. Woodard, L.F. Eastman, Solid State Elect. Vol. 22, 645 (1979).
10. D.M. Larsen, private communication, Phys. Rev. B, Vol. 13, 1681 (1976).
11. C.M. Wolfe, G.E. Stillman, J.O. Dimmock, J. Appl. Phys. 41, 504 (1970).
12. M. Ozeki, K. Kitahara, K. Nakai, A. Shibatomi, K. Dazai, S. Okawa, O. Ryuzan, Jpn. J. Appl. Phys. 16, 1617 (1977).
13. T.S. Low, G.E. Stillman, D.M. Collins, and C.M. Wolfe, to be published.
14. R.A. Stradling, private communication, 1981.

15. J.H.M. Stoelenga, D.M. Larsen, W. Walukiewicz, C.O. Bozler, J. Phys. Chem. Solids, 39, 873 (1978).

16. M.N. Asfar, K.J. Button, G.L. McCoy, Proc. Sym. GaAs and Related Compounds, 1980 (Inst. of Physics, London) pp. 547-555.

17. P.D. Dapkus, H.M. Manasevit, K.L. Hess, T.S. Low, G.E. Stillman, J. Cryst. Growth, 55, 10 (1981).

11. MULTIPLE DOPING EXPERIMENTS

In this section we present the results of a study undertaken to determine the interactions between or complexing of multiple dopants in GaAs. The impurities initially studied are sulfur and oxygen. To examine possible interactions, experiments involving the growth and characterization of samples homogeneously and inhomogeneously doped with H_2O and/or H_2S were undertaken. The inhomogeneously doped layers provide self-calibrating samples for subsequent analysis.

11.1 HOMOGENEOUSLY DOPED LAYERS

All of the homogeneously doped layers were grown on Cr doped, semi-insulating substrates oriented 2^o off {100} towards {110}. An extensive series of growth runs were performed using H_2S(g) diluted to 11 ppm as the only doping source. This series of runs yielded the expected result that sulfur is a well-behaved shallow donor in GaAs. The variation of carrier concentration (given by the effective distribution coefficient) with H_2S flow rate is shown in Fig. 1. Doping levels from $3x10^{15}cm^{-3}$ to $3x10^{17}cm^{-3}$ were reproducibly obtained.

Another series of runs was performed using only H_2O as the doping source. The input partial pressure of H_2O was controlled by a constant temperature bath. The dopant was transported into the reactor by passing H_2 over a bed of solid H_2O for those runs performed with the temperature bath at less than 0^oC, and by bubbling H_2 through liquid H_2O for those runs

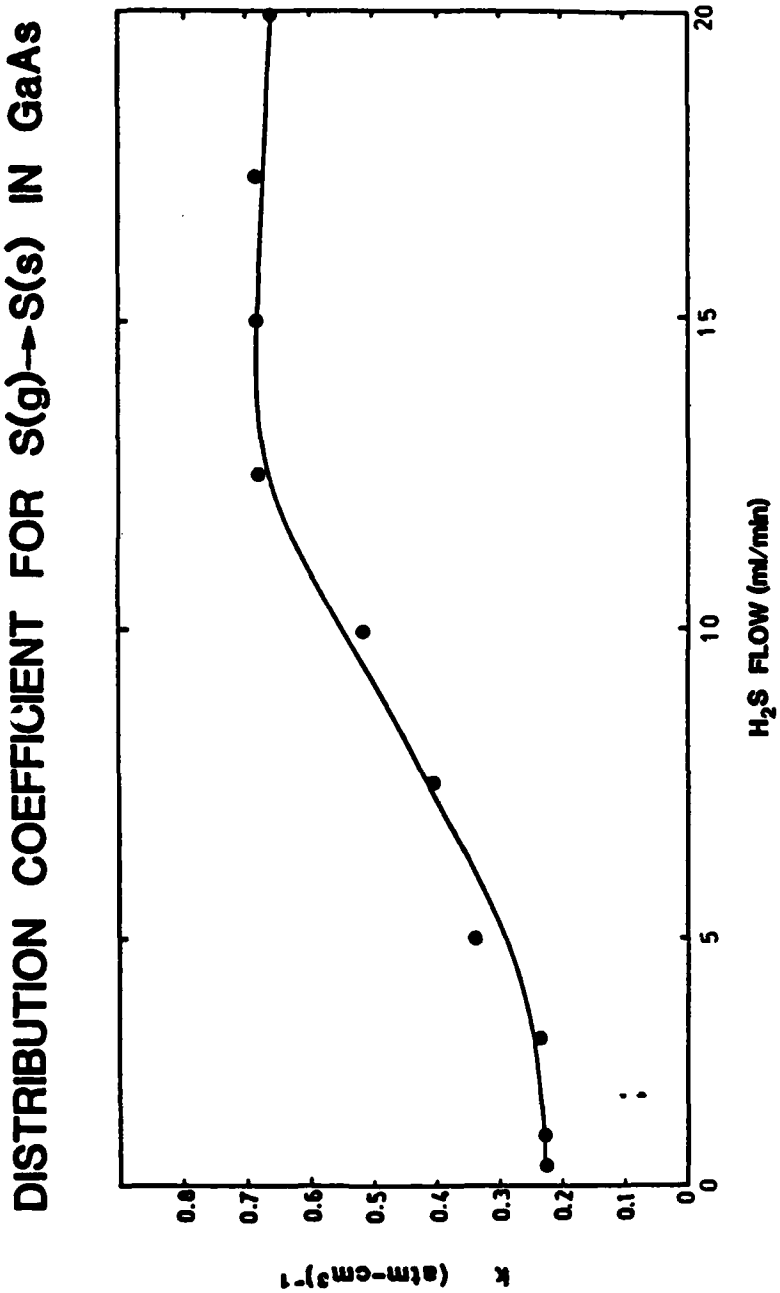
DISTRIBUTION COEFFICIENT FOR S(g)→S(s) IN GaAs
K (atm-cm³)⁻¹
0.8
0.7
0.6
0.5
0.4
0.3
0.2
0.1
0
5
10
15
20
H₂S FLOW (ml/min)

Figure 1

performed with the temperature bath at greater than 0°C. The results of the H_2O doping for the temperature range between -78°C and +24°C were quite striking. For each run the resulting layer was highly compensated with carrier concentrations ranging from $1x10^{14}cm^{-3}$ at -78°C to $8x10^{12}cm^{-3}$ at 24°C.

Growth runs were also performed in which the layers were simultaneously doped with H_2S and H_2O. A series of runs was performed to determine the effect of H_2 flow rate over the H_2O(s). The H_2S flow rate used was 7.5 ml/min and the H_2O source was maintained at a temperature of -78°C. Fig. 2 shows the effect that varying the gas flow over the H_2O(s) has on the carrier concentration obtained from van der Pauw[1] measurements at 300K and 77K. From these data, two effects are demonstrated.

The first effect to be noticed is the increase in carrier concentration with an increase in flow rate over the H_2O. The second effect can be seen in the freeze-out of carriers at 77K. The last column of Fig. 2 shows the difference between the carrier concentrations at 300K and 77K for each of the flow rates given. This shows that the concentration of carriers freezing out is linearly dependent on the flow rate. Such behavior is indicative of a deep donor.

The effect of increasing the partial pressure of H_2O in the system is similar to increasing the flow rate of H_2 through the H_2O, although a definite upper limit to the obtainable carrier concentration is evidenced. Layers were grown with an H_2S flow of 7.5 ml/min and a H_2+H_2O flow of 5.0 ml/min. The temperature of the H_2O was varied from layer to layer

SULFUR/OXYGEN DOPED HOMOGENEOUS LAYERS

H_2+H_2O flow (ml/min)	concentration (cm^{-3}) n_{300}	n_{77}	$n_{300}-n_{77}$
5	2.5×10^{16}	2.0×10^{16}	0.5×10^{16}
10	3.3×10^{16}	2.2×10^{16}	1.1×10^{16}
15	5.0×10^{16}	3.6×10^{16}	1.4×10^{16}

H_2S flow 7.5 (ml/min)

Figure 2

over the range from -78°C to 24°C. Fig. 3 shows the 300K carrier concentration versus H_2O temperature and partial pressure[2]. At the low end of the temperature range (-78°C), the carrier concentration is about $3x10^{16}cm^{-3}$ which is the same as for layers grown in the absence of H_2O. In the high temperature range the carrier concentration is relatively insensitive to changes in H_2O temperature and remains constant at about $2x10^{17}cm^{-3}$.

11.2 SELF-CALIBRATING LAYERS

The self calibrating layer structure used in this work is shown in Fig. 4. N_{D1} and N_{D2} are the dopants added to the layer; in this case N_{D1} and N_{D2} are due to H_2S and H_2O, respectively. The layer is structured into five regions. Regions I and V are the calibration regions in which the chemical and electrical properties of each dopant may be determined independent of any interactions with the other dopant. Regions II and IV are the transition regions for dopants D2 and D1, respectively, which contain the information on how the chemical and electrical concentrations change as a function of concentration of the dopant being switched on or off. Region III is the region in which both dopants are at their maximum levels and the effects of any interactions or complexing should be greatest. Routine analysis of self-calibrating layers consists of SIMS profiling to determine the chemical composition of the layer and C-V profiling to determine the free carrier concentration. The C-V analysis was

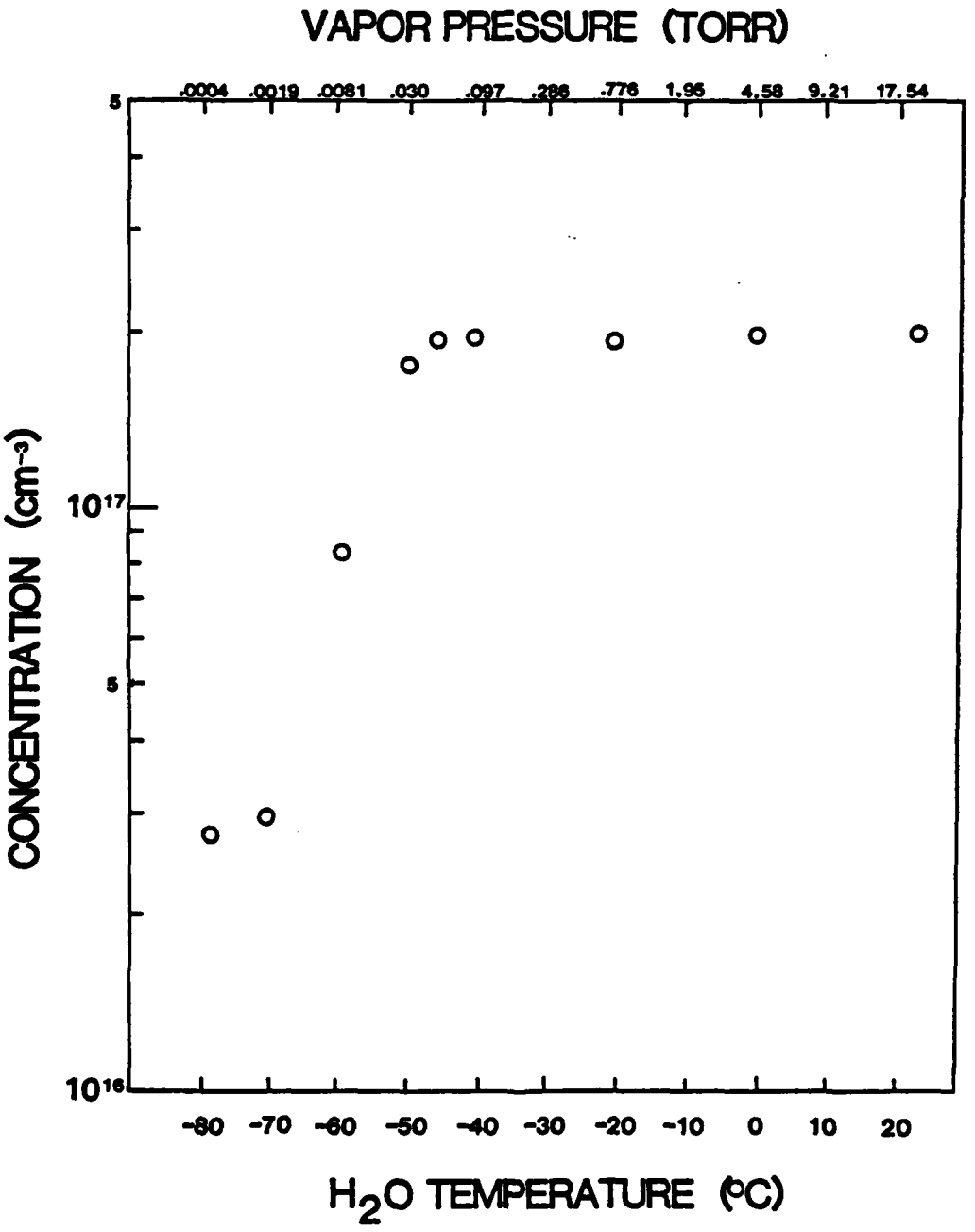

Figure 3. 300K van Der Pauw carrier concentration for layers grown with various levels of H_2O.

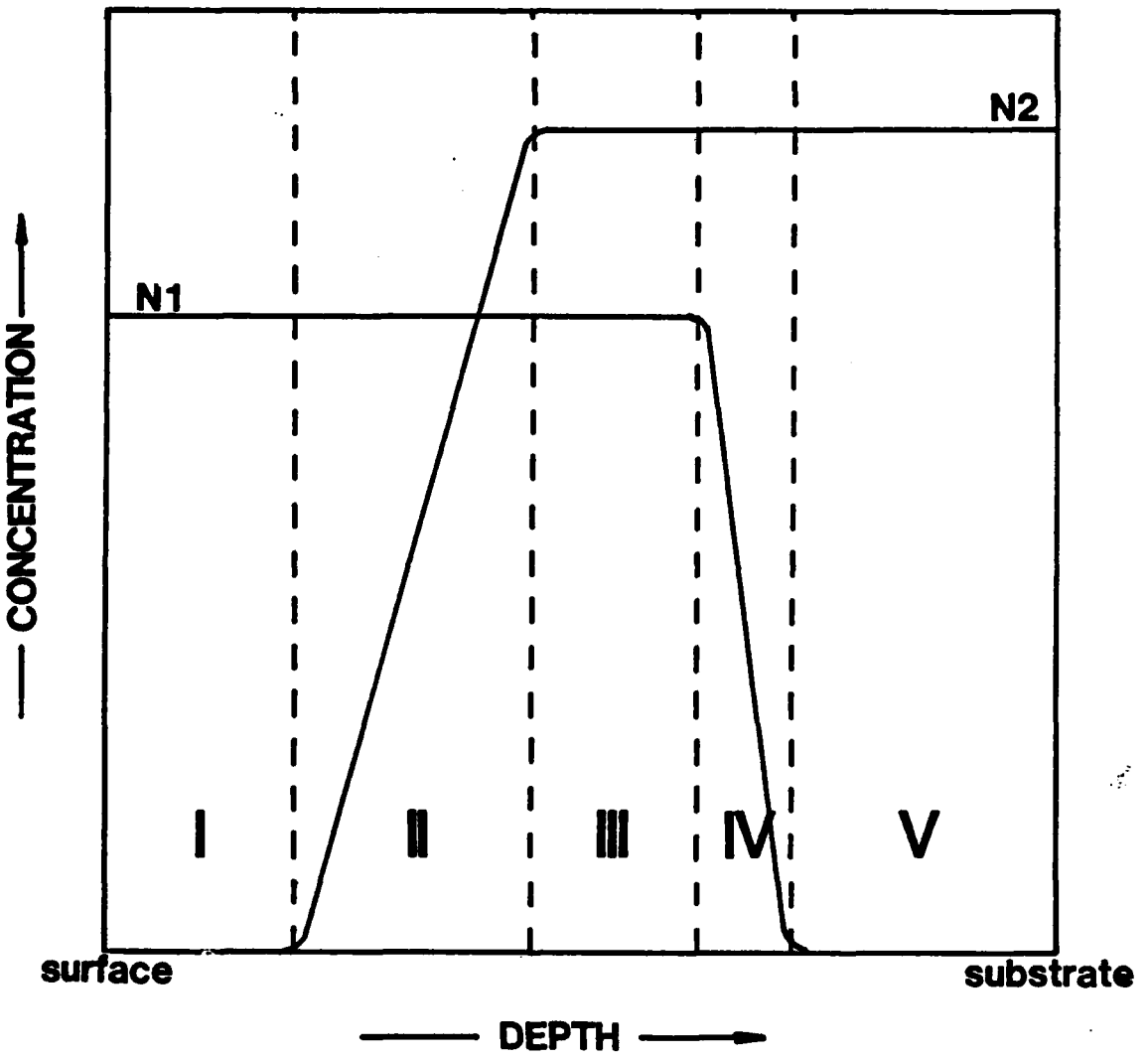

Figure 4. Self-calibrating layer structure.

performed using an electrochemical cell so that thick, heavily doped layers could be examined[4,5,6,7,8].

The self-calibrating layers were grown on Si doped substrates oriented 2^{o} off {100} towards {110} with a carrier concentration between $2x10^{17}cm^{-3}$ and $2x10^{18}cm^{-3}$. The H_2S flow rate, when on, was set for 7.5 ml/min. The flow of H_2+H_2O was 5.0 ml/min with the H_2O temperature ranging from $-78^{o}C$ to $24^{o}C$. Figs. 5, 6, and 7 show the SIMS and C-V analyses for three samples grown with various input partial pressures of H_2O. In these figures n_i is the intrinsic concentration at the growth temperature[9]. In the H_2S calibration region of all three samples, the free carrier concentration at the growth temperature ($740^{o}C$)[9] is between $1x10^{17}cm^{-3}$ and $2x10^{17}cm^{-3}$ which is an order of magnitude higher than the sulfur concentration. This may be due to the influence of a slow turn-off profile for the H_2O as shown in Figs. 6 and 7. A possible effect of the gradual turn-off of H_2O may be seen in the slope of the sulfur profiles in the H_2S calibration region in Figs. 6 and 7. Samples grown without H_2O present or with a very low partial pressure of H_2O exhibit flat sulfur profiles in the calibration region. There are two possible reasons for the dependence of the sulfur profile on the H_2O: (1) the distribution or the diffusion of sulfur in GaAs is altered through some interaction with the H_2O or (2) oxygen incorporated in the layer is detected in the form of O_2 which is indistinguishable from S in normal SIMS analysis[10].

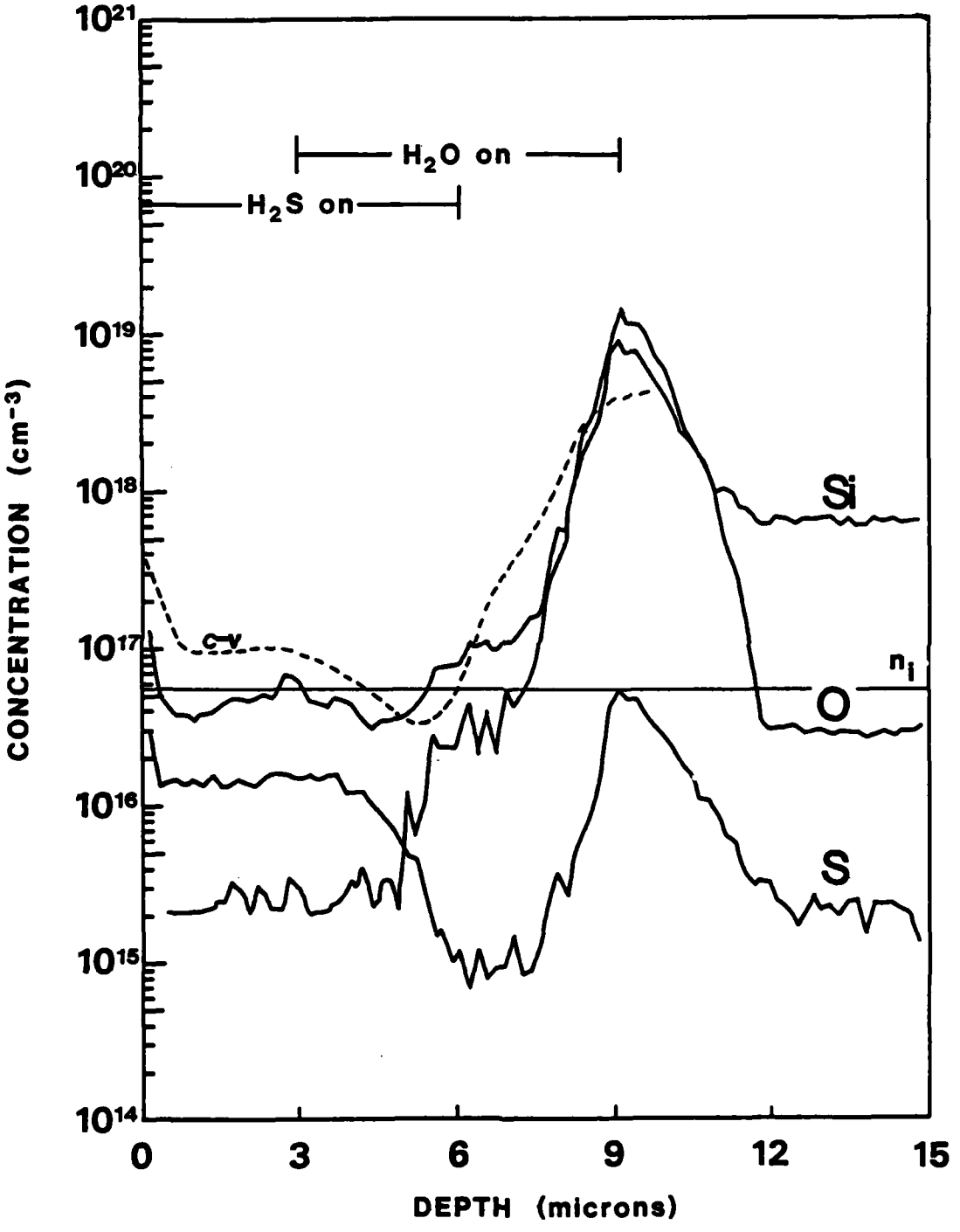

Figure 5. Self-calibrating layer grown with H_2O at -60°C.

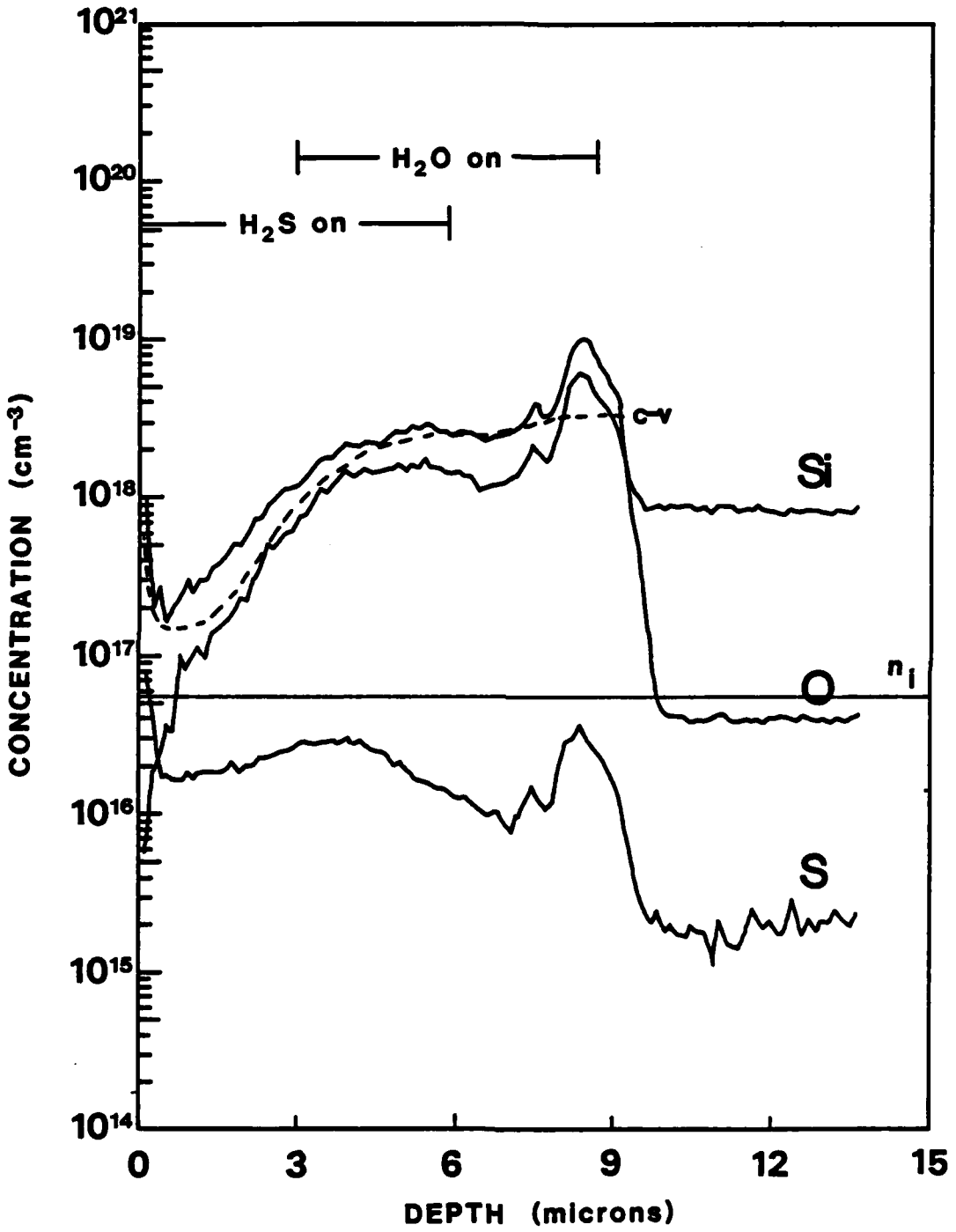

Figure 6. Self-calibrating layer grown with H_2O at -50°C.

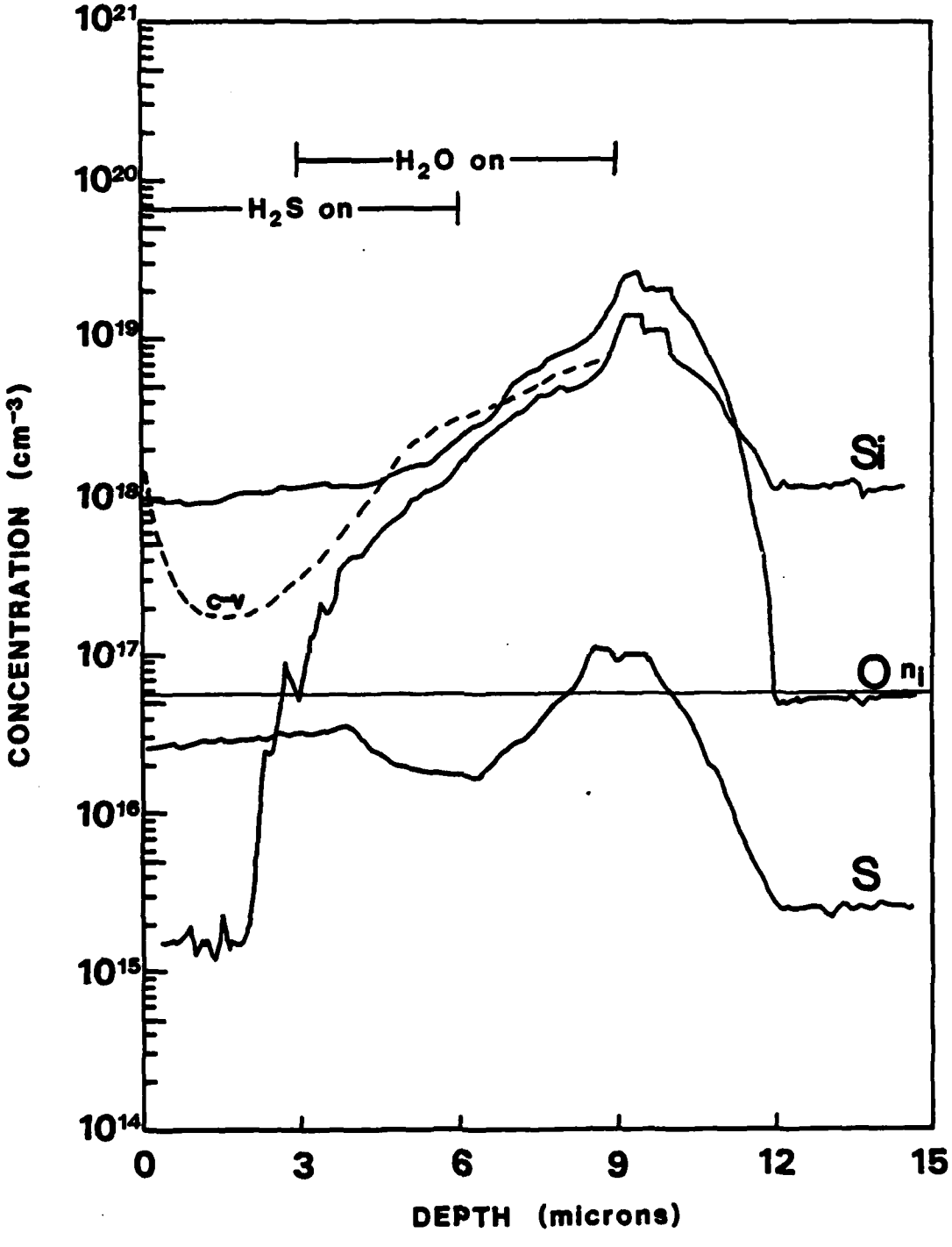

Figure 7. Self-calibrating layer grown with H_2O at -40°C.

Experiments with the homogeneously doped samples indicate that the first explanation is more plausible.

Examination of the behavior of the sulfur in the sulfur transition region shows a dependence of the sulfur turn-on profile on the input partial pressure of the H_2O. From the SIMS analysis, it is evident that the turn-on profile for the sulfur becomes more gradual. Associated with the more gradual turn-on of sulfur is the elevation of the sulfur concentration in the H_2O and H_2S calibration regions.

Some increase in the sulfur concentration with increased H_2O partial pressure in the sulfur calibration region was expected from the work done with the homogeneously doped layer and this was observed. The increase of sulfur in the H_2O calibration region, however, was unexpected. Fig. 5 shows the sulfur concentration in the H_2O calibration region as $1x10^{15}cm^{-3}$ and Fig. 6 shows an order of magnitude increase of sulfur for an increase in H_2O temperature of $10^{o}C$. There are two possible explanations for this behavior. One explanation is, as before, that O_2 may be mistaken for S in the SIMS analysis. The other possibilty is reactive diffusion of sulfur with the impurity introduced or defect induced by the H_2O. The corresponding softening of the sulfur turn-on profile favors the latter explanation.

Finally, notice must be taken of the large concentration of Si throughout the layers of Figs. 6 and 7. It is believed that the source of Si is the substrate and that the profile is the result of autodoping or H_2O enhanced outdiffusion.

The C-V profiles confirm that Si is the major contributor to the carrier concentration when incorporated at such a high concentration.

11.3 DISCUSSION

Experiments performed with homogeneously doped layers demonstrate that H_2O introduces some impurity or defect into the growing layer and that there are two interactions which should be considered. These are (1) the H_2O-residual or intentionally-added impurity interaction responsible for the highly compensated H_2O doped samples and deep donor behavior and (2) the H_2O-H_2S interaction responsible for the change in the sulfur distribution or diffusion. Analysis of self-calibrating layers yields more evidence that H_2O increases the distribution or diffusion of sulfur in GaAs and, at high input partial pressures, contributes significantly to the free carrier concentration. Experiments are currently being performed to separate growth incorporation from reactive diffusion effects.

11.4 REFERENCES

1. L.J. van der Pauw, Philips Res. Repts. 13, 1, (1958).

2. Handbook of Chemistry and Physics 54th edition, CRC Press, 1973.

3. D.P. Kennedy, P.C. Murley, W. Kleinfelder, IBM J. Res. Dev. 13, 409B (1968).

4. T. Ambridge, C.R. Elliott, and M.M. Faktor, J. Appl. Electrochem. 3, 1(1973).

5. T. Ambridge and M.M. Faktor, J. Appl. Electrochem. 5, 319 (1975).

6. T. Ambridge and M.M. Faktor, Electronic Lett. 10, 204 (1974).

7. D.G. Fiddyment and M.R. Taylor, J. Electrochem. Soc. 122, 1567 (1975).

8. T. Ambridge, D.J. Ashen, Electronic Lett. 15, 647 (1979).

9. K.H. Nichols, Camellia M.L. Yee, and C.M. Wolfe, Solid State Electronics 23, 109 (1980).

10. Charles Evans and Associates, private communication.

12. PUBLICATIONS

1. P.A Fedders, "Effects of Interactions Between Hopping Particles on T_1 Relaxation Rates at Low Concentrations", Phys. Rev. B 25, 78 (1982).

2. P.A. Fedders, "Electrostatic Effects of Hydrogenic Donor Complexes on Magneto-Optical Spectra", Phys. Rev. B 25, 3846 (1982).

3. T.S. Low, G.E. Stillman, and C.M. Wolfe, "Identification of Residual Donor Impurities in Gallium Arsenide", Proc. 1981 Int. Symp. GaAs and Related Compounds (Inst. Phys., London, 1982) p. 143.

4. T.S. Low, G.E. Stillman, A.Y. Cho, H. Morkoc, and A.R. Calawa, "Spectroscopy of Donors in High-Purity GaAs Grown by Molecular Beam Epitaxy", Appl. Phys. Lett. 40, 611 (1982).

5. H. Rohdin, M.W. Muller, and C.M. Wolfe, "Impurity Redistribution During Epitaxial Growth", J. Electron. Mat. 11, 517 (1982).

6. T.S. Low, G.E. Stillman, D.M. Collins, C.M. Wolfe, S. Tiwari, and L.F. Eastman, "Spectroscopic Identification of Si Donors in GaAs", Appl. Phys. Lett. 40, 1034 (1982).

7. T.S. Low, G.E. Stillman, T. Nakanisi, T. Udagawa, and C.M. Wolfe, "Photothermal Ionization Identification of Sulfur Donors in GaAs", Appl. Phys. Lett. 41, 183 (1982).

8. P.A. Fedders, "Potential Fluctuations in High-Purity n-Type III-V Semiconductors", J. Appl. Phys. 53, 6154 (1982).

9. D.L. Rode, C.M. Wolfe, and G.E. Stillman, "Magnetic Field Dependence of the Hall Factor of Gallium Arsenide", Proc. 1982 Int. Symp. GaAs and Related Compounds, (Inst. Phys., London, 1983) to be published.

10. B.J. Skromme, T.S. Low, and G.E. Stillman, "Spectroscopic Characterization Studies of the Residual Donors and Acceptors in High-Purity LPE GaAs", Proc. 1982 Int. Symp. GaAs and Related Compounds, (Inst. Phys., London, 1983) to be published.

11. T.S. Low, B.J. Skromme, and G.E. Stillman, "Incorporation of Amphoteric Impurities in High Purity GaAs", Proc. 1982 Int. Symp. GaAs and Related Compounds, (Inst. Phys., London, 1983) to be published.

12. P.A. Fedders, "Coulomb Potential Fluctuations in High-Purity n-Type III-V Semiconductors", Proc. 1982 Int. Symp. GaAs and Related Compounds, (Inst. Phys., London, 1983) to be published.

13. P.A. Fedders, "Strain Scattering of Electrons in Piezoelectric Semiconductors", submitted to J. Appl. Phys.

14. Camellia M.L. Yee, P.A. Fedders, and C.M. Wolfe, "The Effect of Electric Fields on Cr Redistribution at GaAs Surfaces", submitted to Appl. Phys. Lett.

15. H. Rohdin, M.W. Muller, and C.M. Wolfe, "A Model of Cr in GaAs", submitted to J. Phys. Chem. Solids.

13. MEETING TALKS

1. C.M. Wolfe, "Amphoteric Dopants and Compensation in GaAs", Workshop on Shallow Impurities in Semiconductors, Wright-Patterson AFB, Ohio, 21-22 May 1981.

2. G.E. Stillman, "Identification of Shallow Donors in GaAs", Workshop on Shallow Impurities in Semiconductors, Wright-Patterson AFB, Ohio, 21-22 May 1981.

3. H. Rohdin, M.W. Muller, and C.M. Wolfe, "Impurity Redistribution During Epitaxial Growth", Electronic Materials Conference, Santa Barbara, Calif., 24-26 June 1981.

4. T.S. Low, G.E. Stillman, and C.M. Wolfe, "Identification of Residual Donor Impurities in GaAs", Int. Symp. GaAs and Related Compounds, Oiso, Japan, 20-23 September 1981.

5. C.M. Wolfe, "Impurity Complexing in GaAs", Materials Research Meeting, Tokyo, Japan, 24 September 1981.

6. H. Rohdin, M.W. Muller, and C.M. Wolfe, "A Model of Cr in GaAs", Workshop on Compound Semiconductor Microwave Materials and Devices, Scottsdale, Arizona, 22-23 February 1982.

7. T.S. Low, G.E. Stillman, and C.M. Wolfe, "Identification of Residual Donor Impurities in Gallium Arsenide", Workshop on Compound Semiconductor Microwave Materials and Devices, Scottsdale, Arizona, 22-23 February 1982.

8. Camellia M.L. Yee, R.T. Green, P.A. Fedders, and C.M. Wolfe, "Cr-Redistribution at GaAs surfaces", Electronic Materials Conf., Fort Collins, Colorado, 23-25 June 1982.

9. R.T. Green, Camellia M.L. Yee, and C.M. Wolfe, "Impurity Interactions in Vapor-Phase Epitaxial GaAs", Electronic Materials Conf., Fort Collins, Colorado, 23-25 June 1982.

10. T.S. Low, B.J. Skromme, and G.E. Stillman, "Spectroscopic Characterization of Residual Donors and Acceptors in High Purity MOCVD GaAs", Electronic Materials Conf., Fort Collins, Colorado, 23-25 June 1982.

11. D.L. Rode, C.M. Wolfe, and G.E. Stillman, "Magnetic Field Dependence of the Hall Factor of Gallium Arsenide", Int. Symp. GaAs and Related Compounds, Albuquerque, New Mexico, 19-22 September 1982.

12. B.J. Skromme, T.S. Low, and G.E. Stillman, "Spectroscopic Characterization Studies of the Residual Donors and Acceptors in High-Purity LPE GaAs", Int. Symp. GaAs and Related Compounds, Albuquerque, New Mexico, 19-22 September 1982.

13. T.S. Low, B.J. Skromme, and G.E. Stillman, "Incorporation of Amphoteric Impurities in High Purity GaAs", Int. Symp. GaAs and Related Compounds, Albuquerque, New Mexico, 19-22 September 1982.

14. P.A. Fedders, "Coulomb Potential Fluctuations in High-Purity n-Type III-V Semiconductors", Int. Symp. GaAs and Related Compounds, Albuquerque, New Mexico, 19-22 September 1982.

14. DISTRIBUTION LIST

CONTRACT N00014-80-C-0762

Office of Naval Research — 4
Code 414
Arlington, VA 22217

Naval Research Laboratory
4555 Overlook Avenue, S.W.
Washington, DC 20375
Code 6810 — 1
Code 6820 — 1
Code 6870 — 1

Defense Documentation Center — 12
Building 5, Cameron Station
Alexandria, VA 22314

Dr. Y. S. Park — 1
AFWAL/DHR
Building 450
Wright-Patterson AFB
OH 45433

Dr. W. Wisseman — 1
Texas Instruments
Central Research Lab
M.S. 134
13500 North Central Expressway
Dallas, TX 75265

Dr. R. Bierig — 1
Raytheon Company
141 Spring Street
Waltham, MA 02173

Dr. Mike Driver — 1
Westinghouse Research and
Development Center
Beulah Road
Pittsburgh, PA 15235

Dr. F. Eisen — 1
Rockwell International
Science Center
P.O. Box 1085
Thousand Oaks, CA 91360

Mr. Lothar Wandinger — 1
ECOM/AMSEL/TL/IJ
Fort Monmouth, NJ 07003

Dr. William Lindley — 1
MIT
Lincoln Laboratory
F124 A, P.O. Box 73
Lexington, MA 02173

Commander — 1
U.S. Army/ERADCOM
Attn: V. Gelnovatch, DELET-M
Fort Monmouth, NJ 07703

Dr. F. Sterzer — 1
RCA
Microwave Technology Center
Princeton, NJ 08540

Commander — 1
Naval Electronics Systems Command
Attn: J. P. Letellier, Code 6142
Washington, DC 20360

Commander — 1
Naval Air Systems Command
Attn: A. Glista, Jr., AIR 34
Washington, DC 20361

Dr. R. Bell, K-101 — 1
Varian Associates, Inc.
611 Hansen Way
Palo Alto, CA 94304

Dr. Robert Archer — 1
Hewlett-Packard Corporation
1501 Page Road
Palo Alto, CA 94306

Drs. E. J. Crescenzi, Jr. and — 1
K. Niclas
Watkins-Johnson Company
3333 Hillview Avenue
Stanford Industrial Park
Palo Alto, CA 94304

Commandant 1
Marine Corps
Scientific Adviser (Code AX)
Washington, DC 20380

Dr. W. Weisenberger 1
Communications Transistor Corp.
301 Industrial Way
San Carlos, CA 94070

Drs. F. A. Brand and 1
J. Saloom
Microwave Associates
Northwest Industrial Park
Burlington, MA 01803

Commander, AFAL 1
AFWAL/AADM
Attn: Dr. Don Rees
Wright-Patterson AFB
OH 45433

Professor Walter Ku 1
Cornell University
Phillips Hall
Ithaca, NY 14853

Mr. Horst W. A. Gerlach 1
Harry Diamond Laboratories
800 Powder Mill Road
Adelphia, MD 20783

A.G.E.D. 1
201 Varick Street
9th Floor
New York, NY 10014

Dr. Ken Weller 1
TRW Systems
MS/1414
One Space Park
Redondo Beach, CA 90278

Professor L. Eastman 1
Cornell University
Phillips Hall
Ithaca, NY 14853

Dr. T. J. Magee 1
Advanced Research and
Applications Corporation
Sunnyvale, CA 94086

Professors Hauser and 1
Littlejohn
North Carolina State University
Department of Electrical Engineering
Raleigh, NC 27607

Professor J. Beyer 1
University of Wisconsin
Department of Electrical and
Computer Engineering
Madison, WI 53706

Professors Rosenbaum and Wolfe 1
Washington University
Semiconductor Research Laboratory
St. Louis, MO 63130

Dr. W. H. Perkins 1
General Electric Company
Electronics Lab 3-115/B4
P.O. Box 4840
Syracuse, NY 13221

Dr. Bryan Hill 1
AFWAL/AADE
Wright-Patterson AFB
OH 45433

Dr. J. Schellenberg 1
Hughes Aircraft Company
Electron Dynamics Division
3100 W. Lomita Boulevard
P.O. Box 2999
Torrance, CA 90509

Mr. H. Willing 1
Radar Directorate
BMD - Advanced Technical Center
P.O. Box 1500
Huntsville, AL 35807

Dr. C. Krumm 1
Hughes Research Laboratory
3011 Malibu Canyon Road
Malibu, CA 90265

Dr. E. Silberg 1
Bell Telephone Laboratories
Holmdel, NJ 07733

Dr. Harvey Nathenson 1
Westinghouse Research and
Development Center
Beulah Road
Pittsburgh, PA 15235

Dr. S. Wanuga 1
General Electric Company
Electronics Lab 134
Electronics Park
Syracuse, New York 13221

Professor D. Navon 1
University of Massachusetts
Department of Electrical and
Computer Engineering
Amherst, MA 01003